NONLINEAR PROCESSING OF SENSORY INTERFERENCE DRIVES SOCIAL BEHAVIOR IN WEAKLY ELECTRIC FISH

by

Manu S. Madhav

A dissertation submitted to The Johns Hopkins University in conformity with the requirements for the degree of Doctor of Philosophy.

Baltimore, Maryland

March, 2014

Abstract

Sensory systems in animals and robots can receive information from the environment via modulations of sensory signals. Environmental features and conspecifics generate these modulations, and effective computational algorithms in sensory systems can demodulate signals to perceive the features. However, interaction of multiple modulations can themselves generate emergent modulations, which can encode relative information between environmental features. These emergent modulations create sensory interference which can be detrimental or beneficial to sensing. Organisms that probe their environment using autogenous sensory signals are prone to such interference from other nearby individuals in the same social group. Some animals have evolved behaviors that allow them to retain a high level of sensory performance in such a social context. For example, the weakly electric glass knifefish, *Eigenmannia virescens*, produces a pseudo-sinusoidal oscillating electric signal used for electrolocation and social communication. In my thesis, I explore how the electrosensory system of weakly electric fish use nonlinear processing to respond to interference from conspecifics.

ABSTRACT

In *Eigenmannia* and other wave-type electric fishes, the interaction between two individuals produces first-order modulations termed *beats*, and interaction between three or more individuals produce "beats of beats", termed *envelopes*. In this thesis, I provide an analytical basis for the emergence of beats and envelopes in sensory systems. I derive conditions where these emergent modulations arise, and show how biologically plausible nonlinear mechanisms can extract information embedded in them.

Experimentally, I characterize the Jamming Avoidance Response (JAR) in *Eigenmannia* in terms of an input-output model. The JAR is a widely studied response to beats. The JAR is locally unstable; it is an escape response. An experimental closed-loop around the electrosensory system of the animal "stabilized" the behavior, facilitating system identification analysis. The experimental input–output responses were parsed into a global nonlinear model of the JAR.

I also describe our discovery of a new behavior in these fish, termed the Social Envelope Response (SER). The SER is a behavioral response to envelopes. We experimentally determined the properties of the SER for *Eigenmannia*.

Primary Reader: Noah J. Cowan

Secondary Reader: Eric S. Fortune and Dennice F. Gayme

Acknowledgments

This thesis, though it carries my name proudly on the cover, would not have been possible without the guidance, help, support and dogged persuasion of a select group of friends and colleagues.

First and foremost, I would like to thank my advisor, Dr. Noah Cowan for welcoming me into his lab. Over the years, he has played the roles of teacher, colleague, mentor, counsellor, and even confidant. His curiosity inspires me, his skills bewilder me, and his unwavering, sometimes annoying adherence to the highest standards of scholarship and the scientific method helps me become a better academician and person.

Dr. Eric Fortune has served as my unofficial co-advisor, and helped me as I spent countless hours in his fish lab taking the first steps from being a freshly minted engineer to a (still in progress) scientist. His sense of humor uplifts me, and his ability to tackle a seemingly complex experimental problem with a simple, clever, elegant solution is a skill that I aspire to.

I have to (under duress) thank Dr. Sarah Stamper, my partner in all the work

that contributed to this thesis. As a colleague, she exemplifies resolve—she is able to perform behavioral experiments for hours on end, and determinedly pursue problems until a solution is found. She helps me clarify the image seen through my "engineering goggles" and find the appropriate scientific questions. I feel myself lucky to have been paired with her.

The Locomotion in Mechanical and Biological Systems (LIMBS) laboratory has not only helped me improve myself academically, but also has provided me with an amazing group of friends. I would like to thank lab members past and present: Shahin Sefati, Mert Ankarali, Ravikrishnan Jayakumar, Alican Demir, Erin Sutton, Eatai Roth, John Swensen, Robert Nickl, Jusuk Lee, Sean Carver and Eric Tytell.

I would also like to thank the grad students, staff, faculty and friends at JHU and especially at LCSR. They are too many to name, but my experiences in this esteemed institution has been enriched by the interactions with each and every one of them.

Dedication

This thesis is dedicated to my parents, Sreekumari and Sasidharan, who shared my burdens from half a world away, and to my brother, Chettanmon, who filled our home with laughter, and departed before I had a chance to know him.

Contents

List of Tables

List of Figures

Chapter 1

Introduction

Biological organisms thrive in a wide variety of natural and even artificial environments. An organism's environment provides it with a rich set of sensory signals. Accessing appropriate information encoded in these sensory signals is essential for the organism to utilize its environment. This sensory challenge is relevant not only to biologists in understanding animal behavior, but also to engineers trying to get the most out of the sensing capabilities in a robot.

In the following sections, I discuss the nature of information encoded in sensory signals, and how this information can be extracted and utilized by organisms. In social settings, interference between sensory signals provides additional, potentially confounding, nonlinear information. My thesis focuses on the mechanisms for extraction of emergent oscillations resulting from sensory interference, and behavioral responses to these nonlinear features. In the following discussion, the term "agent"

can refer to either an organism or a robot. Similarly, both a biological sensory organ and an artificial sensor are lumped together under the term "sensor".

1.1 Information in modulations

Most environments can be sensed through a large number of possible cues, for example, light, sound, mechanical perturbations, electric and magnetic fields, chemical composition, temperature, and pressure. In some sensory systems, the source of the sensory signals can be the agent itself (e.g. echolocation and electrolocation in biology; radar and sonar in engineering). Sensory systems can also rely on signals generated and present in the ambient environment (e.g. vision, hearing, and magnetoception in biology; cameras, microphones, and GPS receivers in engineering).

These myriad signals are conducive to sensing due to the environment being able to influence and change them. Environmental features interact with sensory signals to produce modulations in the signal. A modulation is simply a change in one or more of the parameters of the sensory signal. The modulation in a sensory signal produced by an environmental feature tends to "encode" some parameter of the feature. This encoding is generally the result of the physics of the interaction; the feature leaves a signature of itself in the signal that it interacts with. An example of this is viewing shadows. An object in the presence of a visible light source physically obstructs the light, producing a shadow: a distorted two-dimensional projection of the object. A

sensor that perceives visible light, e.g. an eye or a camera, measures a contrast pattern, which is the modulation of the signal absent the object. The spatial frequencies of this modulation correspond, in large part, to dimensions of the object that caused the modulation. Thus, the modulation carries information relevant to perception of the object.

Sensory organs as well as their associated neural circuits are typically tuned to the properties of their associated sensory signal. For instance, the visual receptors (rods and cones) in the human retina are tuned to the specific frequencies of electromagnetic radiation which we term "visible light". In fact, there are three different types of cones which are sensitive to specific frequency bands, allowing us to perceive and interpret color [9, 73]. Similarly, the cochlea in the human ear is susceptible to mechanical vibration in the so-called "audio frequency" range (10–10000 Hz). However, visual features in nature are generally much lower frequency (higher wavelength) than visible light [25], and human speech is much lower frequency than audio frequencies [68]. Visible light and audible sound are just signals that are "carriers" of relevant low-frequency information. An object in the visual scene, for example, produces a modulation of the light, and it is this modulation of the carrier signal which provides the visual system with the information to perceive and process the feature.

1.2 Emergent modulations in sensing

The role of a sensor is to measure the modulated sensory signal. A successful sensory system will additionally use this measured signal to extract relevant information about the environment. In the simplest case, the sensory signal undergoes one type of modulation from a specific environmental feature, and the sensory system performs one set of operations on the signal in order to extract the modulation, thereby revealing characteristics of the feature. However, this is rarely the case in real-world environments, where different features and conspecifics are present. A sensory signal may undergo multiple similar or dissimilar modulations. In these conditions, the role of the sensory system is decidedly complex: the sensory system has to demodulate the signal, and then process the modulations in order to estimate the properties of the features that created those modulations.

The layered nature of information in sensory modulation is made more complicated by the emergence of *second-order* modulations which are not due to a specific environmental feature, but instead due to the interaction of multiple feature-driven *first-order* modulations. For example, if a carrier signal (say a pure cosine wave $\cos \omega t$) is modulated by two different amplitude functions $a_1(t)$ and $a_2(t)$, either additively

$$(a_1(t) + a_2(t)) \cos(\omega t),$$

or sequentially

$$a_2(t)[a_1(t) \cos(\omega t)];$$

either of these operations can result in emergent (second-order) modulations. The first case represents the interaction of two independently modulated carrier signals (e.g. diffraction patterns in interacting light from two spatially separated sources). The second case represents tiered modulations, where a signal modulated by an environmental feature is further modulated by a second feature. (e.g. patterns around the image of an object viewed through a lens with spherical aberrations).

Emergent modulations are generally *nonlinear*, i.e. they cannot be extracted by a linear process such as the Fourier transform. In my thesis, I investigate two types of emergent nonlinear modulations, termed *beats* and *social envelopes*. These features can, under the appropriate conditions, emerge in sensory systems that generate their own signals to probe the environment. The sensory signals from these systems could interfere under conditions where multiple agents are in close proximity. For example, several species of animals prefer to be in social settings, and some animals even lead their lives in large social groups [24]. Under the assumption that each agent does not know its conspecific's signal properties, there is a large chance that signal interference could occur. These types of interference might be detrimental to sensory processing, or may even be beneficial by providing information on conspecifics.

How do organisms process these complex, interfering, degraded, sensory signals in order to effect complex behavior such as social communication, obstacle and predator avoidance, and prey capture? How do they balance the beneficent effects of large social groups with the resulting increased complexity of sensory tuning and motor

action? To answer some of these questions, I look at the effect of interacting sensory fields and the production of sensory modulations, termed beats and envelopes, using the weakly electric fish electrosensory system as a model.

1.3 Weakly electric fish

Two orders of weakly electric fish inhabit fresh water habitats all over South America (*Gymnotiforms*) and parts of Africa (*Mormyriforms*). Research suggests that these fish independently evolved a structure in the tail called the electric organ (EO) [26,42,48]. The EO acts as a current source [10,15], discharging electricity generated by either modified muscle cells (myogenic) or nerve cells (neurogenic) [8] into the water surrounding it. In an aquatic environment filled with obstacles, obstructions, predators and prey, the electric organ discharge (EOD) is modulated by objects with impedances that are different from the surrounding water [3,44,82]. Lower impedance objects "attract" the field lines whereas higher impedance objects "repel" them. The local potentials of this modulated field are sensed by electroreceptors distributed over the surface of the fish's body, and used in *electrolocation* [12,15,50,51,81]. The fields create a two-dimensional projection of the surrounding three-dimensional field, called the *electric image* (akin to images on a retina in the visual system) [10]. As described above, neighboring objects, including obstacles, conspecifics, predators and prey, cast "shadows" in this electric image, and thus can be sensed by the fish. Previous work

has shown that weakly electric fish can discriminate the size, shape and distance of objects in range of their electric field [1, 4, 31, 65].

Weakly electric fish can be classified broadly by the spatiotemporal properties of their electric signal. "Pulse-type" fish emit discrete, periodic pulses followed by a silent period until the next pulse [20, 29]. In contrast, "wave-type" fish emit a continuously modulating periodic signal, without any breaks in between. [17] Pulse- and wave-type electric fish experience similar but distinct challenges during social communication and gathering electrosensory information from the environment. Wave-type species have distinct EOD patterns, and species differences can be reflected in frequency, harmonic content and spatial distribution of EOD [20, 23, 45, 61].

I will be focusing on wave-type fish, whose EOD potential oscillates periodically at the EOD frequency (f_1). EOD frequencies span a wide range, from 25 to 2000 Hz [23]. The frequency of any given individual remains relatively constant over time, but is subject to change from environmental factors [16, 43, 87].

1.3.1 Emergent modulations in electrosensory signals

The weakly electric fish EOD can be modulated in a number of ways. Objects in the environment influence the amplitude of the electric field sensed by the receptors according to their impedance, creating local amplitude modulations (AMs) and phase

modulations (PMs). These local modulations carry information on the size, shape and distance of objects [1,4,31,65]. Movement of objects and other organisms relative to the fish can create spatiotemporal AMs across its skin surface, termed *movement envelopes* [84].

Weakly electric fish live in social groups in the wild, and frequently swim close enough to each other for EOD interactions to occur [74]. Interaction with a conspecific of similar frequency creates a specific combination of amplitude and phase modulations, termed a *beat*. Interaction between multiple conspecifics can create second-order effects such as 'beats of beats', which are termed 'envelopes' in the electric-fish literature. Beats are predominantly at the pairwise difference frequencies (*df*s) and envelopes are at the difference of difference frequencies (*ddf*s). The weakly electric fish electrosensory system is the source of the relevant sensory signal, and these emergent modulations are caused by additive interactions of unmodulated sensory signals from multiple individuals, and not by any environmental features.

AMs and PMs caused by objects with differing impedance, movement envelopes due to relative motion of objects and conspecifics, as well as beats and envelopes due to interfering conspecific signals all occur simultaneously in the electrosensory milieu, and it is up to the nervous system in these animals to categorize, declutter and interpret signals and use them to generate behavior. All the modulations described above have the common characteristic that they are *nonlinear*. Accordingly, a linear analysis such as the Fourier transform is unable to extract this rich set of information,

i.e. they cannot be detected in the frequency spectrum of the received signal. However, neural circuits are inherently nonlinear, and there are several proposed mechanisms like saturation and rectification that the nervous system can utilize in order to extract nonlinear modulations.

1.4 Thesis synopsis

In Chap. 2, I provide an analytical explanation of the generation of envelopes in sensory systems. I begin with an analysis of a seemingly simple case, interfering sinusoids, and show that by applying elementary nonlinear operations such as rectification, information emerges at the beat and envelope frequencies. [76]. Many of these operations are biologically relevant, and already being explored as candidate neural correlates of envelope processing. I also provide a mathematical justification of the algorithm which computes difference frequencies in the electrosensory system of these fish. This algorithm proposed by Heiligenberg et al. [34, 35] involves information collected from electroreceptors across the body surface compared and compiled into a "democratic" estimate of the frequency difference with a conspecific.

In the third chapter, I explore the behavior that is iconic of the weakly electric fish model: the Jamming Avoidance Response (JAR) in the glass knifefish *Eigenmannia virescens*. In this behavior, the EOD frequency of the fish moves away from that of an interfering conspecific. The JAR is initiated when the two frequencies are close

but not identical. This condition gives rise to low-frequency beats (Chap. 2), which have been shown to be detrimental to electrosensory processing [5, 30, 54]. JAR was discovered in *Eigenmannia* over half a century ago [47, 83], and the neural circuitry and computational algorithm underlying this behavior have been deciphered [6, 35].

In this chapter, I describe a set of experiments used to fit a "black-box" input–output model to the JAR. [53]. Closed-loop experiments, where the frequency of an artificial signal was tied to the instantaneous frequency of the fish, was used to characterize this behavior. This characterization was done at multiple operating points: at the resting frequency of the fish as well as at surrounding frequencies. This allowed a global nonlinear model to be constructed that could simulate the behavior given a particular frequency input.

In groups of two or more fish, higher-order sensory modulations, called envelopes, emerge as a result of EOD interactions (Chap. 2). Do these fish detect and respond to envelopes as well? Recent studies have shown responses at envelope frequencies at various levels of neural electrosensory processing [55, 60, 70]. However, a behavioral response to envelope stimuli was unknown. I describe in Chap. 4 work by Dr. Sarah Stamper and I resulting in discovery of the Social Envelope Response (SER) and its properties [76]. Characterizing the JAR was a necessary step to differentiate it from responses to envelopes. Stimuli that would not elicit a low-frequency beat, but do produce low-frequency envelopes were shown to elicit responses similar to the JAR. These responses could be a behavior correlate to envelope-sensitive neural circuits

discovered previously [55, 60, 70]; however, these responses can also be described by a small addition to the already existing JAR circuitry. One such mechanism is proposed in Chap. 4, although the neural mechanism underlying envelope processing is still unclear.

Chapter 2

A Mathematical Treatment of Sensory Envelopes

2.1 Representation of sensory signals

2.1.1 Time series

Animals perceive their environment using a myriad of sensory signals. These signals are measured and converted into neural code by a similarly large variety of sensory organs, which are generally highly tuned to the specific stimuli and environments. A metric of the property of the environment being measured as a function of time forms the relevant sensory signal, which can thus be expressed as a *time series*, i.e. a time-varying amplitude $s(t)$.

2.1.2 Frequency domain representation

A signal can also be represented in the *frequency domain*. The common way of effecting this is the Fourier transform:

$$S(\omega) = \int_{-\infty}^{+\infty} s(t)e^{-i\omega t}dt. \tag{2.1}$$

where at each frequency ω, $S(\omega)$ is a complex number whose magnitude and phase correspond to the amplitude and phase of a sinusoid of frequency ω. The integral (sum) of these sinusoids mathematically gives rise to the same time series $s(t)$.

Mathematically, a Fourier transform is simply a projection of the signal onto an infinite-dimensional basis vector, the elements of which are the complex sinusoids $e^{i\omega t} = \cos\omega t + i\sin\omega t$.

The time and frequency domain representations are interchangeable and contain the same information. Then why is the frequency domain representation advantageous? Instead of viewing the signal as amplitudes in time, the frequency domain adds the perspective of periodicity, i.e. it quantifies the presence and relative contribution of periodic signals which contribute to the overall signal. Several physical processes, including inertial dynamics, can be described using *linear models*. A linear system effects relative amplification and phase change on each periodic component of a signal without changing the periodicity itself. Thus, the effect of the system on each frequency is independent of other frequency components, which makes the frequency domain an efficient method to model and understand physical systems. Similarly,

frequency domain models of biological systems may also be constructed and utilized, as I have done with the JAR in Chap. 3.

2.1.3 FM representation

Even though time series and frequency-domain representations are used in the majority of signal processing applications, there are many other useful representations of signals. One relevant example is the so-called *Frequency Modulation* (FM) representation.

In FM representation, the signal is synthesized as modulations of modulations of a carrier signal. A simple case is a sinusoidal carrier whose frequency is modulated around its initial value, ω_c, by a sinusoidal modulator of frequency ω_m. This produces a combined signal of the form

$$s(t) = A\sin(\omega_c t + I\sin\omega_b t) \tag{2.2}$$

The modulated function $s(t)$ can be expanded [22] as:

$$\begin{aligned} s(t) =& A\Big\{ J_0(I)\sin\omega_c t \\ &+ J_1(I)\left[\sin(\omega_c+\omega_m)t - \sin(\omega_c-\omega_m)t\right] \\ &+ J_2(I)\left[\sin(\omega_c+2\omega_m)t + \sin(\omega_c-2\omega_m)t\right] \\ &+ J_3(I)\left[\sin(\omega_c+3\omega_m)t - \sin(\omega_c-3\omega_m)t\right] + \ldots \Big\} \end{aligned} \tag{2.3}$$

where $J_n(I)$ represents the Bessel function of the first kind and n^{th} order evaluated at the *modulation index* I, which is the ratio of the peak deviation to the modulating

frequency ω_m. Note that this equation clarifies what a frequency modulation does to the spectrum of a "pure" sinusoidal carrier — power which was concentrated at the carrier frequency ω_c is distributed into the sidebands $(\omega_c - \omega_m), (\omega_c + \omega_m), (\omega_c - 2\omega_m), (\omega_c + 2\omega_m), \ldots$, according to the Bessel functions, which decay with increasing order. The sidebands are separated from each other by the modulating frequency, ω_m.

A time series, $s(t)$ can similarly be synthesized as a (possibly infinite) series of nested modulations, in the following manner:

$$s(t) = I_c \sin(\omega_c t + I_{m1} \sin(\omega_{m1} t + I_{m2} \sin(\omega_{m3} + \ldots))) \tag{2.4}$$

and the modulating frequencies ω_c, ω_{m1}, ω_{m2}, ... and the modulating envelopes I_c, I_{m1}, I_{m2}, ... can be evaluated by performing the analytic signal analysis described in [40] "*ad infinitum* or *ad nauseum* if we so desire." The FM representation is useful as a way to synthesize complex "naturalistic" music, with a large number of harmonics, using relatively few parameters [22, 40].

Envisioning a sensory signal using the FM representation, i.e. as "modulations of modulations" turns out to be useful to understand the emergence of envelopes in these systems. In the following section, we explore this topic in the context of the electrosensory system of weakly electric fish.

2.2 Beats and envelopes in the electrosensory system

This section focuses on emergent modulations arising from multiple interacting motionless wave-type weakly electric fish. We address the following questions:

- What are beats and envelopes in the context of interacting EODs?
- How do beats and envelopes emerge from sums of sinusoids?
- What are the constraints on biological mechanisms for the extraction of beats and envelopes?

2.3 Definition of beats and envelopes

Interactions of the electric fields of two motionless fish with different EOD frequencies give rise to a beat pattern at the difference frequency (df) of the two EOD signals. The sum of two sinusoids can be mathematically decomposed into an amplitude and phase modulated signal:

$$a_1 \cos(\omega_1 t) + a_2 \cos(\omega_2 t) = M(t) \cos(\psi(t)). \tag{2.5}$$

However, the structure of $M(t)$ and $\psi(t)$ is complicated:

$$\begin{aligned} M(t) &= \sqrt{a_1^2 + a_2^2 + 2a_1 a_2 \cos((\omega_2 - \omega_1)t)}, \\ \psi(t) &= \frac{\omega_1 + \omega_2}{2}\, t + \tan^{-1}\left(\frac{a_1 - a_2}{a_1 + a_2} \tan\left(\frac{\omega_1 - \omega_2}{2} t\right)\right). \end{aligned} \tag{2.6}$$

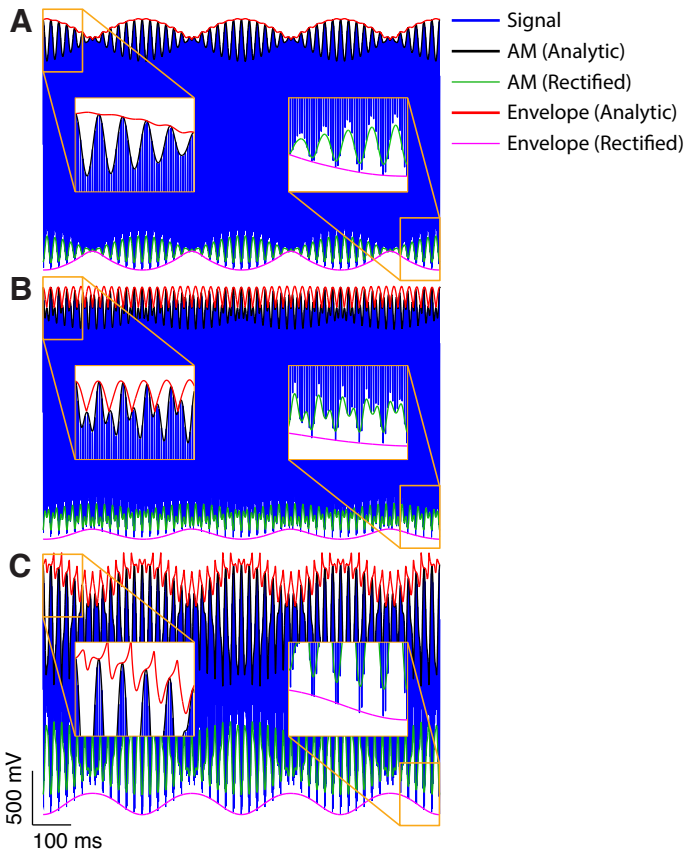

Figure 2.1: A sum of three sinusoids (blue), S_1, S_2 and S_3, with amplitudes a_1, a_2 and a_3, and frequencies f_1, f_2 and f_3, along with the AM (black) and envelope (red), as calculated from the magnitude of the analytic signal. The AM (green) and envelope (magenta) as calculated from full-wave rectification and filtering are inverted and shifted to the bottom of the combined signal. Enlarged sections of both the top and bottom profiles are shown in each of the plots. f_1 is 500 Hz in all cases. (A) For df at -52 and 48 Hz (with $a_1 : a_2 : a_3 = 10 : 1 : 1$), the signal has a meaningful envelope at the $|ddf|$ at 4 Hz. (B) This is not the case when df values are -48 and 100 Hz, and there is no spectral separation with the $|ddf|$ of 52 Hz. The analytic envelope does not follow the amplitude profile of the AMs; here the low-frequency profile is created by a secondary interaction between the $|df|$ at 48 Hz and the $|ddf|$ at 52 Hz. The rectification envelope with a low-pass cut-off set at 10 Hz captures this envelope. (C) When the amplitude of S_1 does not dominate ($a_1 : a_2 : a_3 = 5 : 5 : 2$), the analytic envelope deviates from the extrema of the AM, while the rectified signal produces an 'envelope' in the sense that it tracks some overall structure of the EOD, although the carrier signal is not well defined. It should be noted that the rectification envelope (magenta) in B and C have been amplified; thus this method has the penalty of reduced gain.

When $a_1 \gg a_2 > 0$ these signals can simplified to an intuitive expression:

$$\begin{aligned} M(t) &\simeq a_1 + \frac{a_2}{a_1}\cos\big((\omega_2 - \omega_1)t\big), \\ \psi(t) &\simeq \omega_1 t. \end{aligned} \tag{2.7}$$

This holds for electric fish because the amplitude of the self-generated EOD for a fish generally dominates the amplitudes of EODs of conspecifics.

Mathematically, the "modulator" $M(t)$ above is referred to as the envelope of the signal. However, this quantity is termed the AM by the electric fish community, because envelope coding in electric fish is observed in the afferents of P-type electroreceptors, which code EOD amplitude increases. Thus the source signal for envelope extraction is the AM of the EOD, not the underlying EOD signal itself. However, as shown in Eq. (2.6), both the amplitude and phase are modulated simultaneously. This particular combination of amplitude and phase modulations is termed the *beat* of the EOD.

The AM itself can be written in terms of amplitude and phase modulations:

$$M(t) = E(t)\cos(\gamma(t)) \tag{2.8}$$

The second-order envelope $E(t)$, i.e. the modulator of the AM, will be referred to as, simply, the *envelope*. Of course, we can further express $E(t)$ as modulations, and so on, resulting in a nested modulation representation similar to Eq. (2.4).

For three interacting, motionless EODs (modeled as sinusoids), $M(t)$ and $\psi(t)$ are more complicated. These interactions can produce a combined signal with higher

order features such as "beats of beats" (primarily at the *ddf*), which are termed *social envelopes*.

The AM $M(t)$, of a signal, $s(t)$, is the signal such that, when multiplied by a carrier signal, $\cos\psi(t)$, reproduces $s(t)$, namely $s(t) = M(t)\cos\psi(t)$. Under appropriate assumptions, $M(t)$ is a smooth curve that approximately traces the local maxima of $s(t)$, and $-M(t)$ its minima, and these local extrema approximately correspond to the peaks and troughs of $\cos\psi(t)$. Thus, for an AM to be "well defined" (in a sense formalized below), the extrema should oscillate at slower frequencies than the carrier. In the case of two sinusoids, the expression for $M(t)$ in Eq. (2.6) represents a pure AM only if it is in a lower frequency band than the carrier signal $\cos\psi(t)$, i.e. the signals are spectrally separated. In fact the Hilbert transform can be used to decompose such a signal into a product of its amplitude and carrier if those signals are spectrally separated [7,66]. $M(t)$ and $\cos\psi(t)$ resulting from mixing of two sinusoids as in Eq. (2.6) generally results in infinite harmonics; however, when $a_1 \gg a_2 > 0$ and $|\omega_2 - \omega_1| < \omega_1$, the majority of the spectral content of the $M(t)$ and $\cos\psi(t)$ are band-separated, so they form well-defined AMs [49,66]. These restrictions can also be explained in the context of a signal, initially constructed as $s(t) = \hat{M}(t)\cos\hat{\psi}_1(t)$. The AM and carrier extracted by the Hilbert transform, $M(t)$ and $\cos\psi(t)$ will generally not be equal to $\hat{M}(t)$ and $\cos\hat{\psi}(t)$ unless $\hat{M}(t)$ and $\cos\hat{\psi}_1(t)$ are themselves band separated. For three or more sinusoidal EODs, there are analogous constraints on amplitudes and frequencies of the individual EODs in order that their sum produces

a well-defined envelope of the AM (See Fig. 2.1).

Consider a group of N weakly electric fish, assumed motionless, with approximated sinusoidal EODs. The EOD of fish k, where $k \in \{1, 2, \ldots, N\}$, is perceived at an electroreceptor of fish 1 as $a_k c_k$, where a_k is the amplitude, and $\omega_k = 2\pi f_k$ is in radians, where f_k is the frequency of fish k in Hz. a_k is a function of the relative distance and orientation between fish 1 and fish k for $k \neq 1$, and a_1 would depend on body bending of fish 1. The total signal at the electroreceptor is:

$$s(t) = \sum_{k=1}^{N} a_k \cos(\omega_k t + \phi_k) = \sum_{k=1}^{N} a_k c_k(t), \tag{2.9}$$

where $\cos(\omega_k t + \phi_k) = \cos(\theta_k) = c_k$. Since $s(t)$ is assumed to be the signal at a receptor of fish 1, the amplitude of fish 1 will generally be greatest, i.e. $a_1 \gg a_k$, $k = 2, 3, \ldots N$.

We have stated that amplitudes and envelopes contain the dfs and ddfs, but it is clear from Eq. (2.9) that the signal at the electroreceptor has only components at ω_k. Thus, a nonlinear method is required to extract AMs and envelopes.

2.4 Methods for envelope extraction

2.4.1 Magnitude of the analytic signal

A common definition of AMs is as the magnitude of the *analytic signal*. For a given real input signal $s(t)$, its *complex analytic signal* is defined as $\mathcal{A}(t) = s(t) + i\hat{s}(t)$,

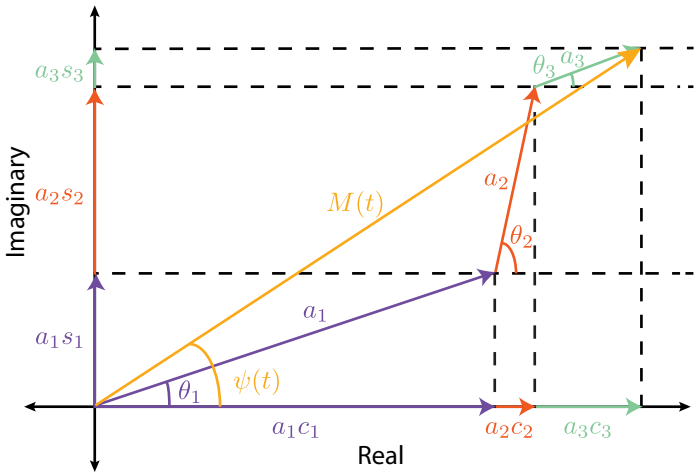

Figure 2.2: Analytic representation of sum of cosines signal at time t. Each of the three short vectors represents an analytic signal; the original signals are shown on the 'Real' axis, and their Hilbert transforms on the 'Imaginary' axis. Over time, each vector rotates, tracing a circular path at its angular velocity ω_k. However, because they rotate around the tip of the previous vector, the combined signal (orange vector) traces out a complex Lissajous figure. This combined signal can be parameterized by the magnitude, $M(t)$, and phase, $\psi(t)$, of the analytic signal.

where $\hat{s}$ is obtained by the Hilbert transform:

$$\hat{s}(t) = \mathcal{H}(s)(t) = \frac{1}{\pi} P \int_{-\infty}^{\infty} \frac{s(\tau)}{t-\tau} d\tau = s(t) * \frac{1}{\pi t}, \tag{2.10}$$

where P denotes Cauchy principal value, and $*$ denotes the convolution operator.

There are two key properties of the Hilbert transform used extensively below. First, the Hilbert transform is linear:

$$\mathcal{H}(au(t) + bv(t)) = a\mathcal{H}(u(t)) + b\mathcal{H}(v(t)).$$

Second, the Hilbert transform of sinusoids is given by:

$$\mathcal{H}(\cos(\omega t)) = \sin(\omega t),$$

$$\mathcal{H}(\sin(\omega t)) = -\cos(\omega t).$$

We can express the analytic signal in polar form as $\mathcal{A}(t) = M(t)e^{i\psi(t)}$. The AM is $M(t) = |\mathcal{A}(t)|$ and the phase function is $\psi(t) = \angle\mathcal{A}(t)$. The nonlinearity in this form of AM extraction arises not from the Hilbert transform or analytic signal construction—which are both linear—but rather from the magnitude operation.

To apply this to the sum of sinusoids signal, let $\mathcal{A}_k$ be the complex analytic signal corresponding to $a_k c_k$, namely $\mathcal{A}_k = a_k c_k + i a_k s_k = a_k e^{i\theta_k}$. Then

$$\mathcal{A} = \sum_{k=1}^{N} \mathcal{A}_k = \sum_{k=1}^{N} a_k e^{i\theta_k} = M(t)e^{i\psi(t)} \tag{2.11}$$

is the analytic signal of $s(t)$ in Eq. (2.9). Graphical representation of this decomposition is shown in Fig. 2.2, for the three sinusoid case. The real part of the analytic

signal is the real signal $s(t) = M(t)\cos\psi(t)$. The magnitude is calculated via

$$\begin{aligned} M^2(t) &= \left|\sum_{k=1}^{N} a_k e^{i\theta_k}\right|^2 = \left(\sum_{k=1}^{N} a_k e^{i\theta_k}\right)\left(\sum_{k=1}^{N} a_k e^{-i\theta_k}\right) \\ &= \sum_{k=1}^{N} a_k^2 + \sum_{k=1}^{N-1}\sum_{j=k+1}^{N} a_k a_j \left(e^{i(\theta_k-\theta_j)} + e^{-i(\theta_k-\theta_j)}\right) \\ &= \sum_{k=1}^{N} a_k^2 + 2\sum_{k\neq j} a_k a_j c_{k-j}(t) \\ &= \alpha^2 + 2\sum_{k\neq j} a_k a_j (c_{k-j} - 1), \end{aligned} \tag{2.12}$$

where $\sum_{k=1}^{n} a_k = \alpha$, and the summation notation $k \neq j$ refers to the $\binom{N}{2} = \frac{N(N-1)}{2}$ combinations of $k, j \in \{1, \ldots, N\}$, $k \neq j$.

$$M(t) = \alpha\sqrt{1 + \frac{2}{\alpha^2}\sum_{k\neq j} a_k a_j (c_{k-j} - 1)} \tag{2.13}$$

The Taylor series expansion can be approximated, to first order, as

$$\sqrt{1+x} = 1 + \frac{1}{2}x - \frac{1}{8}x^2 + \frac{1}{16}x^3 + \ldots \simeq 1 + \frac{x}{2}, \tag{2.14}$$

when $|x|$ is small. To apply this first order approximation to Eq. (2.13), note that

$$x = \frac{2}{\alpha^2}\sum_{k\neq j} a_k a_j (c_{k-j} - 1)\ ,\ 0 \leq |x| \leq \frac{4}{\alpha^2}\sum_{k\neq j} a_k a_j.$$

When a_1 dominates, the upper bound is approximately $\frac{4(a_2+\ldots+a_N)}{a_1}$, which for sufficiently large a_1 is small, and the approximation in Eq. (2.14) is justified. Thus,

$$\begin{aligned} M(t) &\simeq \alpha + \frac{1}{\alpha}\sum_{k\neq j} a_k a_j (c_{k-j} - 1) \\ &= \underbrace{\alpha - \frac{1}{\alpha}\sum_{k\neq j} a_k a_j}_{\text{DC}} + \underbrace{\frac{1}{\alpha}\sum_{k\neq j} a_k a_j c_{k-j}}_{df\text{s}}. \end{aligned} \tag{2.15}$$

Subtracting DC, we obtain a "Hilbert approximation," M_H, of the AM:

$$\begin{aligned} M_H(t) &= \frac{1}{\alpha}\sum_{k\neq j} a_k a_j c_{k-j} \\ &= \sum_{k\neq j} b_{kj}\cos((\omega_k-\omega_j)t+(\phi_k-\phi_j)) \end{aligned} \tag{2.16}$$

where $b_{kj}=\frac{a_k a_j}{\alpha}$. The AM is approximately a sum of $\binom{N}{2}$ cosines at the dfs $|\omega_k-\omega_j|$.

The envelope of this AM is obtained as the magnitude of the analytic signal of the expression in Eq. (2.16). Repeating steps in Eqs. (2.12–2.16),

$$\begin{aligned} E_H(t) &= \sum e_{kjpq} c_{|k-j|-|p-q|} \\ &= \sum e_{kjpq}\cos((|\omega_k-\omega_j|-|\omega_p-\omega_q|)t+(|\phi_k-\phi_j|-|\phi_p-\phi_q|)), \end{aligned} \tag{2.17}$$

where the summation is over the set of all $\binom{\binom{N}{2}}{2} = \frac{N(N^2-1)(N-2)}{8}$ combinations of $\{\{k,j\},\{p,q\}\}$ such that $k,j,p,q\in\{1,\ldots,N\}$, $k\neq j$, $p\neq q$ and $\{k,j\}\neq\{p,q\}$, and

$$e_{kjpq}=\frac{b_{kj}b_{pq}}{\beta}=\frac{a_k a_j a_p a_q}{\alpha^2\beta}\ ,\ \beta=\sum_{k\neq j} b_{kj}.$$

The envelope can be approximated as the sum of sinusoids at ddfs of the frequencies contained in the original sum of sinusoids. In the context of this chapter (mixing of three EODs), from 2.17,

$$E_{H3}(t)\simeq \frac{\begin{array}{r} a_1^2 a_2 a_3\cos(|\Delta\theta_{21}|-|\Delta\theta_{31}|)+a_1 a_2^2 a_3\cos(|\Delta\theta_{21}|-|\Delta\theta_{32}|) \\ +\,a_1 a_2 a_3^2\cos(|\Delta\theta_{32}|-|\Delta\theta_{31}|)\end{array}}{a_1a_2+a_2a_3+a_3a_1},$$

where $\Delta\theta_{21}=(\omega_2-\omega_1)t+(\phi_2-\phi_1)=2\pi(df_2)t+(\phi_2-\phi_1)$. Similarly, $\Delta\theta_{31}=2\pi(df_3)t+(\phi_3-\phi_1)$, and $\Delta\theta_{32}=2\pi(df_1)t+(\phi_3-\phi_2)$. If we assume $a_1\gg a_2$ and $a_1\gg a_3$, we can further approximate this as

$$E_{H3}(t)\simeq\frac{a_1a_2a_3}{a_2+a_3}\cos(2\pi(ddf)t+\Phi), \tag{2.18}$$

where $ddf = |df_3| - |df_2|$, and $\Phi = (|\phi_3 - \phi_1| - |\phi_2 - \phi_1|)$ Thus the envelope is primarily composed of the ddf, namely the difference of difference frequencies between fish 1 and other conspecifics.

2.4.1.1 Caveats of the analytic signal method

Real-time envelope extraction using the analytic signal is not biologically plausible, since the Hilbert transform is a noncausal operator. The analytic envelope of a narrow-band Gaussian white noise, as discussed in [60], is generally well-defined. However, this breaks down as the number of sinusoidal components are reduced (unless one of the amplitudes is dominant), as shown in the case of three EODs in Fig. 2.1C. The approximation in Eq. (2.18) is not applicable for a wide range of parameters, e.g. any conspecific amplitude is non-negligible relative to a_1, or insufficient band separation between Fs, dfs and ddf. These limitations do not apply to our experimental setup because (1) the combined signal perceived by the fish is dominated by its own EOD and (2) the ddf and dfs used were sufficiently separated.

2.4.2 Envelope extraction via rectification and low-pass filtering

A commonly used method of envelope extraction is rectification of the signal followed by filtering. A similar mechanism may be used in electric fish via rectification

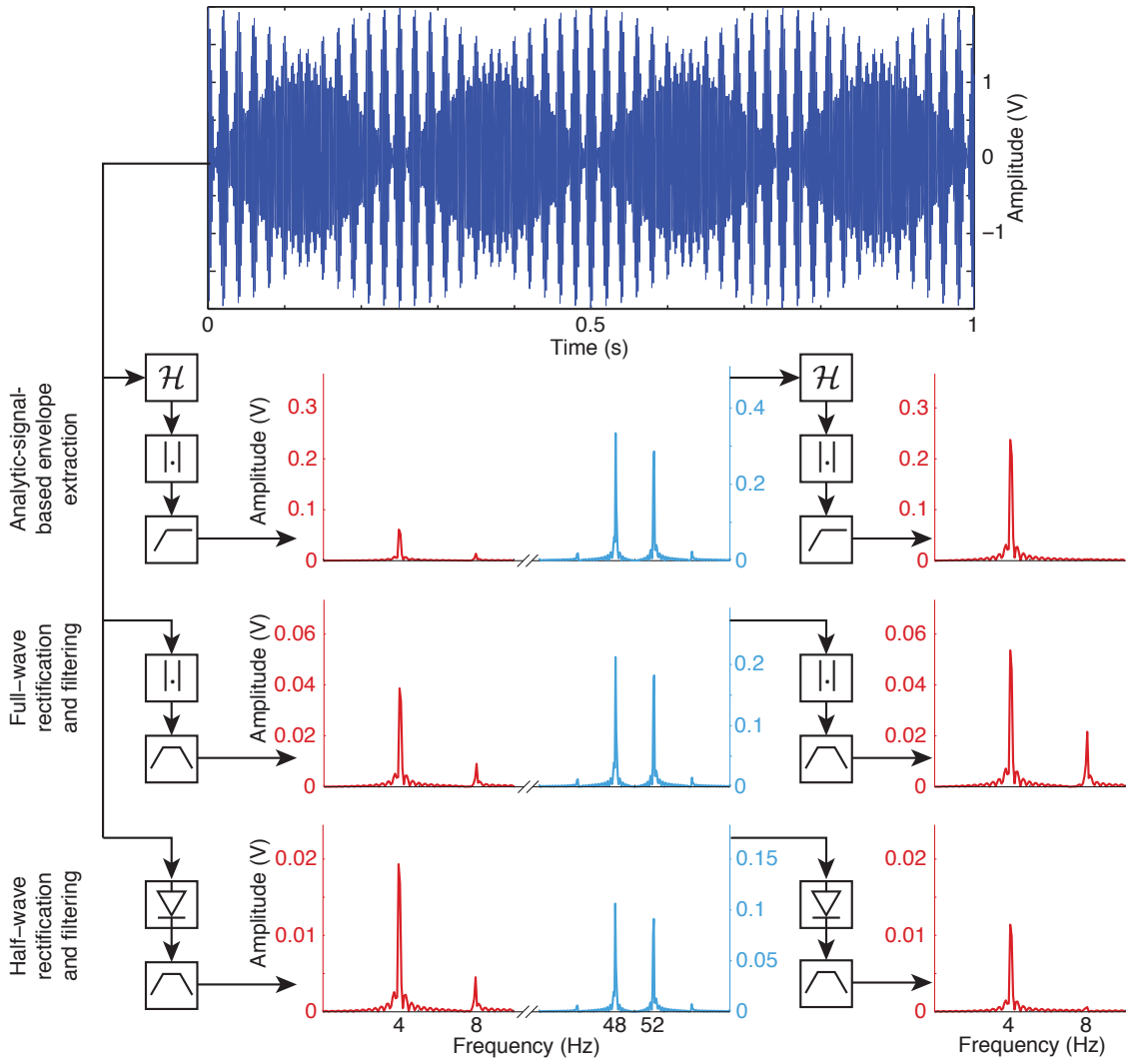

Figure 2.3: Envelope extraction methods comparison. The input (top) is the sum of three sinusoids, S_1, S_2 and S_3, at $f_1 = 500$, $f_2 = 452$ and $f_3 = 552$ Hz. S_2 and S_3 had amplitudes $a_2 = a_3 = 0.5$, while S_1 had amplitude $a_1 = 1$. The first plot in each row is the spectrum of the output of a particular method of envelope extraction, and the second column is the output when the method is used twice in succession. The methods are mnemonically depicted by a sequence of filters, $\mathcal{H}$ depicts extraction via the analytic signal, $||$ depicts full-wave rectification and the diode depicts half-wave rectification. High-pass and band-pass filters are depicted by frequency response gain functions. It can be seen that all resulting signals from one application of each method have maximum amplitude at the $|df|$ frequencies (48 and 52 Hz), with an additional component at the ddf (5 Hz). Applying the method twice extracts out the $|ddf|$ component alone. When used twice, each method extracts out the ddf component alone, but with varying amplitudes.

by having the firing threshold of a neuron close to the mean of the input, and then filtering through a slow synapse [52, 59].

2.4.2.1 Full-wave rectification

Full-wave rectification of a zero-mean signal produces the absolute value of the signal. For the sum of sines from Eq. (2.9),

$$\begin{aligned} |s| &= \left|\sum_{k=1}^{N} a_k c_k\right| = \sqrt{\left(\sum_{k=1}^{N} a_k c_k\right)^2} \\ &= \sqrt{\sum_{k=1}^{N} a_k^2 \left(\frac{1+c_{2k}}{2}\right) + 2\sum_{k\neq j} a_k a_j \left(\frac{c_{k+j}+c_{k-j}}{2}\right)} \\ |s| &= \sqrt{\frac{\alpha^2}{2}\left(1 + \frac{1}{\alpha^2}\sum_{k=1}^{N} a_k^2 c_{2k} + \frac{2}{\alpha^2}\sum_{k\neq j} a_k a_j (c_{k+j}+c_{k-j}-1)\right)}. \end{aligned} \tag{2.19}$$

By using the first order Taylor approximation from Eq. (2.14),

$$|s| \simeq \underbrace{\frac{\alpha}{\sqrt{2}} - \frac{1}{\sqrt{2}\alpha}\sum_{k\neq j} a_k a_j}_{\text{DC}} + \underbrace{\frac{1}{\sqrt{2}\alpha}\sum_{k\neq j} a_k a_j c_{k-j}}_{df\text{s}} + \underbrace{\frac{1}{\sqrt{2}\alpha}\sum_{k\neq j} a_k a_j c_{k+j} + \frac{1}{2\sqrt{2}\alpha}\sum_{k=1}^{N} a_k^2 c_{2k}}_{\text{Sum frequencies}} \tag{2.20}$$

If the band of difference frequencies $|\omega_k - \omega_j|$ is spectrally separate from the sum frequencies $|\omega_k + \omega_j|$, an appropriate filter can extract the dfs only, which form the AM. Let $L_F(.)$ be such a filter, which high-passes DC and low-passes sum frequencies, and define

$$I_F(t) = L_F(|s|) \simeq \frac{1}{\sqrt{2}}\sum_{k\neq j} b_{kj} c_{k-j} = \frac{I_H}{\sqrt{2}} \tag{2.21}$$

One more rectification and low-pass filtering step provides us with the envelope, at the *ddf*:

$$E_F(t) = \frac{1}{2}\sum e_{kjpq} c_{|k-j|-|p-q|} = \frac{E_H}{2} \tag{2.22}$$

Envelopes extracted by both methods thus have similar spectral content, and the difference frequency components are separated only by scale.

2.4.2.2 Half-wave rectification

Envelopes can also be extracted by half-wave rectification. For a signal $s(t)$, let $h(s)$ denote the positive half-wave operator, as follows:

$$h(s) = \begin{cases} s & : s > 0 \\ 0 & : s \leq 0 \end{cases} \tag{2.23}$$

$h(-s)$ is thus the negative half wave, inverted to be positive. The signal itself can be written as the difference of these two "half-waves":

$$s = h(s) - h(-s) \tag{2.24}$$

Similarly, the full-wave rectification is the sum of the two half-waves:

$$|s| = h(s) + h(-s) \tag{2.25}$$

Using Eq. (2.24) and Eq. (2.25), the half-wave rectified signal is simply the average of the full-wave rectification and the signal itself (in the zero-mean case):

$$h(s) = \frac{s + |s|}{2} \tag{2.26}$$

Thus the half-wave rectified signal contains the frequencies from the full-wave rectification (DC, *df*s and sums) and the signal frequencies themselves. Using Eq. (2.20),

$$\begin{aligned} |s| \simeq & \underbrace{\frac{\alpha}{2\sqrt{2}} - \frac{1}{2\sqrt{2}\alpha}\sum_{k\neq j} a_k a_j}_{\text{DC}} + \underbrace{\frac{1}{2\sqrt{2}\alpha}\sum_{k\neq j} a_k a_j c_{k-j}}_{df\text{s}} + \underbrace{\frac{1}{2}\sum_{k=1}^{N} a_k c_k}_{f\text{s}} \\ & + \underbrace{\frac{1}{2\sqrt{2}\alpha}\sum_{k\neq j} a_k a_j c_{k+j} + \frac{1}{2\sqrt{2}\alpha}\sum_{k=1}^{N} a_k^2 c_{2k}}_{\text{Sum frequencies}} \end{aligned} \tag{2.27}$$

Comparing Eq. (2.27) with Eq. (2.20), it is possible to extract *df*s if the band of difference frequencies $|\omega_k - \omega_j|$ is spectrally separate from both the band of sum frequencies $|\omega_k + \omega_j|$ and the band of signal frequencies ω_k. The filter $L_H(.)$ which extracts *df*s will have to, in this case, high-pass DC and low-pass signal as well as sum frequencies. Applying this filter,

$$I_H(t) = L_H(h(s)) \simeq \frac{1}{2\sqrt{2}}\sum_{k\neq j} b_{kj} c_{k-j} = \frac{I_F}{2} = \frac{I_H}{2\sqrt{2}} \tag{2.28}$$

After one more rectification and low-pass filtering step, the envelope emerges:

$$E_H(t) = \frac{1}{4}\sum e_{kjpq} c_{|k-j|-|p-q|} = \frac{E_F}{2} = \frac{E_H}{4} \tag{2.29}$$

Comparing this to Eq. (2.22), we can see that half-wave rectification, in the ideal case, only results in half the envelope power of full-wave rectification. In addition, $L_H(.)$ needs to have cut-off frequencies between the signal frequencies and *df*s. These stricter restrictions as compared to $L_F(.)$ could, in practice, cause more signal loss. This further degrades the power at the envelope, as can be seen in Fig. 2.3.

2.5 The amplitude-phase Lissajous

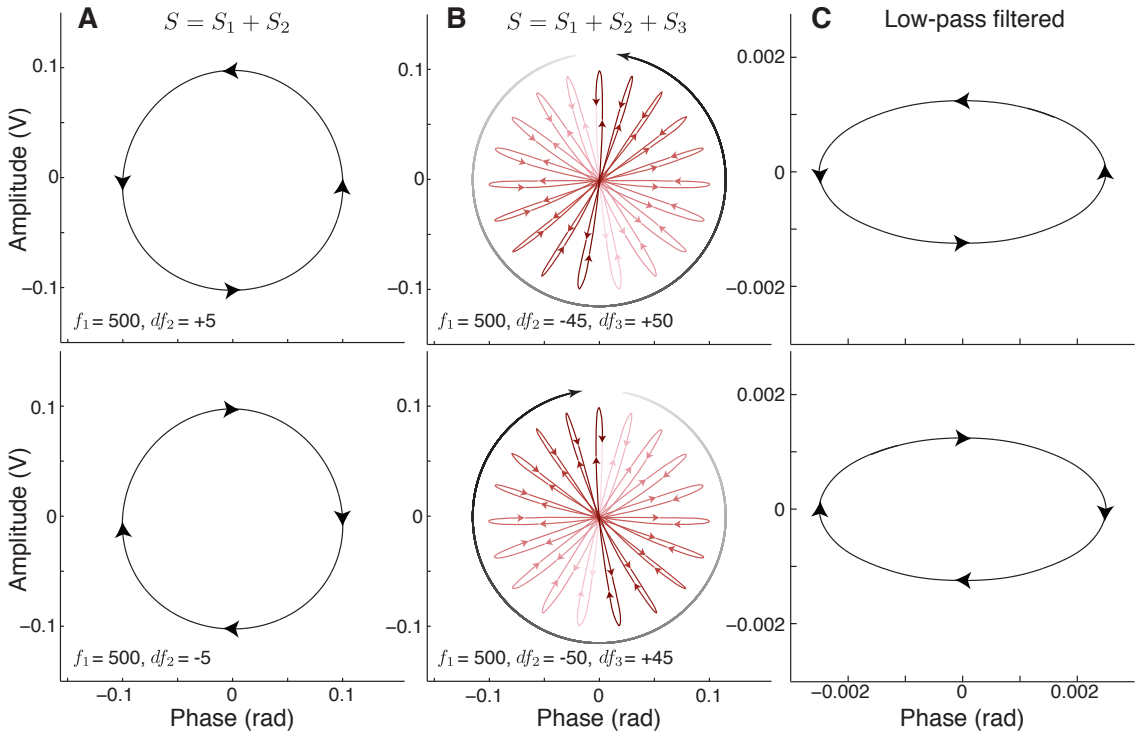

Figure 2.4: Amplitude-phase Lissajous of two or three sinusoidal signals. (A) The parametric curve of analytic signal amplitude vs relative phase for the sum of two signals S_1 and S_2 produces a circular graph that rotates counter-clockwise for positive *df* (top) and clockwise for negative *df* (bottom), at frequency $|df|$. (B) The sum of three signals S_1, S_2 and S_3 results in a more complex Lissajous figure, for positive *ddf* (top) and negative *ddf* (bottom). The Lissajous has a local rotation (arrows on petals) and also a general precession (external arrow and increasing color gradient on petals) (C) The amplitude and phase from B were low-pass filtered (Butterworth, sixth-order, 20 Hz normalized cut-off). This shows that there is a low-frequency precession of the graph in the counter-clockwise direction for positive *ddf* (top) and clockwise for negative *ddf* (bottom). The precession is at frequency $|ddf|$.

In weakly electric fish, extensive research has abstracted the computation of difference frequencies as a comparison between the absolute signal amplitude and signal phase. [33]. This so-called "amplitude-phase Lissajous" figure is illustrated for the

case of two and three interacting sinusoids in Fig. 2.4. Here, we explain why this Lissajous figure is able to extract the *df*s, and why the low-pass filtered version of the Lissajous has a global precession at the *ddf*. Consider the summed signal Eq. (2.9). The phase function $\psi(t)$ is

$$\psi(t) = \tan^{-1} \frac{\sum a_k s_k}{\sum a_k c_k}. \tag{2.30}$$

Using $\tan^{-1} z = \frac{i}{2} \ln \frac{1 - iz}{1 + iz}$,

$$\begin{aligned} \psi(t) &= \frac{i}{2} \ln \frac{\sum a_k e^{-i\theta_k}}{\sum a_k e^{i\theta_k}} = \theta_1 + \frac{i}{2} \ln \frac{\sum a_k e^{-i(\theta_k - \theta_1)}}{\sum a_k e^{i(\theta_k - \theta_1)}} \\ &= \theta_1 + \tan^{-1} \frac{\sum a_k s_{k-1}}{\sum a_k c_{k-1}} \end{aligned}$$

The analytic phase relative to that of fish 1 is

$$P_L(t) = \psi(t) - \theta_1(t) = \tan^{-1} \frac{\sum a_k s_{k-1}}{\sum a_k c_{k-1}}. \tag{2.31}$$

This is the phase of the sum of the *df*s, $\sum_{k=1}^{N} a_k c_{k-1}$. The analytic signal magnitude (2.16), when a_1 dominates, can be further simplified to

$$M_L(t) = \sum_{k=1}^{N} b_{k1} c_{k-1}. \tag{2.32}$$

The Lissajous (M_L vs P_L) consists primarily of *df* components, which is why the graph in Fig. 2.4A rotates in the direction of the *df* in the case of two fish. However, M_L is a first order Taylor approximation. If, instead, we approximate to the second order, we obtain

$$M_L(t) \simeq \alpha + \frac{1}{\alpha} \sum_{k \neq j} a_k a_j (c_{k-j} - 1) - \frac{1}{2\alpha^3} \left(\sum_{k \neq j} a_k a_j (c_{k-j} - 1) \right)^2. \tag{2.33}$$

The square term, when expanded, will contain product terms $c_{k-j}c_{p-q}$, which can be written as their corresponding sums

$$c_{k-j}c_{p-q} = \frac{1}{2}(c_{|k-j|+|p-q|} + c_{|k-j|-|p-q|}).$$

This shows that the amplitude of the analytic signal contains *ddf* terms $\frac{a_k a_j a_p a_q}{2\alpha^3} c_{|k-j|-|p-q|}$. (Fig. 2.3, top). Hence a low-pass filtered version of the Lissajous also serves as a means to extract out components at *ddf*, albeit with reduced magnitudes. This is illustrated by the graph in Fig. 2.4C rotating in the direction of the *ddf*. Fig. 2.3 (middle, bottom) shows that a *ddf* component is also present in the full-wave and half-wave rectified signals. Interestingly, when we apply each extraction method twice in succession, it affects the *ddf* component differently. It turns out that the half-wave rectified signal contains a stronger component at the *ddf* than the half-wave rectified AM.

2.6 Distributed computation of *df*

The amplitude-phase Lissajous described in the previous section is the abstraction of the computation in the Electrosensory Lateral Line (ELL) and midbrain of these fish, which ultimately reveals the *df* [6, 32, 34], without explicit "knowledge" of the self-generated pacemaker frequency [16]. In this section, I describe how a similar computation can be accomplished in a distributed manner, using pairwise comparisons of amplitude and phase information from different areas of the body. Such a distributed

computation does not need a central representation of signal amplitude and phase, and thus is likely a more biologically relevant method. This is indeed what the neural circuitry seems to accomplish [6, 35].

Consider two small areas on the body surface of fish 1, denoted by p and q. There is a single conspecific, fish 2, in the neighborhood, as in the case of JAR, providing a *df*. The signals at the two areas, s_p and s_q are:

$$\begin{aligned} s_p(t) &= a_1 c_1 + a_{2p} c_2(t) \\ s_q(t) &= a_1 c_1 + a_{2q} c_2(t) \end{aligned} \tag{2.34}$$

These expressions assume that the fish's own signal is perceived at a constant amplitude a_1 across the body surface. *Eigenmannia* has such a spatially uniform EOD [1]. Two types of tuberous receptors on the body surface sense high-frequency EOD disturbances. P-units increase their probability of firing upon increasing amplitude of the signal. [71, 72]. Applying Eq. (2.16) to the special case of two signals, the DC-subtracted amplitudes at the two areas are:

$$\begin{aligned} M_p(t) &\simeq \frac{a_1 a_{2p}}{a_1 + a_{2p}} c_{2-1} \\ M_q(t) &\simeq \frac{a_1 a_{2q}}{a_1 + a_{2q}} c_{2-1} \end{aligned} \tag{2.35}$$

T-units are receptors which fire in a phase-locked manner to the EOD, and thus provide an encoding of phase [14, 72]. Similarly, from Eq. (2.30), the phases at the two receptors are:

$$\begin{aligned} \psi_p &= \theta_1 + \tan^{-1} \frac{a_1 s_{1-1} + a_{2p} s_{2-1}}{a_1 c_{1-1} + a_{2p} c_{2-1}} = \theta_1 + \tan^{-1} \frac{a_{2p} s_{2-1}}{a_1 + a_{2p} c_{2-1}} \\ \psi_q &= \theta_1 + \tan^{-1} \frac{a_1 s_{1-1} + a_{2q} s_{2-1}}{a_1 c_{1-1} + a_{2q} c_{2-1}} = \theta_1 + \tan^{-1} \frac{a_{2q} s_{2-1}}{a_1 + a_{2q} c_{2-1}} \end{aligned} \tag{2.36}$$

Again, we make use of the assumption that the fish's own amplitude dominates those perceived from a conspecific, i.e. $a_1 \gg a_{2p}, a_1 \gg a_{2q}$. Under these assumptions, from Eq. (2.35),

$$M_p(t) \simeq a_{2p} c_{2-1}(t),\ M_q(t) \simeq a_{2q} c_{2-1}(t) \tag{2.37}$$

Also adding the small angle assumption of $\tan^{-1} z \simeq z$ for small z:

$$\psi_p(t) \simeq \theta_1 + \frac{a_{2p}}{a_1} s_{2-1}(t),\ \psi_q(t) \simeq \theta_1 + \frac{a_{2q}}{a_1} s_{2-1}(t) \tag{2.38}$$

The amplitude-phase Lissajous for area p, for e.g., is constructed by placing the amplitude M_p on the y-axis, and the pairwise differences between the ψ_p and phases at other areas on the body surface on the x-axis. For simplicity, we can again consider just the areas p and q, which would make the x-axis $\psi_p - \psi_q$. In case of a two-dimensional $X - Y$ curve such as the Lissajous, Greene's theorem gives us the infinitesimal area swept by the curve as a line integral [41]:

$$dA = \frac{1}{2}(x dy - y dx) \tag{2.39}$$

The sum of the differential areas thus obtained at areas p and q are:

$$\begin{aligned} 2dA_{p,q} &= (\psi_p - \psi_q) dM_p - M_p d(\psi_p - \psi_q) + (\psi_q - \psi_p) dM_q - M_q d(\psi_q - \psi_p) \\ &= (\psi_p - \psi_q) d(M_p - M_q) - (M_p - M_q) d(\psi_p - \psi_q) \end{aligned} \tag{2.40}$$

The rate of change of area is:

$$\begin{aligned} 2\frac{dA_{p,q}}{dt} &= (\psi_p - \psi_q)\frac{d}{dt}(M_p - M_q) - (M_p - M_q)\frac{d}{dt}(\psi_p - \psi_q) \\ &= \frac{a_{2p} - a_{2q}}{a_1} s_{2-1}(a_{2p} - a_{2q})\frac{d}{dt}c_{2-1} - (a_{2p} - a_{2q})c_{2-1}\frac{a_{2p} - a_{2q}}{a_1}\frac{d}{dt}s_{2-1} \\ &= -\frac{(a_{2p} - a_{2q})^2}{a_1}(c_{2-1}^2 + s_{2-1}^2)(\omega_2 - \omega_1) \\ \frac{dA_{p,q}}{dt} &= -\frac{(a_{2p} - a_{2q})^2}{2a_1} df \end{aligned} \tag{2.41}$$

The above expression clearly shows that the sign of area, i.e. direction of rotation of the Lissajous clearly depends on the sign of df, and the rate of change of area is proportional to $|df|$ – thus the curve rotates faster with increase in $|df|$ – in fact, it is periodic at frequency $|df|$. Moreover, since the Lissajous can be created with any pair of areas p and q, each pairwise interaction does provide a "vote" towards the democratic computation of the df [32, 34]. The electrosensory behaviors are indeed, as Heiligenberg [33] puts it, a result of "a pandemonium of local computations and competing instructions".

Chapter 3

Modeling the Jamming Avoidance Response

The Jamming Avoidance Response, or JAR, in the weakly electric fish has been analyzed at all levels of organization, from whole-organism behavior down to specific ion channels. Nevertheless, a parsimonious description of the JAR behavior in terms of a dynamical system model has not been achieved at least in part due to the fact that "avoidance" behaviors are both intrinsically unstable and nonlinear. The experimental setup described in [53] overcame the instability of the JAR in *Eigenmannia virescens* by closing a feedback loop around the behavioral response of the animal. Specifically, the instantaneous frequency of a jamming stimulus was tied to the fish's own electrogenic frequency by a feedback law. Without feedback, the fish's own frequency diverges from the stimulus frequency, but appropriate feedback sta-

bilizes the behavior. After stabilizing the system, we measured the responses in the fish's instantaneous frequency to various stimuli. A delayed first-order linear system model fit the behavior near the equilibrium. Coherence to white noise stimuli together with quantitative agreement across stimulus types supported this local linear model. Next, we examined the intrinsic nonlinearity of the behavior using clamped-frequency-difference experiments to extend the model beyond the neighborhood of the equilibrium. The resulting nonlinear model is composed of competing motor return and sensory escape terms. The model reproduces responses to step and ramp changes in the difference frequency (df) and predicts a "snap-through" bifurcation as a function of df that we confirmed experimentally.

3.1 Introduction

Weakly electric fish emit an electric organ discharge (EOD) that is used for electrolocation [18, 80] and communication [27, 38, 39, 79]. In wave-type electric fish, the EOD is quasi-sinusoidal and has a relatively stable baseline frequency when undisturbed [11, 13, 62, 85, 86]. When two or more fish are in close proximity (< 1 m), their EODs interact to produce emergent beats with amplitude and phase modulations at the difference frequency (df) between the fish (Eqs. (2.31),(2.32)). *Eigenmannia virescens* (Fig. 3.1) shift their baseline EOD frequency in response to low-frequency ($<$ 15 Hz) dfs [16, 83], which have been shown to impair aspects of electrolocation [5, 30].

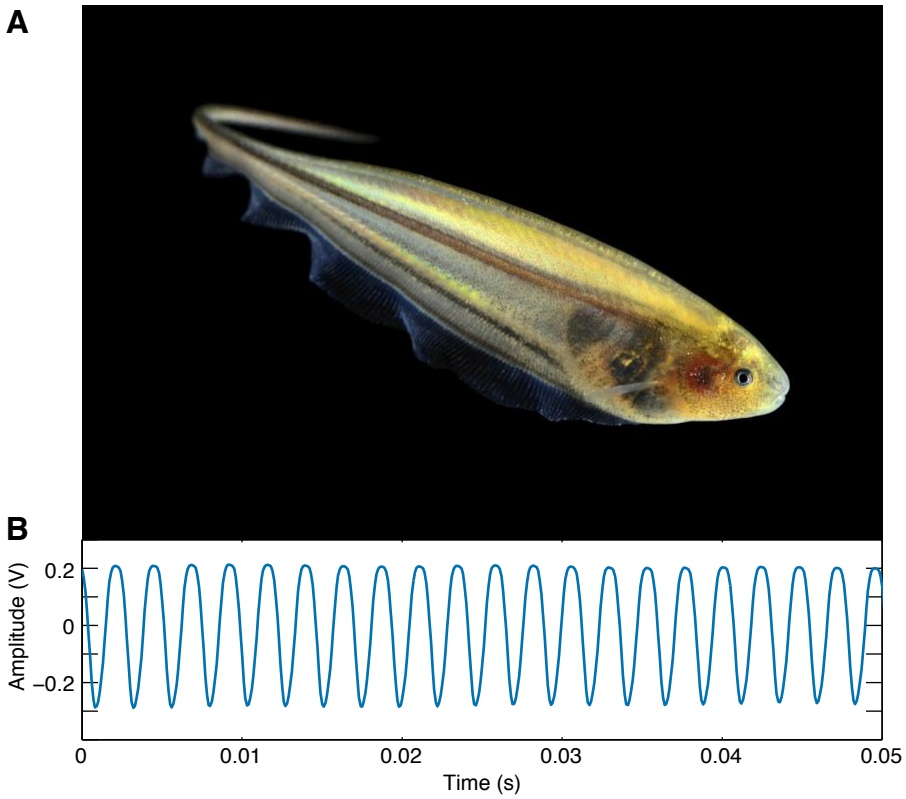

Figure 3.1: (A) *Eigenmannia virescens*, the "glass knifefish". Photo credit: Will Kirk. (B) The pseudo-sinusoidal EOD of *Eigenmannia*. This amplified EOD signal was recorded from a fish with a baseline frequency of approximately 421 Hz.

The direction of the frequency shift is determined by the sign of the df and results in an increase in the magnitude of the df. This behavior is known as the Jamming Avoidance Response (JAR).

The JAR has been analyzed at all levels of organization, from whole-organism behavior down to specific ion channels [6, 28, 33, 35]. Despite the fact that the JAR is among the best understood sensorimotor circuits, the sensorimotor responses have not been modeled as a dynamical system. One challenge to modeling the temporal dynamics arises from the intrinsically 'unstable' nature of the JAR. This is because the fish shifts its EOD frequency (f_1) in the direction away from the frequency of the conspecific (f_2), resulting in an increase of $|df|$, where $df = f_2 - f_1$. We overcame this challenge by closing a feedback loop around the natural behavior: the frequency of a conspecific-like signal was calculated and adjusted in real-time to stabilize the response and drive it to any desired frequency in a neighborhood of the fish's original baseline frequency.

Perturbation experiments on the stabilized closed-loop system were used to characterize the dynamics of the JAR. These perturbations included sinusoids, sums of sinusoids, chirps, and band-limited noise. Responses to these stimuli were used to estimate a non-parametric frequency response function (FRF). The FRF was then used to infer the frequency response of the open-loop behavior, i.e. the JAR itself. A first-order delayed parametric model was fit to the behavior near its equilibrium.

This local model does not, however, capture the nonlinear features of the behavior:

the biological relevance of the JAR lies in its escape from the unstable equilibrium. To address this, we extended the linear model using additional experiments in which the dfs were "clamped" to furnish a complete nonlinear model. The nonlinear model was parsed into terms that capture competing avoidance and return responses and was validated by comparison with responses to open-loop stimuli. The model was also used to predict a saddle–node bifurcation in the vector field of the system, which was exhibited in the behavior as a 'snap-through' of the fish's frequency (f_1) from one stable equilibrium to another.

3.2 Methods

3.2.1 Experimental setup

Adult *Eigenmannia virescens* ($10-15$ cm in length) were obtained from commercial vendors. The fish were housed in group aquarium tanks that had a water temperature of approximately 27°C and a conductivity in the range of $150-500$ μS/cm [36]. All experimental procedures were approved by the Johns Hopkins Animal Care and Use Committee and followed guidelines established by the National Research Council and the Society for Neuroscience.

The experimental tank was maintained at a temperature of 25 ± 3°C and conductivity of 150 ± 25 μS / cm. Each fish ($N=7$; $n=5$ reference-tracking trials, $n=2$ clamp trials) was tested individually. Each fish was acclimated to the testing tank for

a minimum of 24 hours prior to the start of the experiment. After the initial acclimation period the fish was restricted in a chirp chamber for $2-3$ hours to allow the EOD frequency to stabilize. The chirp chamber served to restrict the movement of the fish and prevent changes in orientation during the experiment, resulting in more consistent measurements of the EOD frequency. A pair of measurement electrodes (red) were placed longitudinally (near the fish's head and tail) to record the EOD and a second pair of stimulus electrodes (black) were placed transverse to the fish to provide a frequency-controlled sinusoidal stimulus (Fig. 3.2A). The distance between each pair of electrodes was 25 cm.

The EOD of the fish, recorded via the head-to-tail electrodes (Fig. 3.2A ; red circles), was filtered and amplified (0.1 Hz - 1 kHz bandpass, gain 100 ; A-M Systems Model 1700, Sequim, WA, U.S.A.) and input to a frequency-to-voltage converter (F2V; FV-1400, Ono-Sokki, Yokohama, Japan). The F2V calculates the frequency of the signal using precise time differences. The F2V output was further filtered (Chebyshev low-pass, 30 Hz cutoff). Both the amplified signal and the F2V output were fed into a Power1401 Mk.II signal acquisition device (CED, Cambridge, U.K.) which ran a custom sequencer script that read the input signal, performed the feedback calculation and generated a sinusoid with the desired output frequency. Using this setup enabled regular temporal sampling intervals and provided a lower and more measurable and repeatable computation time than including a standard computer in the feedback. The signal acquisition device received parameters and reference signal

for each trial from the Spike2 software (CED, Cambridge, U.K.) which ran simultaneously on a computer. During the trials, this software received and recorded data from the input, output and intermediate channels. The amplitude of the stimulating sinusoid was 100 μV/cm (unless otherwise noted) which produced approximately 30% contamination of the EOD, as measured at a 1 cm dipole placed adjacent to the head of the fish.

We performed an identification experiment on the feedback system to assess what its characteristics were, especially the delay introduced by the equipment. The contribution was minimal ($\sim$ 2 ms delay) due to fast instrumentation (data not shown). As such, the feedback delay was not incorporated into subsequent calculations.

3.2.2 The closed-loop approach

The fish EOD frequency $f_1(t)$ and the stimulus frequency $f_2(t)$ are functions of time. Under constant lighting, temperature, and conductivity, and without conspecific stimulation, the EOD frequency remains relatively stationary over long periods of time [11]. The initial time $t = 0$ for each trial was preceded by a period of no stimulation for at least 300 s, and we defined the baseline (initial) frequency $f_1(0)$ as the EOD frequency at that initial time.

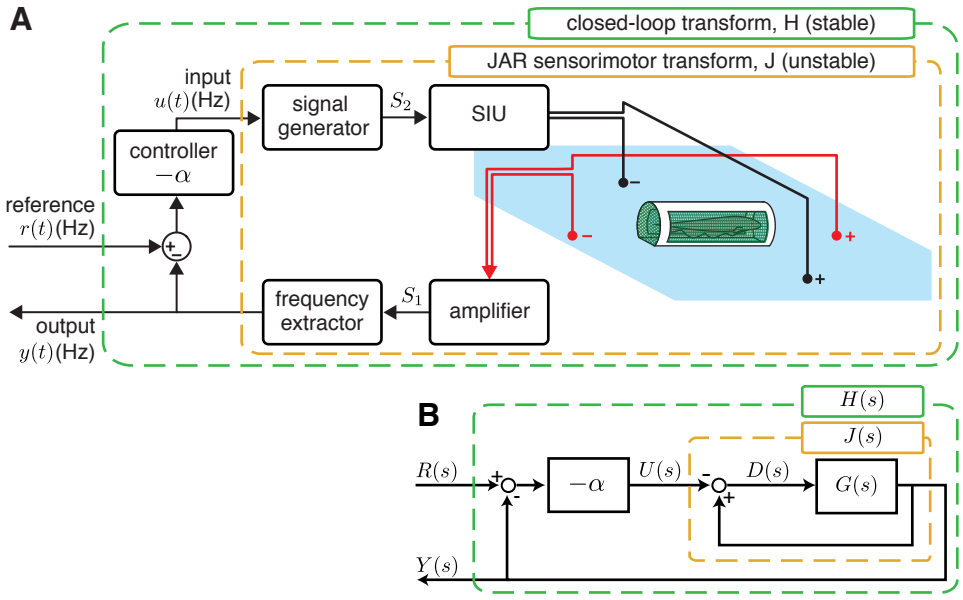

Figure 3.2: Experimental Setup. (A) Schematic of the closed-loop system. The reference frequency, $r(t)$, EOD frequency, $y(t)$, and the frequency of the input signal, $u(t)$, are all baseline subtracted, so that 0 Hz corresponds the fish's baseline EOD frequency. The EOD is measured (recording electrodes, red), amplified, and its frequency, $y(t)$, is extracted. The input frequency $u(t) = \alpha(y(t) - r(t))$ is fed to a signal generator, which outputs a sinusoid of that frequency. This sinusoid is played back through a stimulus isolation unit (SIU) to the fish (stimulating electrodes, black). (B) A block diagram representation of the experimental system. Here, $R(s), Y(s), U(s)$ and $D(s)$ are the Laplace transforms of the reference, input, output and difference frequencies respectively. $J(s)$ represents the (open-loop) JAR behavior, namely the transfer function from $U(s)$ to $Y(s)$. The transfer function from the computed difference $D(s)$ and output $Y(s)$ is The closed-loop transfer function $H(s)$ relates $R(s)$ to $Y(s)$.

The following control variables were chosen as frequencies relative to $f_1(0)$:

$$\begin{aligned} y(t) &= f_1(t) - f_1(0), \\ u(t) &= f_2(t) - f_1(0), \\ d(t) &= y(t) - u(t) \end{aligned} \tag{3.1}$$

The signal $u(t)$ served as the input and $y(t)$ was the measured output of the behavior. The signal $d(t)$ is the difference between these signals, also referred to as the *df*.

Given a reference signal $r(t)$, a simple proportional controller was able to stabilize the system:

$$u(t) = -\alpha(r(t) - y(t)). \tag{3.2}$$

The controller gain was typically selected as $\alpha = 2$ (unless otherwise noted) and was positive for all experiments.

The frequency of the applied signal S_2 was $f_2(t) = f_1(0) + u(t)$. S_2 is calculated as a function of time:

$$S_2(t) = a_2 \sin\left(\int_0^t f_2(t)dt\right) = a_2 \sin\left(f_1(0)t + \int_0^t u(t)dt\right) \tag{3.3}$$

where a_2 is the stimulus amplitude (typically 100 μV/cm). The generation of applied signals from frequency trajectories is illustrated in Fig. 3.3.

In the frequency domain, $J(s)$ denotes the input–output transfer function corresponding to the behavior at frequency $s = j\omega$. Thus $J(s)$ is the *behavior* transfer function from $U(s)$ to $Y(s)$, where $U(s)$ and $Y(s)$ are the Laplace transforms of $u(t)$ and $y(t)$, respectively. $G(s)$ is the *open-loop* transfer function between $D(s) =$

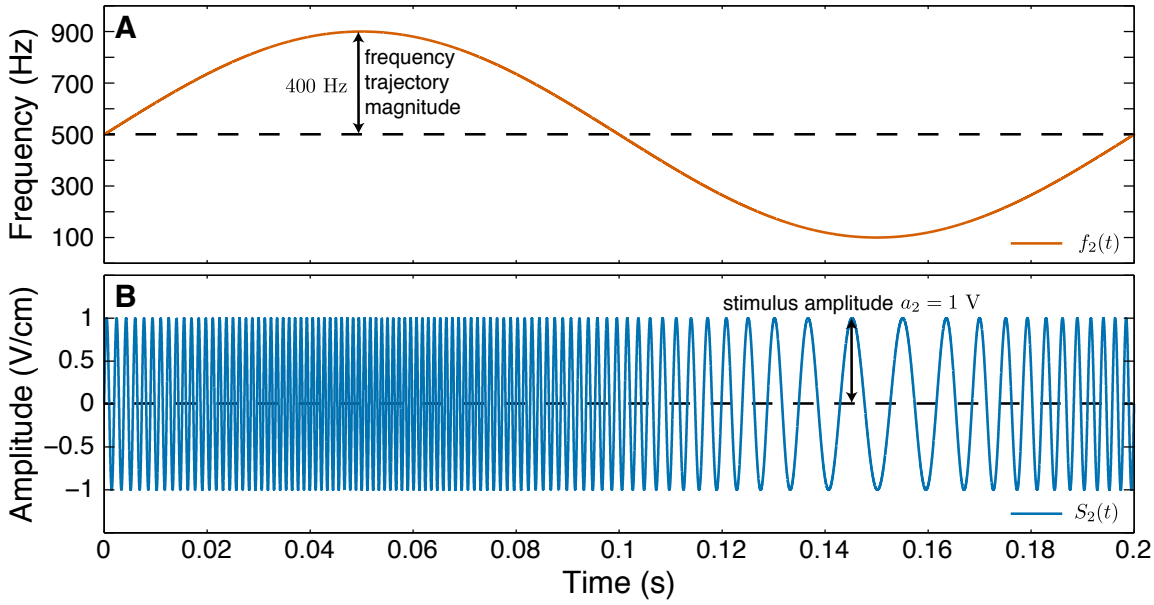

Figure 3.3: Instantaneous frequencies are the primary signals of interest in this chapter, but ultimately voltage signals are applied into, and measured from, the water. This can be confusing because we often wish to create sinusoidally varying frequency trajectories (or chirps, or sums of sines), and then use these frequency trajectories to generate a voltage signal. This figure illustrates the generation of an applied signal $S_2(t)$ from a sinusoidally varying frequency, $f_2(t)$. (A) In this scenario, the fish's baseline frequency is $f_1(0) = 500$ Hz, and the input frequency trajectory is a sinusoid of 400 Hz magnitude and 5 Hz frequency—a single 0.2 second period is shown. Thus $u(t) = 400 \sin 10\pi t$, and the stimulus frequency is $f_2(t) = f_1(0) + u(t)$. (B) A signal of amplitude 1 V is generated with the frequency varying as $f_2(t)$, using Eq. (3.3). Note that for illustration purposes, the stimulus frequency magnitude and stimulus amplitude shown in this figure is exaggerated beyond values applied during experiments. Typical experimental frequency magnitude value is ~ 1 Hz, and stimulus amplitude value is $\sim 100\mu$V/cm.

$(Y(s) - U(s))$ and $Y(s)$. Similarly, $H(s)$ is the *closed-loop* transfer function between $R(s)$ and $Y(s)$ (Fig. 3.2B). The open-loop transfer function, $J(s)$, can be converted to closed loop, $H(s)$, and vice versa. The following equations relate these three transfer functions:

$$\frac{Y(s)}{R(s)} = H(s) = \frac{-\alpha J(s)}{1 - \alpha J(s)} = \frac{-\alpha G(s)}{(1-\alpha)G(s) - 1} \tag{3.4}$$

$$\frac{Y(s)}{U(s)} = J(s) = \frac{H(s)}{\alpha(H(s) - 1)} = \frac{G(s)}{G(s) - 1} \tag{3.5}$$

$$\frac{Y(s)}{D(s)} = G(s) = \frac{J(s)}{J(s) - 1} = \frac{H}{H(1-\alpha) + \alpha} \tag{3.6}$$

3.2.3 Stimulus types

3.2.3.1 Single sines

Sinusoidal stimuli were of frequencies $0.01, 0.055, 0.215$, and 0.995 Hz and of durations $1000, 1000, 500$, and 200 s respectively. The stimulus durations were chosen to have a sufficient number of beat cycles for spectral analysis.

3.2.3.2 Sum of sines

These stimuli were the sum of 10 logarithmically spaced sinusoids with randomized phase, in the range 0.01 to 1 Hz. The sum-of-sine stimuli included the four single sine frequency components. The stimulus duration was 1000 s.

3.2.3.3 Chirps

The chirp stimulus was a sinusoid of increasing frequency, from 0.01 to 1 Hz over 1000 s. The increase of frequency was exponential, ensuring sufficient stimulus power across all frequencies.

3.2.3.4 Long chirps

The long-chirp stimulus was similar to the chirp stimulus except that the frequency increased from 0.001 to 1 Hz. Consequently, the stimulus duration was increased to 10000 s.

3.2.3.5 Band-limited pseudo-random noise

Band-limited noise stimuli consisted of non-overlapping, 2 Hz wide frequency bins from 0 to 20 Hz. For each bin, a stimulus was generated by summing together sinusoids associated with all uniformly spaced frequencies as dictated by the sampling rate. This ensured that the stimulus has uniform power over all the frequencies analyzed within each bin. Each component had randomized phase and was scaled equally so that the sum would have a maximum magnitude of 1 Hz. The trial duration was 300 s, except for the lowest frequency band of 0 to 2 Hz, which was 1000 s long.

3.2.4 Trial types

3.2.4.1 Closed-loop reference-tracking trials

For closed-loop reference-tracking trials, we provided a reference signal $r(t)$ and applied the controller as described in Eq. (3.2). At the start of each trial, the fish's baseline was measured. Subsequently, there was a "balancing" period of 100 s wherein the controller aimed to keep the fish at the initial EOD frequency ($r(t) = 0$). To avoid startling the fish, the amplitude of the stimulus signal was ramped up linearly from 0 μV/cm to 100 μV/cm (unless noted) over the first 50 s of balancing period. After the balancing period a stimulus (single sine, noise, etc.) was introduced as the reference. Trials were pseudo-randomized. All stimuli were pre-generated at 1 KHz and input to the sequencer at the start of the trial. A sample interval of a closed-loop trial with a single-sine stimulus is shown in Fig. 3.4.

Each fish ($N = 5$) completed closed-loop reference-tracking trials ($n = 49$) in a randomized order within a single testing session. The trials consisted of the following:

- Single sine stimuli ($n = 8$), the four frequencies of which were replicated for magnitudes of 1 and 2 Hz.
- Sum-of-sines stimuli ($n = 4$), with two different component magnitudes (0.2 and 0.3 Hz), with two different sets of randomized component phases each. Thus the maximum stimulus magnitude was 2 or 3 Hz.
- Chirps ($n = 2$), with magnitudes 1 Hz and 2 Hz.

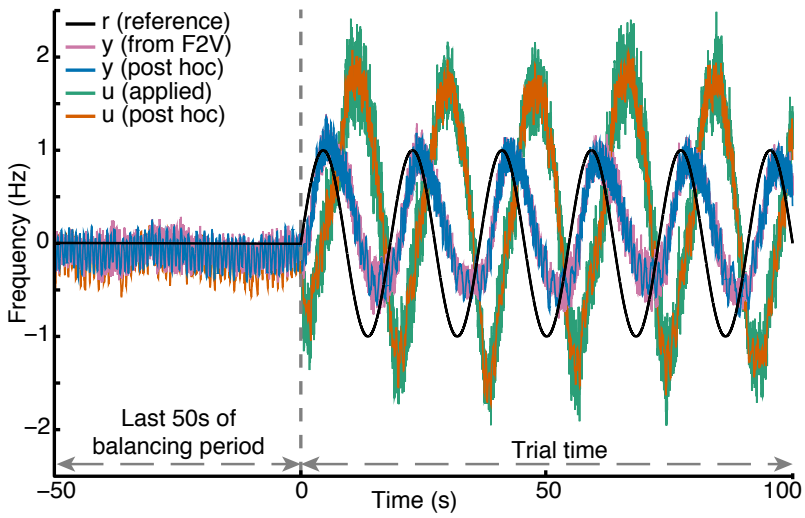

Figure 3.4: Sample closed-loop trial and verification of applied signals via post hoc analysis of measured signals. Output $y(t)$ from the F2V converter (pink) was used during the experiment and its value was verified with a post hoc estimate of frequency (blue) based on the measured EOD signal. The desired input $u(t) = \alpha(y(t) - r(t))$ (green) was verified against a post hoc estimate of the applied frequency (orange) based on a measurement of the input signal.

- White noise stimuli ($n = 30$), with three identical replicates of each of the 10 frequency bands.

- Chirp ($n = 2$) stimuli with signal amplitude 50 μV/cm and 200 μV/cm (typical value = 100 μV/cm). These were to examine sensitivity of the identified system to signal amplitude.

- Chirp ($n = 3$) stimuli with controller gains 1.5, 2.5 and 3 (typical value = 2). These stimuli were, similarly, to examine sensitivity to the feedback gain.

Sample responses to four stimulus types are shown in Fig. 3.5.

In addition, a subset of 3 individual fish were presented with long chirp stimuli at

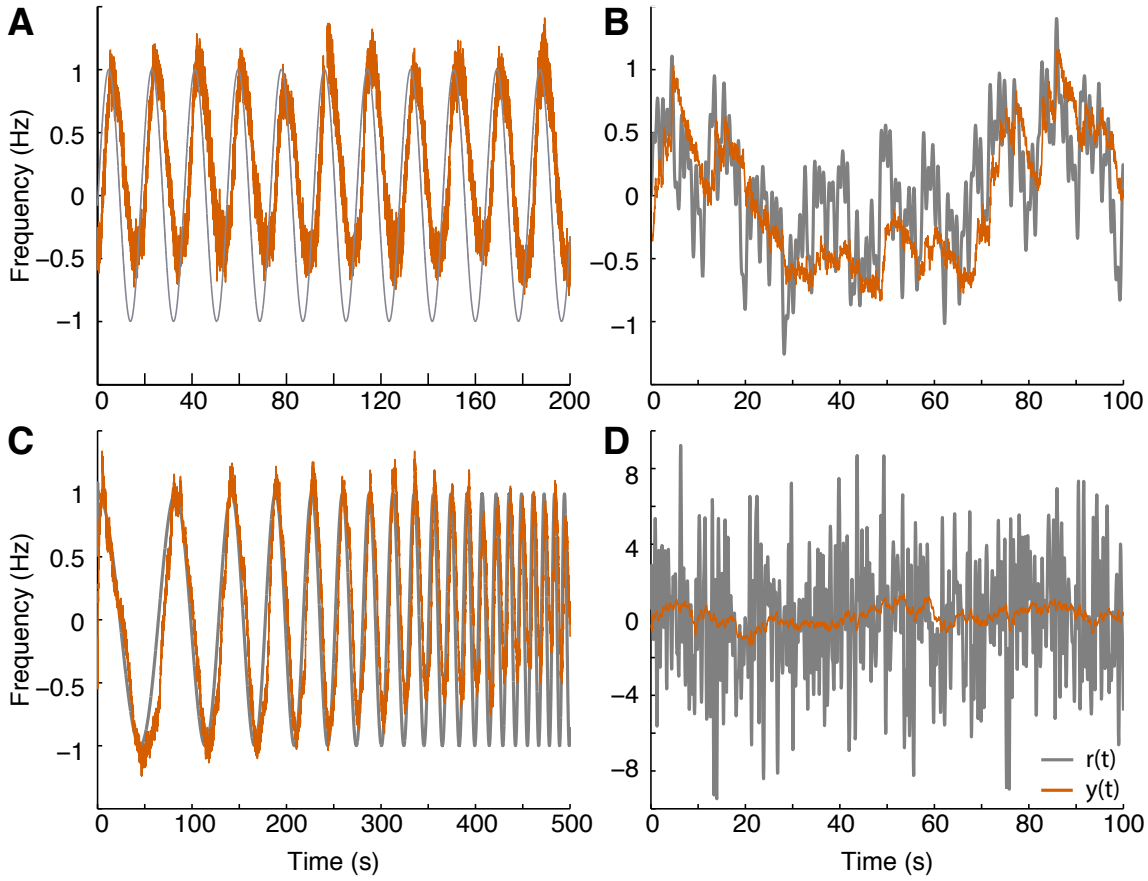

Figure 3.5: Stimulus–response plots for closed-loop reference-tracking trials for different types of reference signals: (A) single sine, (B) sum of sines, (C) chirp, (D) band-limited noise in the 0 to 2 Hz range. The reference trajectory is gray, response is orange.

two magnitudes (1 Hz, 2 Hz).

After each trial, the stimulus was turned off and the EOD frequency was allowed to stabilize over a period of 300 s before the next trial began.

3.2.4.2 Closed-loop clamp trials

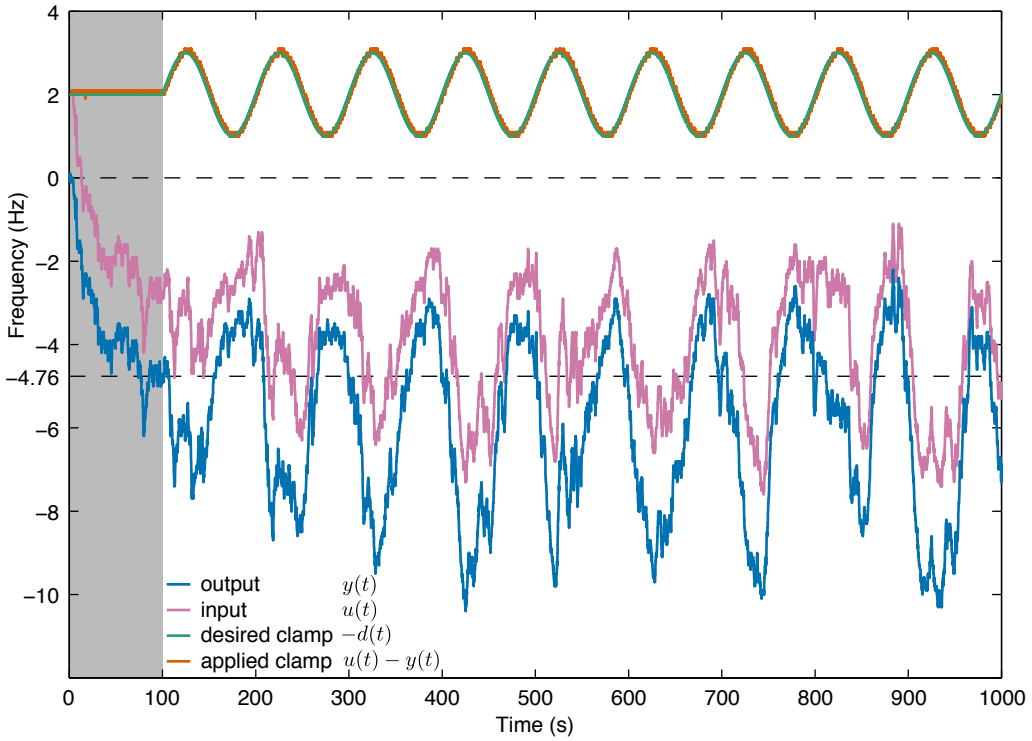

Figure 3.6: Dynamic clamp trial. In this trial, the difference between the baseline-subtracted EOD frequency, $y(t)$ (blue), and applied stimulus frequency, $u(t)$ (pink), is clamped at a constant value, $d_s = -2$ Hz for the first 100 s (gray shaded area). During this time, the EOD frequency settles to the steady-state value, -4.76 Hz. After this static clamp period, the desired clamp (green) is oscillated through a trajectory, in this case a sinusoid of magnitude 1 Hz and frequency 0.01 Hz (100 s period). Since this is a closed-loop trial, the controller maintains $u(t)$ at the appropriate difference from $y(t)$. This is verified by the post-hoc computation of the applied clamp (orange). Note that for clarity in illustration, the negatives of the desired clamp and applied clamp curves are plotted, i.e. $-d(t)$ and $u(t) - y(t)$.

Instead of driving the fish frequency towards a goal, the clamp trials applied a stimulus such that $d(t)$ was maintained at a desired value. Two types of clamp trials were run:

- Static clamps: The clamp was a constant value $d = d_s$ for 300 s.
- Dynamic clamps: The clamp was kept at a particular value $d = d_s$ for 100 s and then oscillated around the value according to a reference trajectory $r(t)$, such that $d(t) = d_s + r(t)$.

Static and dynamic clamps experiments were performed on $N = 2$ individuals, that did not complete the reference-tracking trials. These included $n = 39$ static clamps with d_s from -50 to 50 at higher resolution closer to 0. The dynamic clamp trials had single sine, sum-of-sines, and chirp stimuli as the reference trajectories.

3.2.4.3 Open-loop trials

The objective of these trials was to observe the response of the fish to a stimulus, whose frequency trajectory $u(t)$ was predetermined, and not tied to $y(t)$. Two types of open-loop trials were performed:

- Step inputs: Initially, the fish was driven towards 0 in closed loop for the balancing period of 100 s. The amplitude was linear ramped up to 100 μV/cm for 50 s as described previously. At 100 s, the stimulus switched to open loop,

and $u(t)$ was commanded to a fixed value for a further 100 s. We performed trials at steps with magnitudes from -5 to $+5$ Hz.

- Ramp inputs: The magnitude of u was ramped down from $+30$ to -30 Hz or up from -30 to $+30$ Hz in 300 s at a constant rate of change of 0.2 Hz/s. The stimulus amplitude was ramped to 100 μV/cm in the first 10 s. The initial difference frequency was large, $|df| \approx 30$, well outside the typical range of the JAR.

3.2.5 Data analysis

All data analysis was carried out using custom scripts written in MATLAB (The MathWorks Inc., Natick, MA, U.S.A.).

For each trial, we recorded the reference, EOD, F2V output, and output waveform, sampled at 10 KHz. The voltage signal from the F2V was scaled and offset to convert it into frequency. Extremely rapid, transient changes in frequency (commonly caused by fish movement) were eliminated. The known baseline frequency of the fish was subtracted from all signals, so that a frequency of 0 Hz represents the fish's pre-stimulus (baseline) signal. The processed F2V signal was then subsampled to 100 Hz, and used as the output signal $y(t)$. The input for analysis depended on the type of trial: $r(t)$ was used for reference-tracking trials, $d(t)$ was used for the dynamic clamp trials, and $u(t)$ was used for the open-loop trials. These inputs were pre-generated

trajectories, as mentioned previously.

3.2.5.1 Estimating FRFs for sinusoidal inputs

The frequency domain representations of the input and output signals were calculated using a Fast Fourier Transform (FFT) and peaks corresponding to the known number of frequency components in the input were determined (1 for single sines, 10 for sums of sines). The frequency response at a particular frequency was calculated as the ratio of the Fourier transform of the output to the input of the signal at that particular frequency. Thus we measured 8 data points from 8 single-sine trials and 40 points from 4 sums-of-sines trials. Each data point was represented as a phasor, namely a number in the complex plane. The gain (distance of the phasor to the origin) and phase (angle of the phasor from the positive real axis) for all data were computed.

3.2.5.2 Estimating FRFs for chirp inputs

The input and output signals were filtered, subsampled and transformed via FFT as described above. The data points in this case were the input–output ratios of all the frequency components in the chirp frequency range. Thus, with a single trial, we obtained many data points, but each individual data point is somewhat more susceptible to noise. The data points were binned and averaged at 10 bins per decade of frequency, giving us 20 data points per chirp trial and 30 data points per long chirp

trial.

3.2.5.3 White noise

White noise stimuli were used to evaluate the range over which the behavior is linear. This was done by evaluating the difference of the square root of the response-response coherence ($\sqrt{RR}$) and the stimulus-response coherence (SR) [67]. The coherence between two signals X and Y is a frequency-dependent function:

$$C_{XY}(\omega) = \frac{|G_{XY}|^2}{G_{XX}G_{YY}} \tag{3.7}$$

where G_{XY} is the cross-spectral density between X and Y, and G_{XX} and G_{XY} are the autospectral densities of X and Y respectively. SR is the coherence between each stimulus and its corresponding response. $\sqrt{RR}$ is the square root of the coherence between two responses to the repeated presentation of the same stimulus. In our experiment, there were three replicates of each frequency band, i.e. for a particular stimulus X, there were three independent responses Y_1, Y_2 and Y_3. This gave us 3 data points per frequency per individual for SR (C_{XY_1}, C_{XY_2} and C_{XY_3}) as well as $\sqrt{RR}$ ($\sqrt{C_{Y_1Y_2}}$, $\sqrt{C_{Y_2Y_3}}$ and $\sqrt{C_{Y_3Y_1}}$).

3.2.5.4 Steps and Ramps

These trials were open loop and were used to compare the fish response with model response in the time domain. Hence, no frequency domain analysis was done on these trials.

3.2.6 Modeling approach

Three of the four fish used in the reference frequency tracking trials were tested using long chirp stimuli whose reference frequency started at 0.001 Hz and increased to 1 Hz; the resulting FRF data binned into 30 frequency bands (see Sec. 3.2.5.2). Two chirp magnitudes (1 Hz and 2 Hz) were tested for each individual for a total of six trials that were used for fitting.

The FRF of the closed-loop system was determined as described in Sec. 3.2.5. This data was converted to open-loop as per Eq. (3.6). In open loop, each trial was represented by complex numbers for each frequency bin. At a given frequency ω, the ratio of output $\hat{Y}(j\omega)$ to its corresponding input $\hat{D}(j\omega)$ can be represented by its gain and phase components:

$$\hat{G} = \frac{\hat{Y}}{\hat{D}} = \frac{|\hat{Y}|}{|\hat{D}|} e^{i(\angle Y - \angle D)} = |\hat{G}| e^{i\angle \hat{G}} \tag{3.8}$$

The logarithm of this complex number is:

$$\log(\hat{G}) = \log|\hat{G}| + i\angle\hat{G} = \log\frac{|\hat{Y}|}{|\hat{D}|} + i(\angle\hat{Y} - \angle\hat{D}). \tag{3.9}$$

which is also a complex number, but weights gains logarithmically and phases linearly. This is important since we are interested in ratio of amplitudes and the difference of phases. This is also analogous to computing error directly in the Bode plot, e.g. Figs. 3.9,3.11. Distances in this 'log-complex plane' thus provide a good measure of error for model fitting, as previously used in [69].

We also have to account for the fact that the open loop response will have increased

sensitivity to noise at some frequencies, corresponding to the equation for opening the loop (Eq. (3.5)). The sensitivity of opening the loop can be computed in log-complex plane coordinates:

$$S(\omega) = \left| \frac{d \log G(\omega)}{d \log H(\omega)} \right| = \frac{1}{|H(\omega)(1 - 1/\alpha) - 1|}. \tag{3.10}$$

We use the inverse of this sensitivity to weight the error. The error between model response $M(\omega)$ and the system response $G(\omega)$ at a given frequency ω is then defined as follows:

$$E(\omega) = \left| \log \left(\frac{M(\omega)}{G(\omega)} \right) \right|^2 (|H(\omega)(1 - 1/\alpha) - 1|). \tag{3.11}$$

The total error between model M and response G is the sum of this error over all frequencies.

3.2.6.1 Determining model structure

The next step was to determine the model structure. A model fitting criterion such as reduced χ^2, or information criteria such as AIC or BIC can be generally minimized to determine the model order. However, these criteria assume independent data points. Since the chirp is a time-varying frequency stimulus, the response data is clearly covariant, and the relatively small number of trials (6) is insufficient to determine the covariance structure between 30 bins.

So, we implemented a selection criterion decision technique that takes into account two factors: *Model fit* and *Model consistency*:

3.2.6.1.1 Model fit:

Leave-one-out cross validation (LOOCV) was used as the technique to fit a model while penalizing over fitting. LOOCV is asymptotically equivalent to AIC [77]. For each model, the Matlab nonlinear optimization function *fminsearch* was run with the error function (Eq. (3.11)) to fit parameters to data from five trials, leaving the sixth trial out. This optimization was initialized 100 times (using Matlab to generate pseudo-random initial parameter values), and the parameters with the lowest fit error among them was then compared to the left out trial, using the same error function. The 'leave-one-out' error determined for one trial was averaged over all six trials being left out, providing a combined leave-one-out error for the model structure. See Fig. 3.7, y-axis.

3.2.6.1.2 Model consistency:

Even though a certain model might have low leave-one-out error, the parameters fitted during each of the six leave-one-out minimizations may vary significantly. This variance, which is measure of the uncertainty of the parameters based on our data, needs to be penalized, since we desire to have a consistent model fit with all six trials. To measure model consistency, we calculate the maximum singular value of the $K \times 6$ matrix where each of the six columns contains an estimate of all K parameters, with one column for each fit (one for each of the 6 trials left out). The poles and zeros of each fit are sorted, and mean of each parameter across trials is subtracted, before

finding the maximum singular value.

Altogether, 72 transfer function models of up to seventh order were tested. This includes all combinations $n_z \leq n_p \leq 7$ where n_z is the number of zeros and n_p is the number of poles. The delay was turned on ($n_d = 1$) or off ($n_d = 0$). The models are referred to as (n_z, n_p, n_d), and correspond to the transfer function:

$$(n_z, n_p, n_d) \equiv \frac{k \prod_{i=1}^{n_z} (s - z_i)}{\prod_{i=1}^{n_p} (s - p_i)} e^{-n_d s T}. \tag{3.12}$$

The total number of parameters for a model is $K = n_z + n_p + n_d + 1$, where the extra parameter is due to the gain. The maximum K tested is then $7 + 7 + 1 = 16$. Fig. 3.7 shows leave-one-out error versus maximum singular value. For clarity, only models with maximum singular values below 10^5 are shown. It is clear from the figure that the two initial models $(0, 0, 0)$ (gain: k) and $(0, 0, 1)$ (gain with delay: ke^{-sT}) both have unacceptably high errors. The next two models $(0, 1, 0)$ (gain, zero: $\frac{k}{s-p}$) and $(0, 1, 1)$ (gain, zero, delay:$\frac{k}{s-p}e^{-sT}$) have a combination of low error and high consistency. The higher order models have lower error in some instances, but are much less consistent. As shown in the inset of Fig. 3.7, among the two 'good' models, we choose the model closest to the origin, $(0, 1, 1)$, which corresponds to a first-order system with a delay.

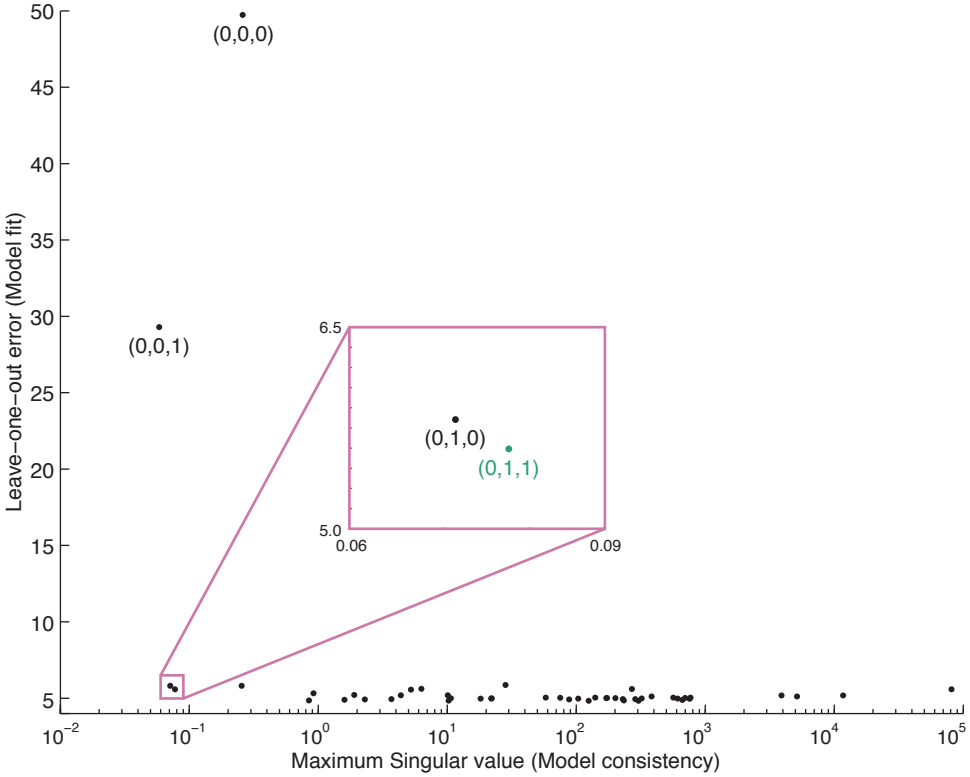

Figure 3.7: Model fit vs. Model consistency. Each data point (black dot) represents a particular model structure (n_z, n_p, n_d). The average leave-one-out error for a particular model structure is on y-axis. The maximum singular value of the $K \times 6$ parameter matrix for each model structure is shown on the x-axis. The first four models are labeled for clarity, and the region containing the two best models is magnified (inset). The model order $(0, 1, 1)$ was ultimately chosen as the best compromise between fit and consistency (inset; green dot)

Model	K	Parameters				Fit error	LOO	MSV
		k	z	p	T			
(0,0,0)	1	0.45				295.17	49.73	0.057
(0,0,1)	2	0.45			0.49	172.34	29.30	0.058
(0,1,0)	**2**	**0.37**		**−0.23**		**28.77**	**5.81**	**0.071**
(0,1,1)	**3**	**0.38**		**−0.24**	**0.057**	**27.12**	**5.59**	**0.077**
(1,1,0)	3	−0.021	16.14	−0.24		26.97	5.56	5.23
(1,1,1)	4	0.085	−3.65	−0.19	0.25	25.42	5.32	0.92
(0,2,0)	3	7.52		-0.25, -19.90		27.33	5.61	6.30
(0,2,1)	4	9.18×10^8		-0.24, -2.45×10^9	0.057	27.12	5.59	1.3×10^8
(1,2,0)	4	0.39	−0.08	-0.04, -0.38		25.67	5.86	28.32
(1,2,1)	5	0.41	−0.16	-0.06, -0.54	0.08	23.03	5.22	1.90
(2,2,0)	5	−0.03	-0.13, 13.18	-0.06, -0.48		23.02	5.19	4.37
(2,2,1)	6	0.06	-0.09, -5.78	-0.04, -0.37	0.21	22.75	5.12	54.25

Table 3.1: Fit parameters, fit error, leave-one-out error, and maximum singular value for the first 12 model structures. The 'best' models $(0, 1, 0)$ and $(0, 1, 1)$ are highlighted in bold.

3.2.6.2 Model fitting

The final fit parameters were determined by initializing the optimization 100 times with random initial parameter guesses, this time with no data left out. The lowest error fit among these was designated the *fit error*, the parameters associated with which were used. For clarity, we present the best parameters and errors of the ten lowest order models shown in Fig. 3.7 in Table 3.1. This is also illustrated in Fig. 3.8. The $(0, 0, 0)$ and $(0, 0, 1)$ models are obviously poor fits to the data, whereas the two parameter model $(0, 1, 0)$ fits the data well except the high frequency region. $(0, 1, 1)$ compensates for that by introducing a phase lag. There is no noticeable advantage to adopting a higher order model than $(0, 1, 1)$. The results from this fitting were reported in the main text; see Eq. (3.14).

3.3 Results

3.3.1 The JAR is approximately linear around the unstable equilibrium

The FRF for single sine, sum of sines, chirp and long chirp closed-loop tracking trials were plotted in a Bode diagram as shown diagram in Fig. 3.9A. The data were converted to open-loop according to Eq. (3.5) as shown in Fig. 3.9B. The agreement between single sine, sum of sines and chirp data indicates that the behavior can be

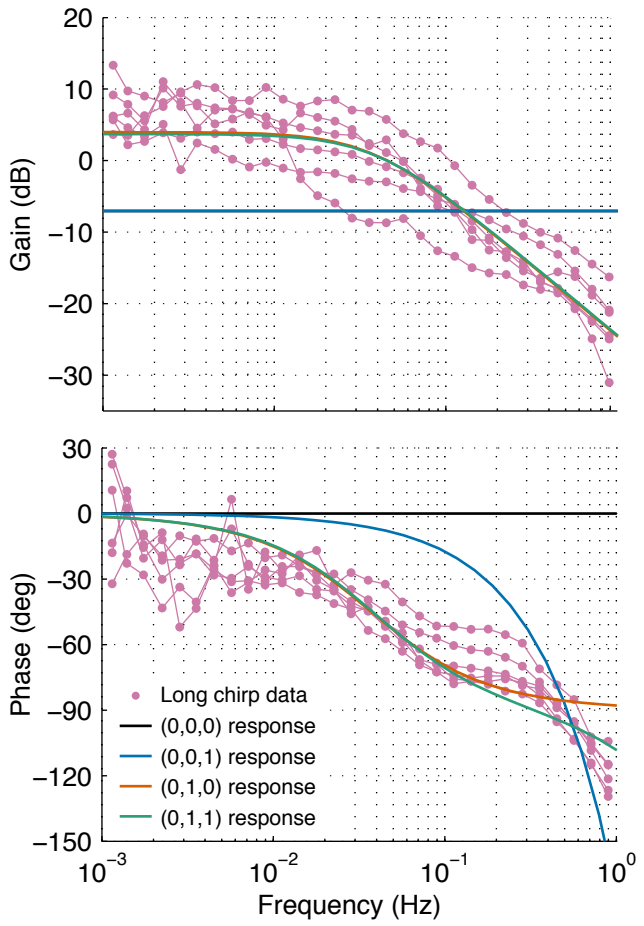

Figure 3.8: Candidate model fits to open-loop data. The FRF data from six long-chirp trials transformed to open loop using Eq. (3.6) is shown, along with the best fits using model structures $(0, 0, 0)$, $(0, 1, 0)$ and $(0, 1, 1)$. It can be seen that fits using $(0, 1, 0)$ and $(0, 1, 1)$ are different only at higher frequencies. Higher-order models with low leave-one-out errors were not substantively different than the $(0, 1, 1)$ model within this frequency range, and thus are not shown.

modeled approximately as a linear system in the neighborhood of the equilibrium, i.e. near the baseline frequency $f_1(0)$. There are small differences in the closed-loop data among different trial types, particularly between long chirps and the others. Sensitivities of opening the loop tend to amplify these, creating significant differences in the open-loop data. The modest difference in closed-loop responses could come from a variety of sources, including nonlinearities and time-dependencies in the behavior.

SR and $\sqrt{RR}$ coherences from white noise trials are shown in Fig. 3.10A. $\sqrt{RR}$ represents the maximum theoretically possible coherence for a linear system in the presence of additive noise. The difference

$$e = \sqrt{RR} - SR \tag{3.13}$$

is an indicator of the nonlinearity of the system [67]. This difference (Eq. (3.13), Fig. 3.10B) does not exceed 0.4, over the white noise stimulation range of 0 to 20 Hz. However, past approximately 6 Hz, $\sqrt{RR}$ drops to around 0.4. In that range and beyond, even the best model will only be able to capture a fraction of the behavior. However the frequency range over which we performed frequency response analysis and modeling ($0.01 - 1$ Hz) is far below this, and would likely encompass most naturally occurring frequency modulations among conspecifics.

As an important control, we investigated the sensitivity of the open-loop dynamics to experimental parameters. Amplitudes were compared at both half and twice the value of 100 μV/cm used in all of the other experiments described in this chapter. Gains were tested at values of 1.5, 2.5, 3 and 4 compared to the value of 2 used in

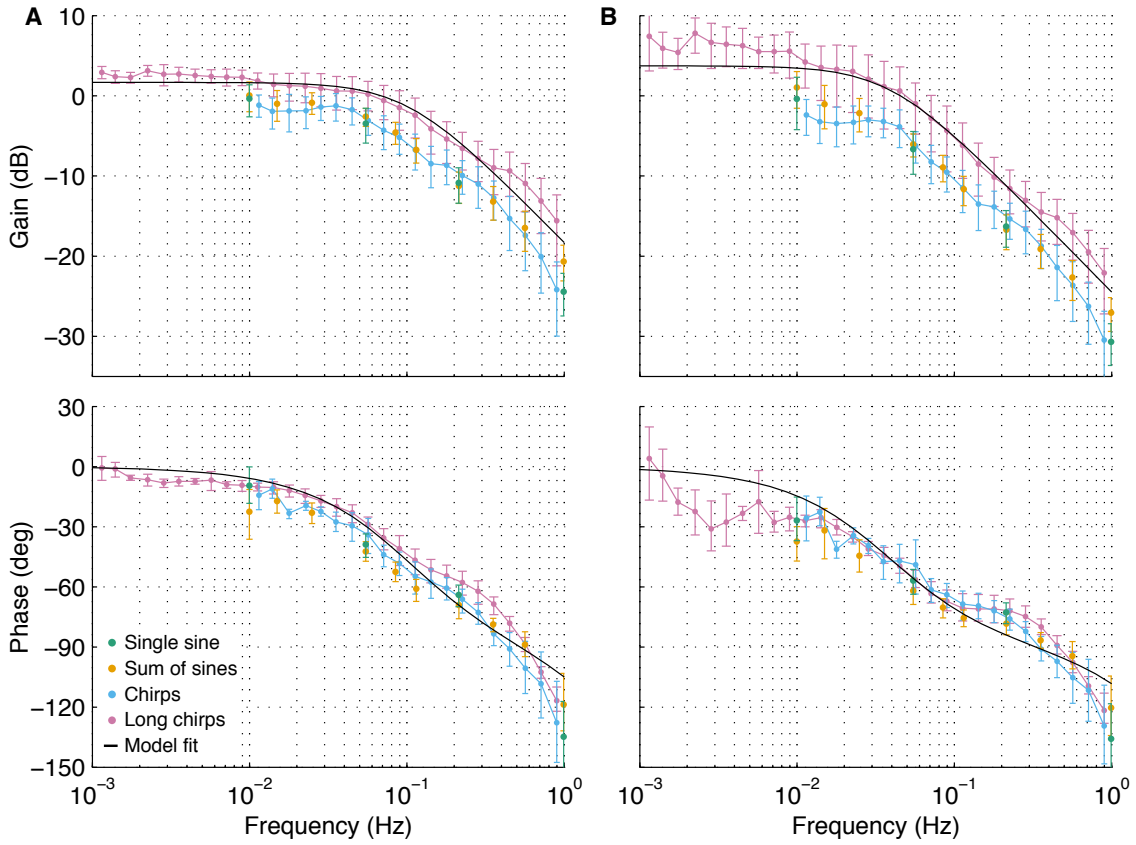

Figure 3.9: Bode diagrams of experimental frequency response functions (FRFs) from single sine, sum of sines, chirp and long chirp trials. In a Bode diagram, the gain of each FRF point, $z = a + ib$, is expressed in decibels ($20 \log_{10}(|z|)$, top) and its phase in degrees ($\frac{180}{\pi} \angle z$, bottom). The single sine and sum of sines data points are slightly offset horizontally to avoid overlapping. (A) Closed-loop FRF. (B) The same data, mapped to open-loop via Eq. (3.6). The model was fit to the open-loop FRF and mapped back to closed loop via Eq. (3.4).

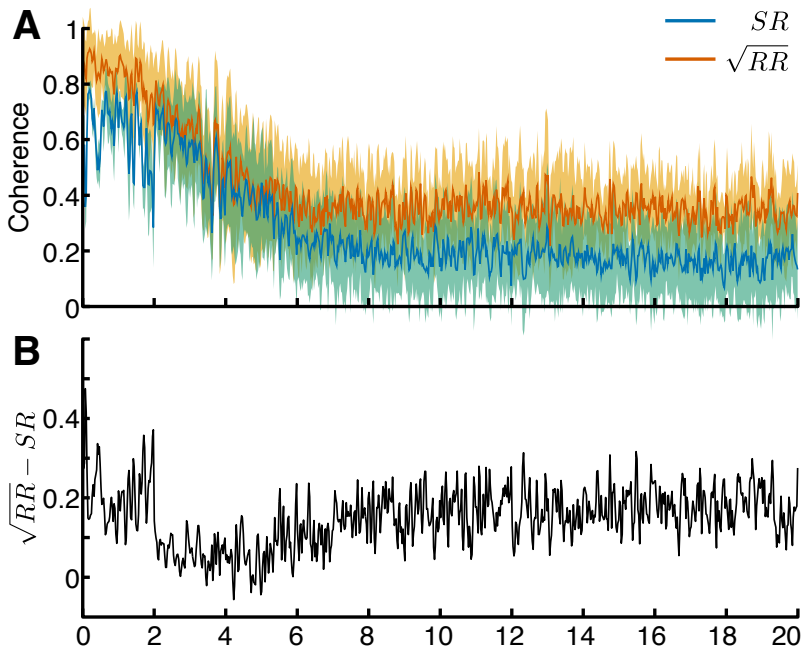

Figure 3.10: Noise coherence plots. (A) SR and $\sqrt{RR}$, as calculated from band-limited white noise trials over all individuals. The solid lines indicate mean value for each frequency and the lighter bands show one standard deviation above and below the mean. (B) Difference between the coherences is an indicator of the linearity of the system [67].

all other experiments. There was little-to-no effect of changing either amplitude of the signal (Fig. 3.11A) or the feedback gain (Fig. 3.11B) on the open-loop frequency response. The amplitude insensitivity results in an experimental advantage, since the size of the fish, or the specific placement of the fish between the stimulus electrodes would have little effect on the dynamics.

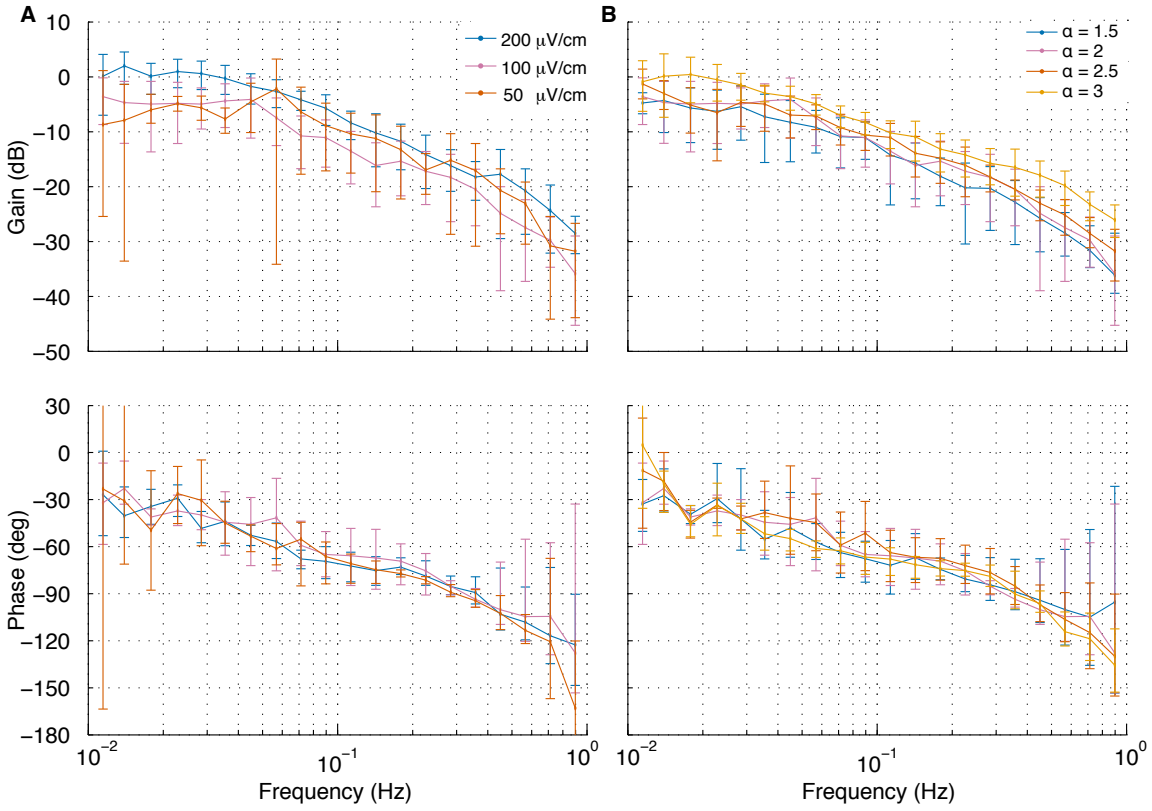

Figure 3.11: Sensitivity to experimental parameters. (A) Open-loop frequency responses to chirp stimuli, for stimulus amplitudes of 50 μV/cm and 200 μV/cm along with the usual experimental value of 100 μV/cm. The stimulus amplitudes were measured at a 1 cm dipole placed adjacent to the head of the fish. (B) Open-loop responses to the feedback gain α being set to 1.5, 2.5, and 3 as opposed to the usual experimental value of 2. Changing the feedback gain causes divergence in the closed-loop response as expected; however the computed open-loop responses do not appear to be sensitive to stimulus amplitude or feedback gain. In both bode plots, the top plot is the gain response and the bottom plot is the phase response.

3.3.2 Determining the local linear model

To fit a model to the JAR behavior at the equilibrium, each of the closed-loop data points was transformed, in the complex plane, to the corresponding open-loop data point using Eq. (3.5); see Fig. 3.9B. As described in the previous section, a simple first order model with delay was fit to the open-loop response:

$$G(s) = \frac{k}{s-p}e^{-sT} \tag{3.14}$$

where $k = 0.38$ Hz, $p = -0.24$ Hz, and $T = 57$ ms. Recall that $G(s)$ represents the transfer function from the *df*, $d(t)$, to the fish's EOD frequency, $y(t)$ (both signals were baseline subtracted). The negative real pole ($p < 0$) confirms that this is a stable system, and the sensorimotor delay of $T = 57$ ms is biologically plausible. The transfer function is plotted as the black curve in Fig. 3.9B. The behavior transfer function $J(s)$ (computed via Eq.(3.5)) is unstable if there are zeros of the denominator $G(s) - 1$ in the open right-half plane. Similarly, the closed-loop transfer function $H(s)$ (computed via Eq. (3.4)) is stable if there are no zeros of $1 - \alpha J(s)$ in the open right-half plane. Based on the Nyquist stability criterion [2], it is easy to confirm that $J(s)$ is unstable (there is exactly one pole in the right-half plane). Furthermore, it is trivial to show that $H(s)$ is stable so long as α is larger than $\alpha_{\min}$.

$$\alpha_{\min} = \frac{p}{k} + 1. \tag{3.15}$$

For the model parameters in Eq. (3.14), the minimum stable gain is $\alpha_{min} = 0.35$. The experimental value of $\alpha = 2$ is much higher than this threshold, thus robustly

stabilizing the closed-loop system.

3.3.3 Determining the global nonlinear model

The model fit using the closed-loop experiment is, effectively, a local linearization of the behavior about the unstable equilibrium $y = 0$ (corresponding to the fish's pre-stimulus baseline frequency). Thus, the transfer function described in Eq. (3.14) is unable to reproduce the full extent of a naturalistic response, which, in addition to avoiding a jamming frequency, involves achieving a steady state frequency at a higher final *df* magnitude. Using the linear model as a starting point, and known features of the JAR neural circuit, we fit a nonlinear model as described below.

The model structure we propose decomposes jamming avoidance responses into competing sensory and motor components. The sensory component captures the primary functional computation in the JAR circuit, namely an 'escape' term, $e(d)$, that depends on the *df*, $d = y - u$. The delay in the linear model fit is lumped into the computation of the *df*, $d(t-T)$, which is in turn passed into the escape term, namely $e(d(t-T))$. The motor component captures the known tendency of the pacemaker nucleus to 'return' to the pre-stimulus (baseline) EOD frequency upon removing a transiently applied jamming stimulus. The combination can be thought of as a leaky nonlinear integrator. When stimulated by a jamming signal, this model settles down to an equilibrium frequency where the sensory and motor components are equal but opposite. By further assuming that the strength of the motor return depends linearly

on the deviation from baseline, we arrive at the following model structure:

$$\tau \dot{y}(t) = -y(t) + e(d(t-T)). \tag{3.16}$$

In this equation, τ is the characteristic time constant of the return to baseline, $-y(t)$ represents the return to baseline, and $e(d(t-T))$ represents the repulsive escape. In the time domain, Eq. (3.14) is expressed as the following differential equation:

$$\dot{y}(t) = py(t) + kd(t-T), \tag{3.17}$$

with $p = -0.24$ Hz and $k = 0.38$ Hz. Upon linearizing the nonlinear dynamics in Eq. (3.16) around the baseline, $d = 0, y = 0$, we compare terms with the linear model in Eq. (3.17) and obtain the following parameters for the nonlinear model:

$$\begin{aligned} \tau &= -p^{-1} = 4.17\, s, \\ \left.\frac{\partial e}{\partial d}\right|_{d=0} &= \tau k = 1.58. \end{aligned} \tag{3.18}$$

To recover the function $e(d)$, note that if d is kept constant at d_s, Eq. (3.16) predicts that y should settle down to the equilibrium corresponding to $\dot{y} = 0$, which is $y_s = e(d_s)$. Hence the steady state values of the clamp trials determine the escape function. We can use both the final values of the static clamp trials, as well as values from the dynamic clamp trials at the end of the static clamp period, before the reference trajectory begins. Panels A and B of Fig. 3.12 show the steady state values of both static and dynamic clamp trials as a function of the clamp d, for two individuals.

For the purpose of generating theoretical predictions from our model, we fit the nonlinear escape curve, $e(d)$, using the a sum of three Gaussians (Matlab curve-fitting

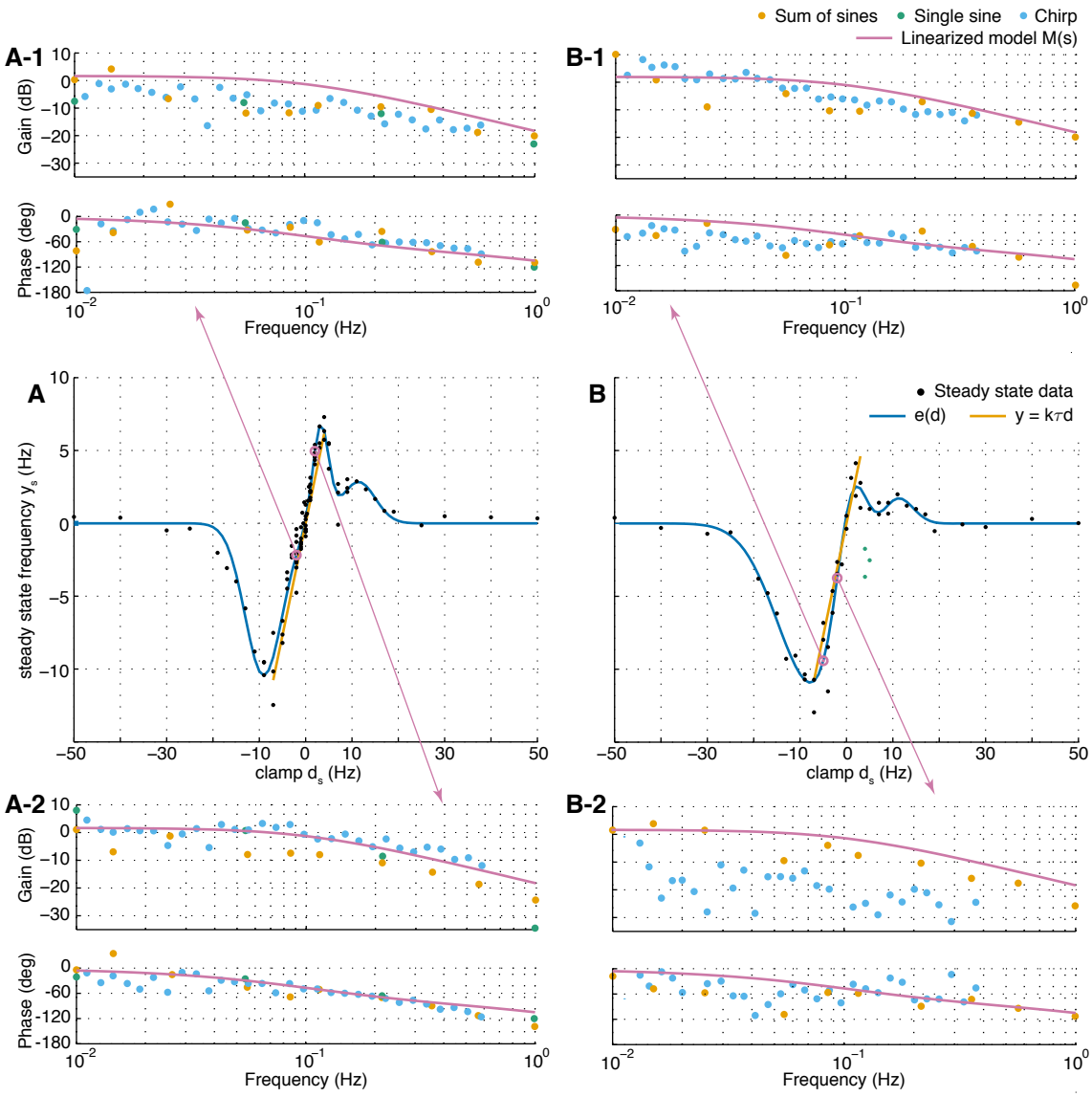

Figure 3.12: Static and dynamic clamps. (A,B) The steady state frequency, y_s (black dots), of two individuals vary nonlinearly as a function of clamped frequency difference, d_s. These data were used to fit distinct escape functions, $e(d)$ (blue curve), for each of the two distinct fish: (A) see Eq. (3.19) and (B) see Eq. (3.20). Green dots represent trials in which the fish frequency shifted in the direction of the input; these data points were removed from fitting. The linearization at origin obtained from reference-tracking trials $y = 1.58d$ is shown (orange line) to compare with the slope of $e(d)$ at the origin. (A-1,A-2,B-1,B-2) Bode plots for the dynamic clamp trials for select clamp values $d = -2.0$ (A-1) and $d = 2.0$ (A-2) for the first individual, and $d = -5.0$ (B-1) and $d = -2.0$ (B-2) for the second individual. On each bode plot, the response of the linearized model (Eq. (3.17)) is also shown (pink curve).

toolbox):

$$e(d) = 2.85e^{-\left(\frac{d-11.39}{5.12}\right)^2} + 6.71e^{-\left(\frac{d-3.26}{2.40}\right)^2} - 10.45e^{-\left(\frac{d+9.05}{5.68}\right)^2} \tag{3.19}$$

$$e(d) = 2.55e^{-\left(\frac{d-10.43}{4.98}\right)^2} + 8.70e^{-\left(\frac{d-1.08}{4.53}\right)^2} - 11.18e^{-\left(\frac{d+6.91}{11.23}\right)^2}. \tag{3.20}$$

The units for all numerical values in the above expression are s^{-1}. The Gaussian mixture approximation of $e(d)$ was somewhat arbitrarily chosen through trial and error to obtain reasonable fits that capture the basic features of the clamp data, and so no mechanistic insights can be drawn from its specific form.

The (dimensionless) slope at the origin for both curves are remarkably similar $(1.68, 1.73)$. Both slopes agree well with the predicted value of 1.58 (Fig. 3.12, orange line), particularly given that the linear system identification data used to predict the escape function slope of 1.58 was categorically different from the clamp experiments, fitting, and analytical differentiation used to determine each individual's slope. Note that three trials (Fig. 3.12, green points), for which the responses were qualitatively different than the other responses, were removed from fitting; including those trials biased the curve toward these outliers, and away from the typical behavior.

3.3.4 Dynamic clamps validate nonlinear model

As a first validation the nonlinear model, we examined the dynamic clamp trials, whose FRF should, in theory, match the prediction of the linearization of Eq. (3.16) at (d_s, y_s). We examined this prediction for two fish (see Fig. 3.12).

For our prediction, we approximated the nonlinear function $e(d)$ as a straight line through the origin, namely $y_s = \tau k d_s$. With this approximation, the FRFs should match the prediction from Eq. (3.17). The FRFs in the insets of Fig. 3.12 (A-1,A-2,B-1,B-2) show the frequency responses to dynamic clamps at two points along $e(d)$, marked in panels (A,B). The response of the linearized model is shown in all four plots and is in good agreement with the frequency responses from the clamp trials. The data shown in Fig. 3.12 were selected to most clearly illustrate the prediction, but among the experimental paradigms we use, clamp trials were the least robust and repeatable. This is evident for e.g. in Fig. 3.12B-1, where the sum-of-sines response is well predicted by the model but the chirp responses have a lower gain response.

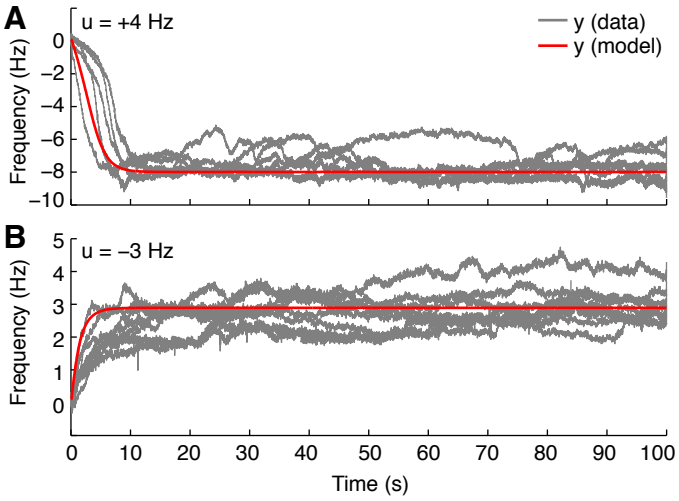

Figure 3.13: Step Responses (A) Responses of one individual to open loop steps of u = 4 Hz (gray) with the model response to the same stimulus (red). (B) Responses of the same individual to steps of u = -3 Hz (gray) with the model response to the same stimulus (red).

3.3.5 Open-loop steps validate nonlinear model

For the same two individuals for which the escape functions were fit, we simulated the model in Eq. (3.16) in response to (open-loop) step inputs. The simulated step responses matched the data from the open-loop step trials remarkably well, particularly given the qualitatively different nature of open-loop step experiments compared to the experiments used to furnish the nonlinear model. Two examples, showing all the data from one individual for steps $u = +4$ and $u = -3$ Hz, along with the model response, are shown in Fig. 3.13.

3.3.6 'Snap-through' bifurcation predicted for ramp stimuli

The model predicts that if the external stimulus frequency were slowly increased or decreased from outside the JAR range, then it should drive the fish's frequency up or down, respectively, until the fish frequency "snaps over" to the other side of the stimulus and then moves away from the stimulus in the opposite direction. Using the open-loop ramp trials (Sec. 3.2.4.3), we tested this prediction of the model.

We now describe the model's snap-through prediction in more detail. Assuming $u(t) =$ constant, the solution(s) to $y(t) = e(u - y(t))$ are the equilibria of the system, i.e. the intersections of functions y and $e(u - y)$. The stability of the equilibrium depends on the derivative of the vector field on the right-hand-side of Eq. (3.16) with

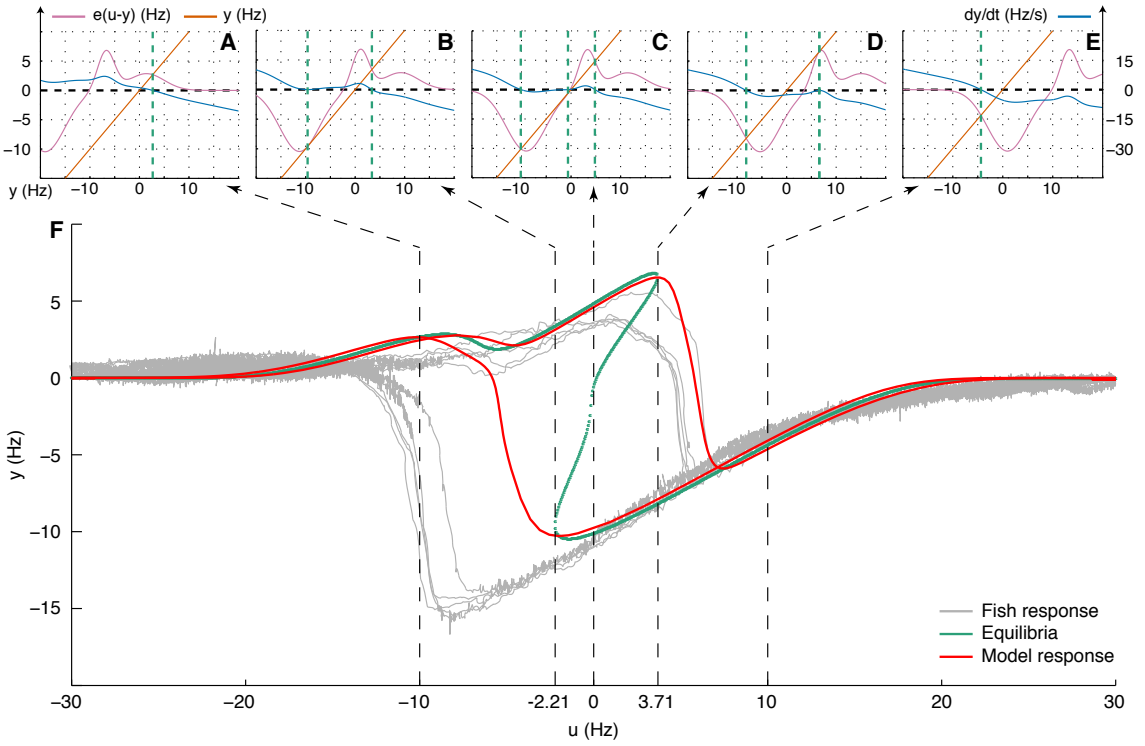

Figure 3.14: Snap-through bifurcation of the dynamics $\dot{y}(t) = \tau^{-1}(e(y(t-T) - u(t-T)) - y(t))$. (A-E) The right-hand-side of the dynamics (blue, right axis) is the scaled difference between two components, $e(y-u)$ (pink, left axis) and y (orange, left axis). The intersection points of y and $e(y-u)$ comprise the equilibrium frequencies (green dashed lines), corresponding to $dy/dt = 0$. The graphs in (A-E) correspond to five distinct values of u, indicated by the black dashed lines originating in Panel (F). (F) As the stimulus, $u(t)$, was ramped linearly up or down from ± 30 Hz, the fish response (gray curves) initially followed the nearest stable equilibrium. For frequencies between approximately -2.21 and 3.71 there are three possible equilibria (green curve); the center branch is unstable. When the input reached a bifurcation frequency, the output "snapped through" to the only remaining equilibrium, as predicted by the model output (red curve). The general hysteretic structure of the responses is well captured by the model.

respect to y: if the derivative is negative, positive or zero the equilibrium is stable, unstable, or a saddle–point, respectively. The subplots along the top in Fig. 3.14 decompose the vector field at different values of u that produce qualitatively different nonlinear dynamics in the sense that the number and type of equilibria change. Assuming u changes sufficiently slowly, the dynamics should track the nearest stable equilibrium.

The number and type of equilibria depend explicitly on the structure of the escape function $e(d)$ (where, recall, $d = u - y$). For the specific fit of $e(d)$ in Fig. 3.12(A) we tested the predictions of the nonlinear model. For this escape function the dynamics are punctuated by two bifurcation points at critical levels of the stimulus input, namely $u \approx -2.21$ and $u \approx 3.69$. For constant stimuli below -2.21 there is one equilibrium (Fig. 3.14A). The single equilibrium (green dotted line) here is stable, since $\dot{y}$ crosses from positive to negative at the equilibrium. At the critical level $u \approx -2.21$, an additional equilibrium is introduced, namely a saddle–node (Fig. 3.14(B)). For $-2.21 < u < 3.69$, one stable and one unstable equilibrium branch out of the saddle–node, while the original stable equilibrium persists; thus in this region there are three equilibrium (Fig. 3.14(C)). But, at $u = +3.69$ the unstable branch intersects with the original stable branch creating a saddle–node (Fig. 3.14(D)), which vanishes for $u > 3.69$, leaving just one lower stable equilibrium (Fig. 3.14(E)). The locus of equilibria at each u is shown in Fig. 3.14(F) (green curve); note that the middle branch of this inverted s-shaped curve is the unstable branch.

We simulated the dynamics for increasing and decreasing ramps between -30 and $+30$ Hz. We started the simulation with an initial condition of $y(0) = 0$, which was near the only equilibrium for the initial values of $u = \pm 30$ Hz. The red curve in Fig. 3.14 shows that, indeed, at each time t, $y(t)$ remained near the closest stable equilibrium point until the output $y(t)$ "snaps through" to the other branch. This occurs when the input $u(t)$ reaches a saddle–node bifurcation. In case of the increasing ramp from -30, both the simulated (red) and actual (grey, multiple trials) $y(t)$ tracked the stable equilibrium on the upper branch of green curve in Fig. 3.14(F), even as the two additional equilibria are introduced at the bifurcation point of $u \approx -2.21$. Eventually, the unstable equilibrium combines with the stable equilibrium that $y(t)$ is tracking, causing both of them to vanish after forming a saddle–node. At that point, the closest (and only) stable equilibrium is the continuation of the lower branch, which causes $y(t)$ to "snap through", ultimately converging to the remaining equilibrium. The responses to decreasing ramps (which follow the lower equilibrium branch for both model and data) exhibit the same qualitative behavior, although the snap-through for the actual data are delayed relative to the model. The overshoot of the model is indicative that either $e(d)$ was underestimated in $d > 0$, or there is a velocity dependence on d that we are not capturing with our first-order model.

Chapter 4

The Social Envelope Response in *Eigenmannia*

Recent studies have shown that central nervous system neurons in weakly electric fish respond to artificially constructed electrosensory envelopes, but the behavioral relevance of such stimuli is unclear. In this chapter, we investigate the possibility that social context creates envelopes that drive behavior. When *Eigenmannia virescens* are in groups of three or more, the interactions between their pseudo-sinusoidal electric fields can generate social envelopes. We developed a simple mathematical prediction for how fish might respond to such social envelopes. To test this prediction, we measured the responses of *E. virescens* to stimuli consisting of two sinusoids, each outside the range of the Jamming Avoidance Response (JAR), that when added to the fish's own electric field produced low-frequency (below 10 Hz) social envelopes.

Fish changed their electric organ discharge (EOD) frequency in response to these envelopes, which we have termed the Social Envelope Response (SER). In 99% of trials, the direction of the SER was consistent with the mathematical prediction. The SER was strongest in response to the lowest initial envelope frequency tested (2 Hz) and depended on stimulus amplitude. The SER generally resulted in an increase of the envelope frequency during the course of a trial, suggesting that this behavior may be a mechanism for avoiding low-frequency social envelopes. Importantly, the direction of the SER was not predicted by the superposition of two JAR responses: the SER was insensitive to the amplitude ratio between the sinusoids used to generate the envelope, but was instead predicted by the sign of the difference of difference frequencies.

4.1 Introduction

Weakly electric fish generate an electric organ discharge (EOD) that results in an electric field that surrounds the fish's body. In *Eigenmannia*, the EOD is quasi-sinusoidal and when fish are in close proximity ($\sim$ 1 m or less) their EODs interact. In the case of two nearby conspecifics, the combined EOD signal has a specific combination of amplitude and phase modulations, termed the beat. If there are more than two nearby conspecifics or relative movements between conspecifics, the combined EOD signal contains modulations of the beat, which has been termed the electrosensory

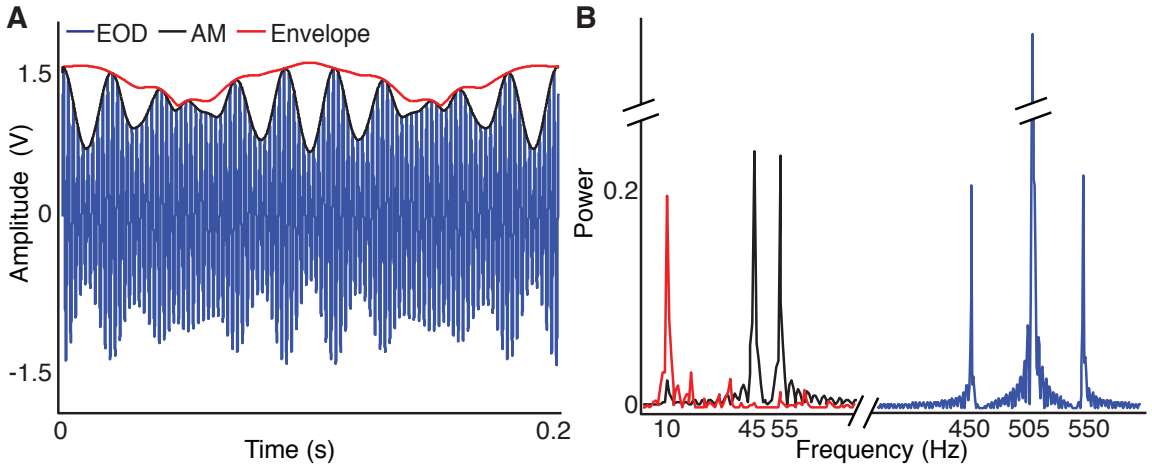

Figure 4.1: Social electrosensory envelopes. (A) A signal (blue) which is the sum of three sinusoids, S_1, S_2, and S_3, with amplitudes $a_1 = 1$ V, $a_2 = 0.3$ V, and $a_3 = 0.3$ V, and at frequencies of $f_1 = 505$ Hz, $f_2 = 450$ Hz, and $f_3 = 550$ Hz respectively. The interactions of these stimuli create a beat which has an amplitude modulation (AM; black), which can be extracted from the signal using a Hilbert transform. Because the $a_1 \gg a_2$ and $a_1 \gg a_3$, a well-defined envelope emerges (red) that can be extracted from the AM using a Hilbert transform. (B) Power spectra of the signal (blue), the AM (black) and the envelope (red). The two peaks of the AM correspond to the $|df|$ values at 45 and 55 Hz and the peak of the envelope corresponds to the $|ddf|$ at 10 Hz.

envelope [60]. The interactions of two EODs have been well studied in relation to the Jamming Avoidance Response (JAR). When two nearby conspecifics have EOD signals S_1 and S_2 at frequencies of f_1 and f_2, respectively, the combined signal, $S_1 + S_2$, has a emergent beat. The AM of this beat oscillates at the frequency difference, $|df|$, where $df = f_2 - f_1$. When two neighboring *Eigenmannia* have EODs of similar frequency (e.g. 500 and 505 Hz, with $|df| = 5$ Hz) they perform the JAR, during which each fish will raise or lower their individual EOD frequency to increase $|df|$, and thus the beat frequency. When there are three or more EOD signals it is possible that fish are responding not only to the beat but also to the emergent envelope. Here we define a *social envelope* as the modulation of the AM of the beat that occurs when at least three EODs are added. For example, if there are three EOD signals, S_1, S_2 and S_3, at frequencies f_1, f_2 and f_3, respectively, the combined signal $S_1 + S_2 + S_3$ can have an AM; the magnitude of this AM also fluctuates over time, referred to here as the envelope of the AM (Fig. 2.1A) (see Sec. 2.3). Thus, it is possible that even with high $|df|$ values there could be a low-frequency envelope (as shown in Fig. 2.1). Understanding the behavioral relevance and sensory processing of envelope information has proven challenging in part because the extraction of envelope information requires nonlinear processing (Fig. 2.1B; see Sec. 2.4). However, recent neurophysiological studies already identified envelope-related neural activity at each level from the receptor afferents to the midbrain in weakly electric fish [52, 55, 59, 60, 70], suggesting that not only can the fish extract envelope information but there might also

be behavioral relevance of these signals for the animals.

4.2 Model-based prediction of the social envelope response

The beauty of the JAR is that the behavioral response can be predicted based on a simple algorithm [33]. For the fish to shift its EOD frequency in the 'correct' direction (e.g. the direction that increases $|df|$), the fish must be able to compute the sign of the df. The fish does this without an efference copy of its own EOD [16] using amplitude and phase modulation information measured across the body (e.g. multiple electroreceptors) [58].

In Chap. 2, I described how the JAR computation is diagrammatically represented as a Lissajous figure in the amplitude-phase plane (Fig. 2.4A), which was pioneered by Heiligenberg and Bastian [35] and has been verified through electrophysiological recordings [6]. The plot is the magnitude (x-axis) versus the phase (y-axis) of the complex representation of the combined signal (see Sec. 2.5). The Lissajous trajectory will rotate clockwise for negative df and counter-clockwise for positive df at a frequency of $|df|$. The direction of rotation of the Lissajous predicts the direction that the fish will shift its EOD during the JAR.

When three sinusoids (or EODs) interact, beats emerge at each of the $|df|$ values, and the Lissajous is more complicated (Fig. 2.4B). For example, if there are three

EOD signals, S_1, S_2 and S_3, at frequencies f_1, f_2 and f_3, there will be beats at the magnitudes of the following df values: $df_2 = f_2 - f_1$, $df_3 = f_3 - f_1$ and $df_1 = f_3 - f_2$. However, the signal measured by each fish is typically dominated by its own EOD. So, for fish 1 the signal S_1 dominates the others (S_2 and S_3) and correspondingly, the beats at $|df_2|$ and $|df_3|$ dominate the beat at $|df_1|$. In this case, the beat at $|df_1|$ can be considered negligible, and the dominant envelope frequency emerges at $ddf = |df_3| - |df_2|$ (see Eq. (2.18)). Note that ddf is a signed quantity, which is important to the predictions stated below.

In this chapter, we hypothesize that the JAR circuit can be extended to predict a behavioral response to signals outside the range of the JAR that nevertheless generate low-frequency envelopes. In some cases, two conspecific signals (S_2 and S_3) when added to S_1 produce a low-frequency envelope (see Sec. 2.4.1.1). Two such cases are depicted in Fig. 2.4B - positive and negative ddf. At first glance, the 'floral' pattern of the Lissajous seems to lack a consistent rotation. However, each of the 'petals' precesses in a direction corresponding to the sign of the ddf, at frequency $|ddf|$ (see Sec. 2.5). Upon low-pass filtering of both the amplitude and phase signals, the petals are filtered out and the general, slow precession emerges (Fig. 2.4C).

Interestingly, as the amplitude ratio between the signals is inverted, the direction of rotation of individual petals flips, but the direction of the precession remains unchanged. Does the fish respond to the direction of the petals (df values and amplitude ratio) or the precession (ddf)? When the df values are within the JAR range the re-

sponse of the fish follows the petals [63]. But what happens when the df values are outside the JAR range? We hypothesize that fish respond to the emergent envelope at the $|ddf|$, governed by the precession as revealed by the low-pass filtered model (see Sec. 2.5). If, as our model predicts, the fish uses a downstream low-pass filter from the JAR circuit to extract envelope information, it could drive a behavioral Social Envelope Response (SER) much like the JAR to beat stimuli.

4.3 Materials and methods

Adult *Eigenmannia virescens* ($10 - 15$ cm in length) were obtained through a commercial vendor and housed in aquarium tanks with a water temperature of $27°C$ and conductivity in the range of $150 - 300\mu$S / cm [37]. All fish used in these experiments were housed in social tanks that contained two to five individuals. These experiments were conducted at the Johns Hopkins University between 2009 and 2012. All experimental procedures were approved by the Johns Hopkins Animal Care and Use Committee and followed guidelines established by the National Research Council and the Society for Neuroscience.

4.3.1 Experimental procedure

Each individual fish ($N = 4$) was transferred to the testing tank ($27 \pm 1°C$ and $175 \pm 25\mu S/cm$) and allowed to acclimate for $2 - 12h$ before experiments began.

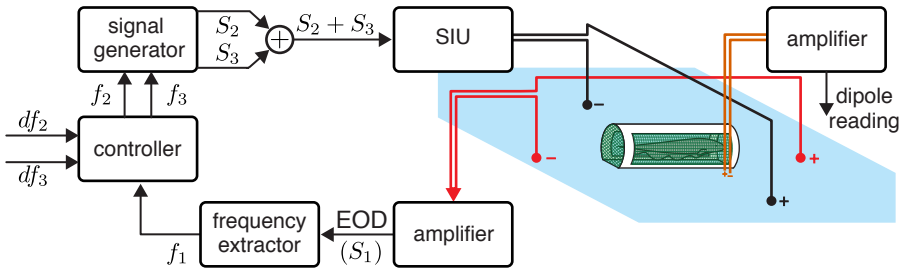

Figure 4.2: The fish's EOD is recorded via head-tail electrodes (red) and amplified. Stimuli to the fish are applied via transverse electrodes (black). Stimuli consist of a single sinusoid (S_2) or a sum of two sinusoids (S_2+S_3). The frequency of the recorded EOD is extracted (f_1), and a controller adds the stimulus values of df_2 and df_3 to f_1 to produce output frequencies f_2 and f_3, respectively. The signal generator produces sinusoids S_2 and S_3 at frequencies f_2 and f_3. S_2 and S_3 are added, and applied to the tank through a stimulus isolation unit (SIU). A dipole with 1 cm spacing (orange) was used to measure the local electric field, and this measurement was amplified and recorded independently.

During the acclimation period a second fish was also in the testing tank, to provide recent social experience, but was removed before the start of the experiment. For testing, the experimental fish was restricted in a chirp chamber to prevent movement. Experiments were started when the EOD frequency did not change by more than ± 1 Hz for at least 25 consecutive minutes, which typically took $1-3$ h.

Trials were presented across multiple testing blocks that lasted $1-3$ h and were completed on different days. Between testing sessions the fish was returned to its home tank to reduce changes in response due to motivation, fatigue or other unknown factors. If the EOD responses of the fish deteriorated over the course of testing the fish was placed back in the home tank for $1-5$ days and then re-tested.

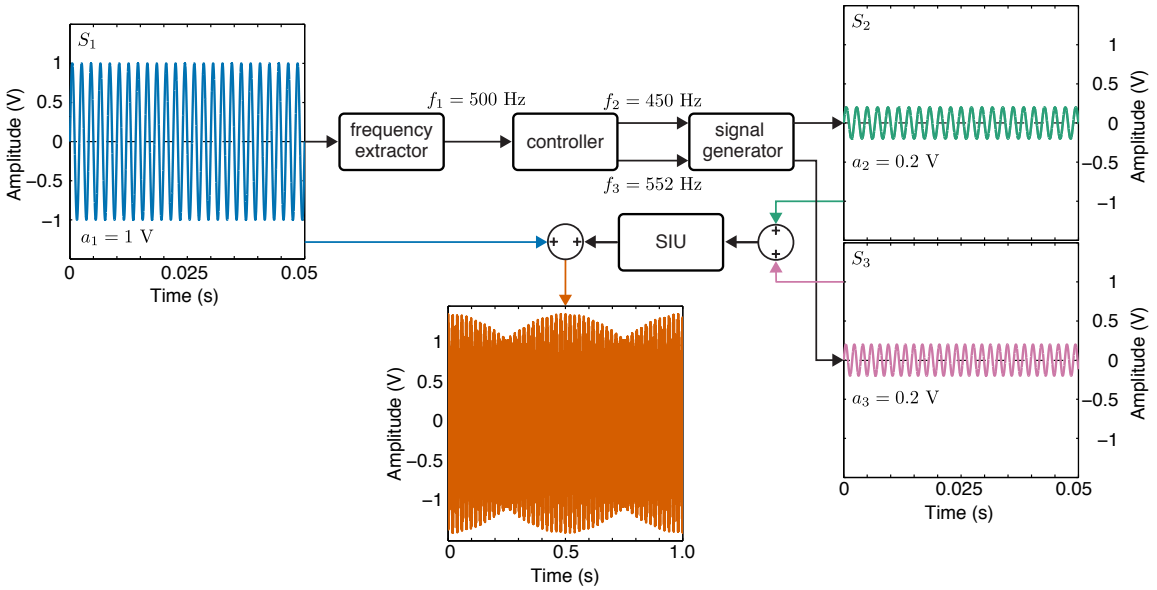

Figure 4.3: Illustration of stimulus generation in envelope experiments. A sinusoid represents the fish EOD (S_1) with amplitude $a_1 = 1$ V. The frequency $f_1 = 500$ Hz is extracted and the controller uses $df_2 = -50$ Hz and $df_3 = +52$ Hz to compute input frequencies $f_2 = 450$ Hz and $f_3 = 552$ Hz. The signal generator produces sinusoids S_2 and S_3 at these frequencies, with the same amplitude, $a_2 = a_3 = 0.2$ V. The signals are added and sent to the stimulus isolation unit (SIU), which introduces the combined signal into the water. The three signals interact in the water to produce a combined signal (orange) with a 2 Hz social envelope.

4.3.2 Experimental setup

The chirp chamber was positioned such that the fish was located in the middle of two electrodes (head-to-tail) separated by 25 m (Fig. 4.2, red electrodes), used to record the EOD. All stimuli were applied into the tank via transverse electrodes separated by 25 cm with the fish located in the middle (Fig. 4.2, black electrodes). A 1 cm transverse dipole (Fig. 4.2, yellow electrodes) adjacent to the head of the fish measured the local electric field, which was used to estimate stimulus amplitude.

At the start of each trial the initial EOD frequency of the fish (f_{1i}) was extracted. All trials within a testing block were presented randomly for each fish. Each trial lasted 200 s with an inter-trial interval of 200 s. For each trial, the fish was presented with a stimulus that was either a single sinusoid (control trials; S_2) or a sum of two sinusoids (envelope trials; $S_2 + S_3$). For the envelope trials, the frequencies of the individual sinusoids (f_2 and f_3) were calculated by adding a specified initial frequency difference (df_i) to f_{1i}, i.e. $f_2 = f_{1i} + df_{2i}$ and $f_3 = f_{1i} + df_{3i}$. Thus S_2 and S_3 were generated as:

$$\begin{aligned} S_2 &= a_2 \sin\left(\int_0^t f_2 dt\right) = a_2 \sin\left((f_{1i} + df_{2i})t\right), \\ S_3 &= a_3 \sin\left(\int_0^t f_3 dt\right) = a_3 \sin\left((f_{1i} + df_{3i})t\right), \end{aligned} \tag{4.1}$$

where a_2 and a_3 are the amplitudes of applied signals S_2 and S_3 (see Fig. 4.3). For control trials, only S_2 was calculated and applied. The frequencies f_2 and f_3 were held constant, i.e. not clamped to f_1, so changes in the fish's EOD frequency results in changes in the value of each df and the ddf.

4.3.3 Experimental stimuli

4.3.3.1 Control trials

All fish completed trials ($N = 20$) with a single sinusoid stimulus (S_2) at a specified high $|df|$ (> 40 Hz). The initial df values used were ± 52, 58, 72, 78, 92 and 98 Hz, which are outside the range of frequencies known to elicit the JAR. These df values were a subset of those used to create the envelope stimuli in other trials (see below). For all control trials the stimulus amplitude was $a_2 = 0.74$ mV/cm and the stimulus amplitude ramp time was 20 s.

4.3.3.2 Amplitude trials

All fish completed trials ($N = 10$), with a sum of two sinusoids ($S_2 + S_3$) that produced a ddf_i of ± 4 Hz. The initial df values used were ± 48 and ± 52, such that there were two trial types: $df_{2i} = -48$ and $df_{3i} = +52$ or $df_{2i} = -52$ and $df_{3i} = +48$, which resulted in a $+4$ Hz and a -4 Hz envelope, respectively. These trials were repeated at five different combined stimulus amplitudes ($a_2 = a_3$, $a_2 + a_3 = 0.15$, 0.45, 0.74, 1.05 and 1.34 mV/cm) with a ramp time of 20 s.

4.3.3.3 Envelope trials

All fish completed trials ($N = 48$) with a sum of two sinusoids ($S_2 + S_3$) that produced a specified ddf_i. Trials were completed with $df_{2i} = \pm 50$, ± 70 or ± 90 with

df_{3i} sweeping from $-df_{2i} - 8$ to $-df_{2i} + 8$ at intervals of 2 Hz. For example, for $df_{2i} = 50$, df_{3i} was set at each of the following values for individual trials: -58, -56, -54 or -52 (resulting in initial ddf values of -8, -6, -4 and -2 Hz) or -48, -46, -44 and -42 (resulting in initial ddf values of 2, 4, 6 and 8 Hz). For trials where $df_{2i} = -50$, the df_{3i} values were the same as the above example, except with a positive sign. This was repeated for $df_{2i} = \pm 70$ and ± 90, resulting in trials with ddf_i values from -8 to $+8$ in increments of 2 Hz (excluding 0), produced by df values of varying frequencies. All trials were completed with $a_2 = a_3$, a combined stimulus amplitude of $a_2 + a_3 = 0.74$ mV/cm and a ramp time of 20 s.

4.3.3.4 Ramp-time trials

One fish completed trials ($N = 30$) with a sum of two sinusoids ($S_1 + S_2$), where three amplitude ramp times were tested (1, 20 and 100 s). Each ramp time was repeated for two envelope frequencies ($+4$ Hz: $df_{2i} = -48$, $df_{3i} = +52$; and -4 Hz: $df_{2i} = -52$, $df_{3i} = +48$) and five stimulus amplitudes ($a_2 = a_3$, $a_2 + a_3 = 0.15$, 0.45, 0.74, 1.05 and 1.34 mV/cm).

4.3.3.5 Ratio trials

One fish completed trials ($N = 10$) with a sum of two sinusoids ($S_2 + S_3$), where the relative amplitudes of each individual component were varied at a ratio of $a_2 : a_3 = 1:1$, $1:3$, $2:3$, $3:2$ and $3:1$ for envelopes of $+4$ Hz ($df_{2i} = -48$, $df_{3i} = +52$)

and -4 Hz ($df_{2i} = -52$, $df_{3i} = +48$).

4.3.4 Data analysis

For each trial the recorded EOD was used to compute the EOD frequency as a function of time, $f_1(t)$. This was achieved via post-processing with a custom script in MATLAB (MathWorks, Natick MA, USA) that computed the spectrogram of the recorded signal and determined $f_1(t)$ as the frequency with the highest power near the fish's baseline EOD frequency. The baseline f_{1i} was measured at the start of each trial using a frequency-to-voltage (F2V) converter (FV-1400, Ono-Sokki, Yokohama, Japan). For 60 trials the output of the F2V converter was verified against post-experiment Fourier analysis. The error between the two measurements was negligible (mean $\pm$ s.d. $= 0.0008 \pm 0.054$ Hz). f_1 stabilized by the last 60 s of each trial; f_{1f} is the mean frequency measured over this period. The change in frequency was calculated as $\Delta f_1 = f_{1f} - f_{1i}$.

For each trial, Δf_1 was normalized to the individual fish's maximum response, $|\Delta f_{1max}|$, to allow responses to be compared across fish. Because fish could raise or lower their EOD frequency, some measures are normalized as $|\Delta f_1|/|\Delta f_{1max}|$. Dependent measures were analyzed using one-way repeated-measures ANOVA. For significant main effects, effect size (ηp^2) is given to allow comparison between measures. Additionally, post hoc Tukey's honestly significant difference (HSD) tests were run on each significant main effect. We indicate the critical value (Q_{crit}) for each test and

provide the obtained values (Q_{obt}) only for those that were statistically significant (i.e. greater than the critical value).

4.4 Results

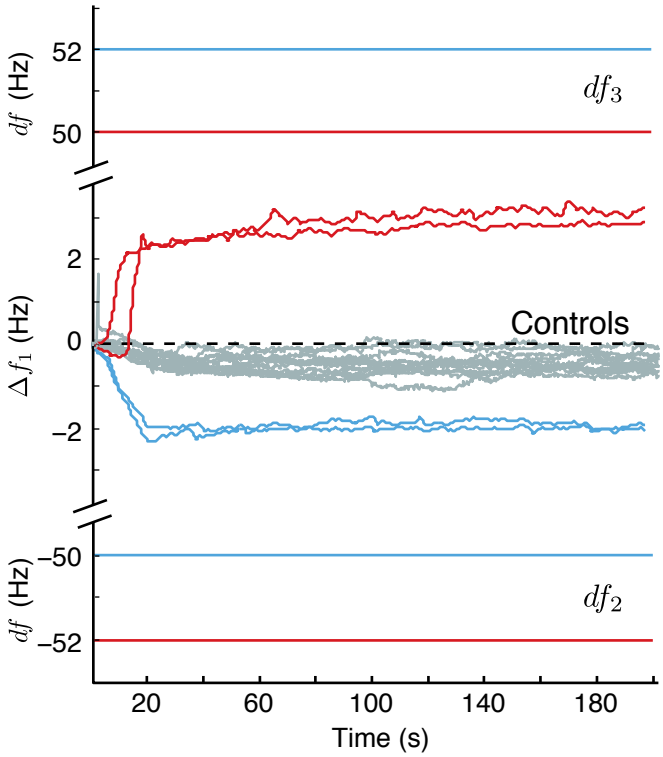

Figure 4.4: *Eigenmannia virescens* do not show a change in EOD frequency (Δf_1) when stimulated with a single sinusoid with $|df| > 50$ Hz (control; gray). The fish respond to sums of two sinusoids that contain a low-frequency envelope. Two trial types are shown, where $df_2 = -50$ and $df_3 = +52$ (+2 Hz envelope; blue lines) and where $df_2 = -52$ and $df_3 = +50$ (−2 Hz envelope; red lines). The fish shift their frequency down for positive envelopes (blue trials) and up for negative envelopes (red trials).

4.4.1 EOD frequency changes were not elicited by high $|df|$ values

To ensure that observed responses were not due to the individual *df* values, we conducted control trials where fish were presented with a single sinusoid stimulus that had a high $|df|$. We measured Δf_1 during the last 60 s of the inter-trial interval and found that the EOD frequency was stable without stimulation (mean ± s.e.m. $= 0.05 \pm 0.006$ Hz). In addition, Δf_1 across the first 10 s (0.23 ± 0.03 Hz) and the last 60 s (0.52 ± 0.04 Hz) of control stimulus presentation produced only nominal changes to the EOD frequency. Responses to all control trials by a single fish are shown in Fig. 4.4. Thus, it is unlikely that the observed Δf_1 to the sum of sinusoid stimuli (which has an emergent envelope) was due to a response to any individual component alone.

4.4.2 Fish exhibited an SER

The sum of two sinusoid stimuli ($S_2 + S_3$) elicited changes in EOD frequency. Fig. 4.4 shows a characteristic SER of a single fish to two replicates of a +2 Hz envelope ($df_2 = -50, df_3 = +52$; blue) and two replicates of a −2 Hz envelope ($df_2 = -52, df_3 = +50$; red). The figure shows that the envelope response differs from the response observed to control stimuli (gray).

Across all fish, responses to control stimuli were minimal (range = 0.05 to 0.74 Hz)

compared with the SERs (range = 1 to 4 Hz). Moreover, the time course of EOD change during control trials was much larger than the time course of the SER, which corresponded to the stimulus ramp time (20 s). In addition, responses to control trials were biased downward, while the SERs were bidirectional. The direction of the SER shows that the fish shifts its EOD frequency down when the envelope frequency (*ddf*) is positive and up when the envelope frequency is negative. The direction of the SER was typically opposite the sign of the *ddf*, resulting in the EOD shifting towards the closer *df* (although the final $|df|$ values were 40 Hz or above).

4.4.3 SER was stronger for lower-frequency envelopes

Fish changed f_1 in response to sum-of-sinusoid stimuli that created initial envelopes in the frequency range of $|ddf_i| = 2$ to 8 Hz as illustrated for a single fish in Fig. 4.5. The figure also illustrates that Δf_1 is qualitatively similar across all *df* values used. However, the strength of the SER (the change in EOD frequency during a trial) is dependent upon on $|ddf_i|$ (Fig. 4.6A). The effect of the initial absolute envelope frequency, $|ddf_i|$, on the normalized absolute EOD frequency change, $|\Delta f_1|/|\Delta f_{1max}|$, was significant ($F_{3,9} = 6.45, P = 0.04, \eta p^2 = 0.68$). Normalized $|\Delta f_1|$ is generally smaller as a function of larger initial *ddf*: mean $\pm$ s.e.m. $= 0.59 \pm 0.04$ for 2 Hz, 0.52 ± 0.03 for 4 Hz, 0.34 ± 0.03 for 6 Hz and 0.39 ± 0.04 for 8 Hz. The only significant

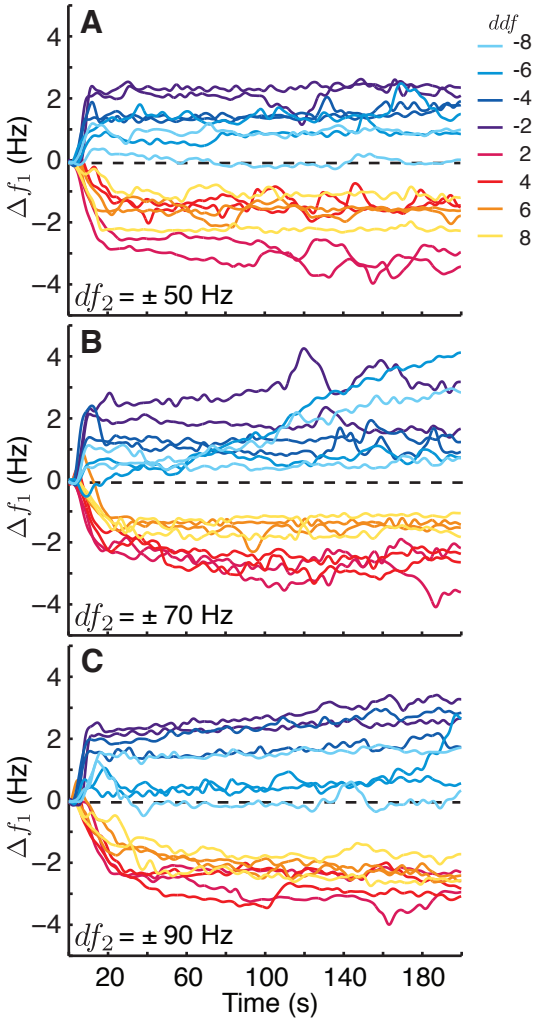

Figure 4.5: The Social Envelope Response (SER) is dependent on *ddf* and not *df*. In each panel, the initial *ddf* was varied from −8 to +8 Hz in 2 Hz intervals (excluding 0). (A) $df_2 = \pm 50$ Hz, (B) $df_2 = \pm 70$ Hz and (C) $df_2 = \pm 90$ Hz. The strength and direction of SER responses was dependent on the *ddf*. In contrast, fish show no systematic differences in responses to *ddf* values as a function of the range of df_2 and df_3 values used.

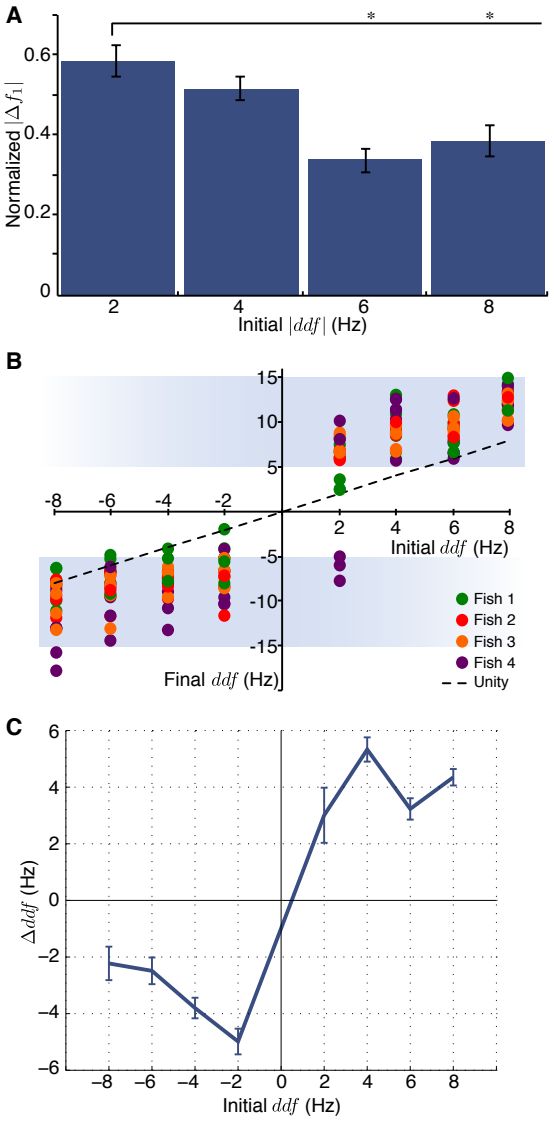

Figure 4.6: SER strength as a function of initial ddf. (A) Normalized $|\Delta f_1|$ (1 indicates greatest response, 0 indicates lowest response) was significantly greater when the initial $|ddf|$ was lower. (B) The f_1 generally shifted in the predicted direction for all fish (colored circles). For most responses, the final envelope frequency was greater than the initial envelope frequency. This is visualized on the plot when the magnitude of the data point is greater than the unity (dashed line). In the three trials that did not go in the predicted direction (purple circles, bottom right), the fish nevertheless increased the envelope by having a stronger response but in the opposite direction. Final $|ddf|$ values were typically between 5 and 15 Hz (shaded band). (C) The change in envelope frequency ($\Delta ddf = |ddf_f| - |ddf_i|$) as a function of ddf_i. The $|\Delta ddf|$ was generally decreased for initial envelopes that were higher in frequency.

pairwise differences (Tukey's HSD, $Q_{crit} = 4.41$) were between the lowest envelope frequency (2 Hz) and those higher than 6 Hz (2 Hz versus 6 Hz: $Q_{obt} = 4.45$; 2 Hz versus 8 Hz: $Q_{obt} = 5.51$; Fig. 4.6A, asterisks). The rest of the pairwise comparisons were not significant ($Q_{obt} < 4.41$).

4.4.4 SER increased the envelope frequency

Fish changed f_1 in response to initial envelope stimuli, which resulted in a change in the envelope frequency (Fig. 4.6B). In general, the final absolute envelope frequency settles in the range of $5 - 15$ Hz (mean $\pm$ s.e.m. $= 8.87 \pm 0.20 Hz$). The change in envelope frequency ($\Delta ddf = |ddf_f| - |ddf_i|$) as a function of ddf_i is shown in Fig. 4.6C. We found a significant effect of the initial envelope frequency ($|ddf_i|$) on the Δddf ($F_{3,9} = 6.32, P = 0.01, \eta p^2 = 0.68$) such that the change in envelope frequency, $|\Delta ddf|$, was smaller as a function of larger $|ddf_i|$: mean $\pm$ s.e.m. $= 4.78 \pm 0.68$ for 2 Hz, 4.57 ± 0.51 for 4 Hz, 2.86 ± 0.36 for 6 Hz and 3.29 ± 0.59 for 8 Hz. The only significant pairwise differences (Tukey's HSD, $Q_{crit} = 4.41$) were between 2 and 6 Hz ($Q_{obt} = 5.05$) and between 4 and 6 Hz ($Q_{obt} = 4.50$), where the change in envelope frequency was greater for the lower initial envelope frequency in each pair.

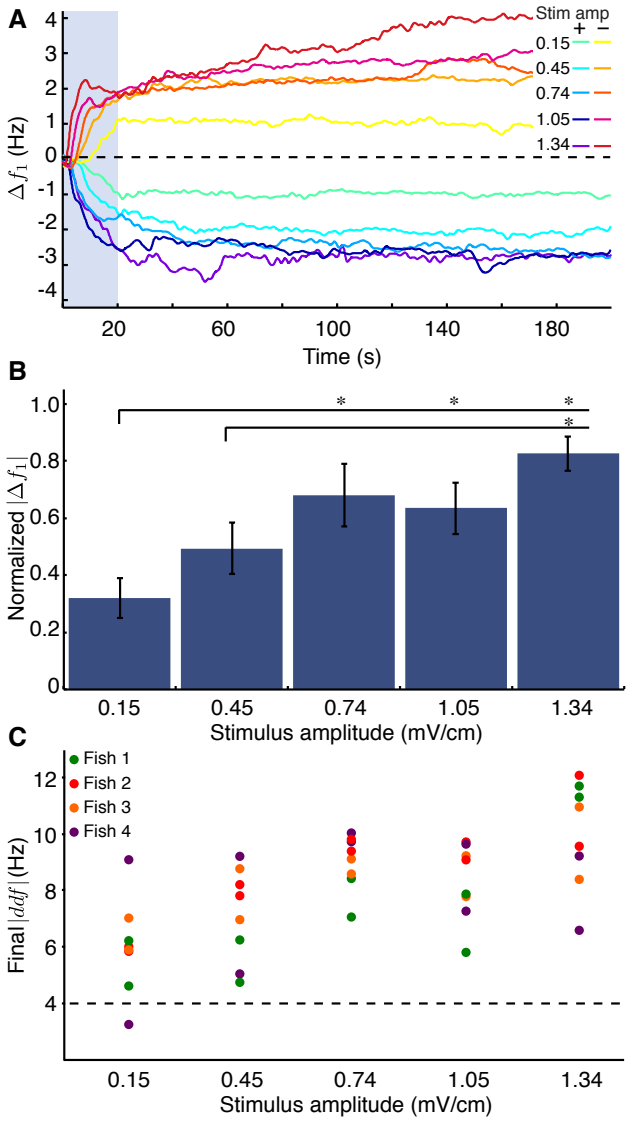

Figure 4.7: SER as a function of stimulus amplitude. (A) EOD frequency traces showing that the strength of the Δf_1 increases as the stimulus amplitude $a_2 + a_3$ was increased from 0.15 to 1.34 mV/cm. The light blue box indicates the period (ramp time) over which the stimulus amplitude was increased from zero to its final value. (B) There was a significant effect of the stimulus amplitude on the strength of the EOD frequency change where stronger responses were observed for higher stimulus amplitudes. (C) The final $|ddf|$ was significantly higher in frequency for larger stimulus amplitudes, across individuals (color-coded).

4.4.5 SER depended on stimulus amplitude and not the rate of amplitude change

The strength of the SER, measured by the magnitude $|\Delta f_1|$, increased as a function of combined stimulus amplitude $a_2 + a_3$ (shown for one fish in Fig. 4.7A). The effect of stimulus amplitude on the normalized $|\Delta f_1|$ was significant ($F_{4,12} = 7.16, P = 0.02, \eta p^2 = 0.71$; Fig. 4.7B). The change in frequency, $|\Delta f_1|$, was generally larger for larger stimulus amplitudes: mean $\pm$ s.e.m. $= 0.32 \pm 0.07$ for 0.15 mV/cm, 0.49 ± 0.09 for 0.45 mV/cm, 0.68 ± 0.11 for 0.74 mV/cm, 0.63 ± 0.09 for 1.05 mV/cm and 0.83 ± 0.06 for 1.34 mV/cm. There were significant pairwise differences (Tukey's HSD, $Q_{crit} = 4.21$) between the lowest stimulus amplitude (0.15 mV/cm) and those higher than 0.74 mV/cm (0.15 versus 0.74: $Q_{obt} = 5.16$; 0.15 versus 1.05: $Q_{obt} = 4.49$ and 0.15 versus 1.34: $Q_{obt} = 7.20$) and between the second lowest stimulus amplitude (0.45 mV/cm) and the highest stimulus amplitude (0.45 versus 1.34: $Q_{obt} = 4.73$; Fig. 4.7B, asterisks). Other pairwise comparisons were not significant ($Q_{obt} < 4.20$). The effect of stimulus amplitude on final $|ddf_f|$ was significant ($F_{4,12} = 7.99, P = 0.04, \eta p^2 = 0.73$; Fig. 4.7C). There was a significant pairwise difference (Tukey's HSD, $Q_{crit} = 4.20$) between the lowest stimulus amplitude (0.15 mV/cm) and those higher than 0.74 mV/cm (0.15 versus 0.74: $Q_{obt} = 5.25$; 0.15 versus 1.05: $Q_{obt} = 4.71$; and 0.15 versus 1.34: $Q_{obt} = 7.65$) and between the second lowest stimulus amplitude (0.45 mV/cm) and the highest stimulus amplitude

(0.45 versus 1.34: $Q_{obt} = 4.83$). Other pairwise comparisons were not significant ($Q_{obt} < 4.20$).

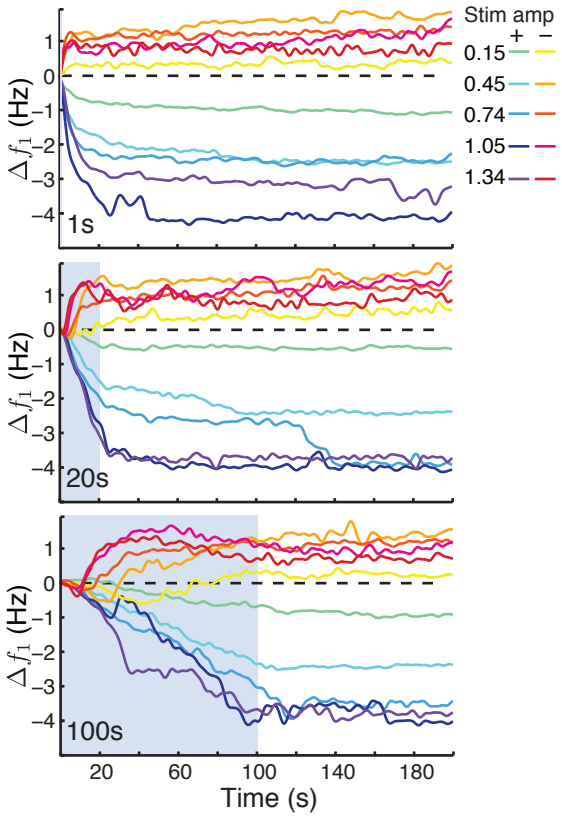

Figure 4.8: The strength of the SER was determined by the final stimulus amplitude value and not the rate of change of amplitude. This was observed by comparing data for one individual fish across multiple stimulus amplitude ramp times (1, 20 and 100 s). The initial time course of the behavior increased as the ramp time increased, but the final change in EOD frequency is equivalent across all ramp times.

In data from one fish, differences in ramp time did not effect the strength of the SER, $|\Delta f_1|$ (Fig. 4.8). Thus, the SER strength depended on the amplitude of the stimulus, but not on the rate of change of amplitude.

4.4.6 SER did not switch direction with changes in amplitude ratio

For a given df_2 and df_3 pair, the relative amplitudes of S_2 and S_3 determine the rotation of the 'petals' of the Lissajous but not the general precession. As can be seen for $ddf = -4$ Hz the petals rotate counter-clockwise for ratios $a_2 : a_3 = 1 : 3$ and $2 : 3$, and clockwise for $1 : 1$, $3 : 1$ and $3 : 2$, but the graph precesses clockwise in all cases (Fig. 4.9, top).

Similarly, for $ddf = +4$ Hz the petals rotate clockwise for ratios $a_2 : a_3 = 3 : 1$ and $3 : 2$ and counter-clockwise for $1 : 1$, $1 : 3$ and $2 : 3$, but the graph precesses counter-clockwise in all cases (Fig. 4.9, bottom). We examined the sign of SER, measured by the sign of Δf_1 in response to different stimulus amplitude ratios $a_2 : a_3$ ($1 : 1$, $1 : 3$, $2 : 3$, $3 : 2$ and $3 : 1$) for $ddf = \pm 4$ Hz (Fig. 4.9). We found that the direction of the SER depended only on the sign of ddf, not the amplitude ratio; i.e. f_1 shifts up when ddf is negative, and f_1 shifts down when ddf is positive (Fig. 4.9, middle). This supports our hypothesis that the SER is driven by the precession of the Lissajous rather than the local rotation of the petals when the df values are outside the JAR range.

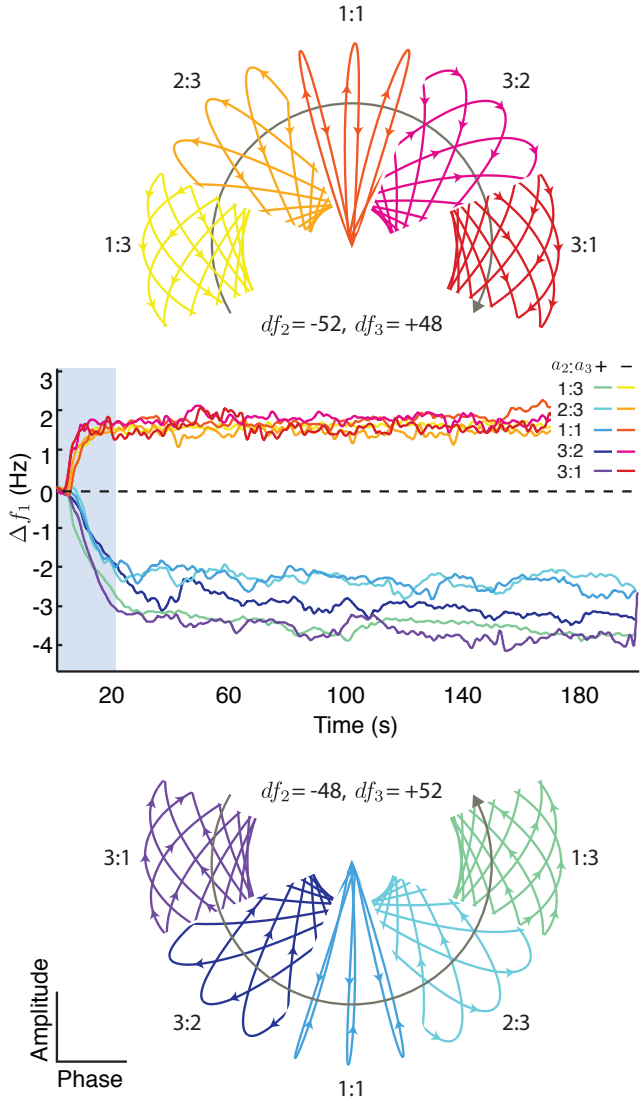

Figure 4.9: EOD frequency traces (middle plot) to envelope stimuli (±4 Hz) with different amplitude ratios ($a_2 : a_3 = 1:3,\ 2:3,\ 1:1,\ 3:2$ and $3:1$). The EOD frequency shifts up for negative *ddf* (red spectrum plots) and shifts down for positive *ddf* (blue spectrum plots). The Lissajous figures are representative angular sections of the plots at each of the tested *ddf* values for each amplitude ratio. As the amplitude ratio is varied the direction of the local rotation of the "petals" can differ from that of the general precession of the Lissajous. The individual petals of amplitude ratios $1:3$ and $2:3$ (negative *ddf*; top) and $3:1$ and $3:2$ (positive *ddf*; bottom) rotate opposite to the precession (gray arrows). The EOD responses follow the precession and not the local rotations, indicating that they are dependent on *ddf* and not the stimulus amplitude ratio.

Chapter 5

Discussion

Sensory conflict, confounds, and interference are inevitable in an environment rich in sensory cues. However, this is not necessarily detrimental to the organism or robot that employs a sensory system. With the appropriate mechanisms, modulations caused by different environmental features can be extracted, and can serve as independent "channels of information". These mechanisms can in principle differentiate between the subtleties of modulations generated by different sources. Emergent modulations such as beats and envelopes are unlike primary sensory modulations; they are caused not due to a specific feature, instead they emerge from the interaction of primary modulations. Thus emergent modulations can also be considered channels of information—they reveal relative relationships between environmental features. This information can either help the perception of these features to a higher accuracy, or instead may be used to directly measure relative traits.

5.1 Relative frequency extraction in electric fish

Electric fish have evolved electrosensory geometry and an underlying computational algorithm which directly measures differential information from conspecifics. The electroreceptors distributed across the body surface [12, 51] enable gathering of spatial electric field information. Two types of tuberous electroreceptors measure independent amplitude and phase information [71, 72] with precision in timing approaching tens of nanoseconds [62]. These parameters of the local electric field are then compared across spatially distributed receptors [6]. This computation can reveal the difference frequency (df) between the sensing fish and its conspecifics (Sec. 2.6) without the sensing fish knowing its own EOD frequency f_1. Indeed, it has been shown through behavioral experiments that these fish lack this feedback from the motor units or electric organ to the sensory regions of the brain [16]. The computation can be visualized as the rotation of the amplitude-phase parametric curve. The direction of the Lissajous trajectory followed by these parameters reveal the sign of df (Secs. 2.5,2.6, Fig. 2.4).

5.2 Characterization of response to beats: the JAR

The nonlinear computation described above allows the extraction of a specific kind of emergent modulation, the beat, which is a specific combination of global amplitude modulation (AM) and phase modulation (PM) at the same df. The electric fish community mistakenly uses the term "Amplitude Modulation" to describe beats, which is an unfortunate nomenclature that I have chosen to use in the publications that contributed to this thesis. However, I have reverted to the mathematically precise terminology in this document. The comparison of amplitude and phase information allow these fish to differentiate beats from other modulations, which may contain different relative contribution and temporal and spatial frequencies of AMs and PMs. Perception of df also facilitates a behavioral response, the JAR, whereby fish change their frequency f_1 to increase $|df|$. In Chap. 3, a complete yet parsimonious model of the JAR is described.

The JAR is a behavior in several species of weakly electric fish that allows individuals to shift their EOD frequency away from that of an interfering conspecific, having low (but nonzero) df. The neural computation of the JAR is conceptually simple yet mechanistically complex: the fish achieve the JAR without an internal reference to their own EOD frequency [16, 34] and instead integrate information from receptive fields across the body surface, ultimately evaluating the single parameter, df, to raise

or lower the EOD frequency so as to increase the magnitude of df.

Despite the mechanistic complexity of the JAR, our goal was to capture its conceptual simplicity and express it as a low-order dynamical system. To achieve this goal, we stabilized the JAR using a computer-controlled feedback system. This stabilization allowed us to reduce the complete computational algorithm of the JAR into a simple parsimonious model comprising a delay, a sensory escape function, and a motor return (see Fig. 5.1).

Comparatively simple experimental measurements can now be used inform the parameters of this model that in turn can predict responses to novel naturalistic or artificial stimuli. For example, this model captures the dynamics of a "snap-through" bifurcation that was not previously appreciated. Further, this model can be used to simulate social interactions between multiple individuals, without considering the mechanistic details of the internal dynamics underlying each individual's response.

5.2.1 Local and global modeling

A stimulus whose frequency perfectly matches that of the fish's own steady-state EOD would not elicit a JAR response; there would be no amplitude modulations or changes in the timings of zero crossings, as is necessary to drive the JAR circuit. This situation is an unstable equilibrium, because any deviations of either the stimulus or response frequency would cause the fish to shift its frequency away from it. The EOD frequency does not escape indefinitely, however, as it settles down into a new

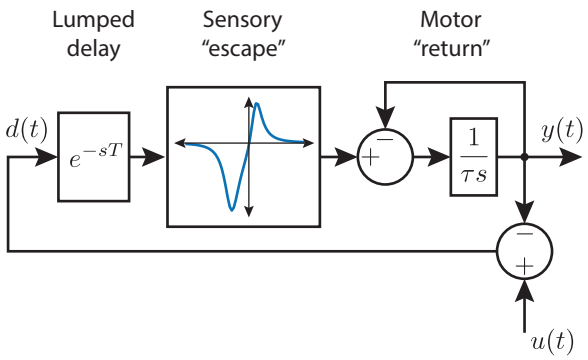

Figure 5.1: A parsimonious nonlinear model for the JAR. The motor output of the EOD is represented in terms of the frequency of the pacemaker, $y(t)$. As is well known, the nervous system extracts the df, $d(t) = y(t) - u(t)$, where $u(t)$ is the frequency of an external stimulus (e.g. from a nearby conspecific). The sensorimotor transform includes a delay T, an sensory escape function, $e(d)$, and autogenous motor return with time constant, τ.

equilibrium that is a function of the applied stimulus frequency. The existence of additional stable equilibria reveals the inherent nonlinear nature of the behavior.

Further, it is known that there are two parallel motor pathways, one that shifts the EOD frequency up and the other down [57]. This implies that there could well be significant nonlinearities or even non-smoothness of the dynamics at the switching point between the two circuits, i.e. the baseline. Thus it is imperative that we understand the local dynamics at baseline, in addition to capturing the nonlinear escape dynamics. Indeed, it is the global asymmetric shape of the nonlinear escape curve $e(d)$—and not a local discontinuity—that captures the asymmetry that was described previously by Metzner [57].

5.2.2 Closed-loop stabilization of unstable behavior

The JAR is an escape response, which makes the examination of the behavior around the baseline challenging. It is the instability of the equilibrium at baseline that underlies this difficulty. However, the stabilization of an unstable system using feedback is a classical application of control theory. In the case of the fish, we stabilized the unstable equilibrium by setting up a closed-loop feedback system that used the error signal between the fish's own frequency and a predefined reference frequency trajectory as the basis for the feedback. This system allows us to "dictate" the frequency of the fish. We showed experimentally (Fig 3.4) and confirmed analytically after modeling (Eq. (3.15)) that this feedback did indeed stabilize the open-loop system.

This artificially closed loop system was systematically perturbed (Fig 3.5), and the resulting FRF data was numerically transformed to open loop using the known feedback transformation (Eq. (3.5), Fig 3.9B). This allowed us to identify a model structure (Fig 3.8) and verify it on the experimentally obtained closed-loop FRF data (Fig 3.9A). In this manner, by knowing the feedback parameters and the closed loop response, we were able to fit a frequency domain model to an unstable behavior. This procedure is relevant and applicable to a wide range of unstable biological behaviors, especially robust escape behaviors.

5.2.3 Evaluating the JAR in relation to the model

In all of the fish that we tested (5 for reference-tracking and 2 for clamp) the linearization at baseline was found to be identical. This was an unexpected result, since it is certainly possible to avoid jamming frequencies while having different slopes for $e(d)$ at the origin, provided they are positive. This result is a testament to the robustness of the JAR. This also means that small excursions around baseline should appear extremely similar across individuals.

This consistency also means that the escape curve, which can be identified by clamped-*df* experiments, serves as a possible "signature" for the behavior. By quantifying the escape curve for two individuals, jamming interactions between them can be modeled and predicted. Reducing the JAR to this curve also allows us to examine social aspects of the JAR without considering the mechanistic details underlying its dynamics. For instance, previous research, interpreted in the context of our model, suggests that the escape curves may vary across development and be dependent on gender [46]. This means that the distribution of frequencies in a social group might be tailored by the individuals over time by modification of their escape curves. Future work might include identifying a general model structure that works across individuals and across stimulus amplitudes so that a complete interaction between freely swimming individuals in the wild can be modeled.

5.2.4 Refining and extending the model

The effect of stimulus amplitude on the dynamics has not been fully explored in this work. While we found no significant dependence on *constant* amplitude (see Fig. 3.11), the JAR certainly depends on *changing* amplitude since a changing amplitude is simply an AM. In a natural environment, the amplitude of EOD signals from nearby conspecifics will depend on the time-varying distance and orientation between the animals. If the goal is to model the interaction of groups of fish, it becomes necessary to quantify the effect of stimulus amplitude dynamics on the JAR.

In addition, the escape function may depend on higher order time derivatives of d, taking the form $e(d, \dot{d}, \ddot{d}, \ldots)$. An asymmetry in this kind of velocity dependence may explain the difference between the model response and data in case of the decreasing ramps. Experiments similar to the dynamic clamp trials described in this chapter are required to fully understand the contribution of these higher order terms.

Our assumption that the return function can be modeled as a linear spring-like term accurately captured the data; however, nonlinearities in the return function could also affect the behavior. In this case, the model will be

$$\dot{y} = -\hat{r}(y) + \hat{e}(d), \tag{5.1}$$

with $\hat{r}(y)$ and $\hat{e}(d)$ denoting return and escape respectively. This would imply that the steady state frequencies are $y_s = \hat{r}^{-1}(\hat{e}(d_s))$. Further behavioral or neural experiments will then be required to tease apart $\hat{r}$ and $\hat{e}$, as this cannot be done with input–output

behavior alone.

In their natural habitat, weakly electric fish are often found in groups of two or more individuals [74,78]. In these groups, the complex interaction of electric fields can give rise to envelopes [75], through the relative movement between individuals [84], or the higher order interaction of their EODs [76]. Evidence of envelope processing has been revealed in the electrosensory system in weakly electric fish [52,55,60,70]. In addition, Chap. 4 described a behavioral response in *Eigenmannia* to low-frequency 'social envelopes' [76]. Extending the JAR model described in Chap. 3 to incorporate not only pair-wise differences between individuals, but also to capture envelope responses would ultimately provide a powerful tool to predict and interpret complex social behavior in these fish.

5.3 Discovery of response to social envelopes

Forty years of analysis of the JAR [16,83] have focused on mapping a well-defined computation [33] through all stages of neural processing, from sensory receptors to motor units [58]. This work was successful mainly due to a sharp focus on the specific parameters that were necessary and sufficient to drive the behavior, thereby putting aside potentially complex temporal features—such as social and movement envelopes—that are likely to be ubiquitous in a fish's electrosensory milieu [74, 78].

Recent neurophysiological studies have identified neurons that respond to such electrosensory envelopes [52, 55, 59, 60, 70], but the function of this brain activity was unknown.

Here we show the behavioral relevance of one category of electrosensory envelopes. We measured the EOD responses of *Eigenmannia virescens* to envelope stimuli like those that would arise from the electrical interactions of three or more motionless conspecifics. We call this behavior the SER. We also proposed a simple extension of the algorithm for the JAR, a low-pass filter of the instantaneous amplitude and phase of the combined signal, which accurately predicts SER behavior. In the SER, *E. virescens* raised or lowered their EOD frequency, which resulted in an increase in frequency of the envelope by approximately $2-6$ Hz, with final envelope frequencies between 5 and 15 Hz. The strength of the SER depended on the initial envelope frequency and the stimulus amplitude: low initial frequencies and high stimulus amplitudes elicited the largest changes in EOD frequency. The SER direction was insensitive to the relative amplitude ratio between stimulus signals, indicating dependence on the slow precession of the Lissajous, as opposed to fast local rotations of the petals, as predicted by our model (see Fig. 4.9).

5.3.1 Mechanisms for the SER

We extended the widely known model for the control of the JAR with the addition of a low-pass filter that eliminates responses to the local rotations of the Lis-

sajous while retaining its precession. The model does not predict where and how this computation may be implemented in the brain. Part of this computation could be implemented as a saturation nonlinearity of amplitude-coding P-receptors, which would cause them to encode envelopes [70]. When combined with a rectification circuit in the electrosensory lateral line lobe (ELL) [52, 59, 60], the amplitude axis of the Lissajous would oscillate at the envelope frequency 2.33. In this case, the phase axis would be filtered independently in downstream circuits to yield the circular Lissajous that precesses at the $|ddf|$. Alternatively, amplitude and phase filtering may both occur in downstream circuits. In this case, the higher response thresholds (as compared with the JAR) may be necessary to overcome the attenuation caused by the filter.

5.3.2 Possible functional relevance of the SER

In their natural habitat, weakly electric fish are commonly found in groups of three or more conspecifics [74, 78], which is a necessary condition for the SER. We showed that fish exhibited SERs that increased the frequency of envelopes to higher frequencies (up to 15 Hz). The SER appears to be analogous to the JAR, in which fish also shift their EOD frequency, effecting an increase in the frequency of the beat [33]. It has been shown that low-frequency beats impair aspects of electrolocation and that the JAR may allow fish to avoid this detrimental interference [5, 30]. In addition to the behavioral impairment, it has also been shown that neural responses to moving objects are impaired by low-frequency jamming [64]. If the SER functions

analogously to the JAR, one would predict that low-frequency envelopes might also degrade electrosensory performance and impair the underlying neural responses to moving objects.

5.3.3 Movement envelopes

Fish are rarely completely motionless; therefore, we expect that movement-related envelopes commonly emerge in groups of two or more fish. These envelopes can encode the relative velocity between fish and possibly provide reliable cues about distance [84]. We suspect that fish may also exhibit a 'movement envelope response' that can be driven by modulations due to the relative movement between individuals. These movement-based envelopes indeed arise in a social context, but for clarity we distinguish them from 'social envelopes' as defined in Chap. 4. This distinction is important because social envelopes constitute a special class of signals that arises solely due to the details of the interactions between electric fields of three or more wave-type weakly electric fish. Movement-related envelopes, however, can arise in a variety of contexts, including from non-social sources such as the interaction of fish with objects in their environment. In the natural habitat, a cacophony of stimuli contribute to modulations of the EOD in *Eigenmannia*, including simple moving objects [21], summations of multiple electric signals (as examined in this chapter) and movements of nearby electrogenic animals [56]. In addition, amplitude and phase modulations influence each other, creating cross interactions, which also have behav-

ioral implications [19]. These and related behaviors appear to be mediated by sets of simple computational rules that are instantiated in the ascending electrosensory pathways of *Eigenmannia* and other closely related species of weakly electric fishes. The behavioral results in Chap. 4 provide yet another platform for the analysis and re-analysis of a well-described neural circuit that is used in the control of multiple behaviors.

Bibliography

[1] C. Assad, B. Rasnow, and P. Stoddard. Electric organ discharges and electric images during electrolocation. *J Exp Biol*, 202(10):1185, 1999.

[2] K. Astrom and R. Murray. *Feedback systems: an introduction for scientists and engineers*. Princeton university press, 2008.

[3] D. Babineau, A. Longtin, and J. E. Lewis. Modeling the electric field of weakly electric fish. *J Exp Biol*, 209(18):3636–51, Sept. 2006.

[4] M. Bacher. A new method for the simulation of electric fields, generated by electric fish, and their distorsions by objects. *Biol Cybern*, 47(1):51–58, 1983.

[5] J. Bastian. Electrolocation in the presence of jamming signals: behavior. *J Comp Physiol A*, 161(6):811–824, 1987.

[6] J. Bastian and W. Heiligenberg. Neural correlates of the jamming avoidance response of *Eigenmannia*. *J Comp Physiol A*, 136(2):135–152, 1980.

BIBLIOGRAPHY

[7] E. Bedrosian. A product theorem for Hilbert transforms. *Proc IEEE*, 51(5):868–869, 1963.

[8] M. Bennett. Electrolocation in fish. *Annals of the New York Academy of Sciences*, 188(1):242–269, 1971.

[9] J. Bowmaker and H. Dartnall. Visual pigments of rods and cones in a human retina. *J Physiol*, 298(1):501–511, 1980.

[10] T. H. Bullock. Biological sensors. *Vistas in science*, pages 176–206, 1968.

[11] T. H. Bullock. Species differences in effect of electroreceptor input on electric organ pacemakers and other aspects of behavior in electric fish. *Brain Behav and Evol*, 2:85–118, 1969.

[12] T. H. Bullock. Electroreception. *Annu Rev Neurosci*, 5(1):121–170, Nov. 1982.

[13] T. H. Bullock, K. Behrend, and W. Heiligenberg. Comparison of the jamming avoidance responses in gymnotoid and gymnarchid electric fish: A case of convergent evolution of behavior and its sensory basis. *J Comp Physiol A*, 103(1):97–121, Feb. 1975.

[14] T. H. Bullock and S. Chichibu. Further analysis of sensory coding in electroreceptors of electric fish. *Proc Natl Acad Sci U S A*, 54(2):422–429, 1965.

[15] T. H. Bullock, R. R. Fay, C. D. Hopkins, and A. N. Popper. *Electroreception. Springer Handbook of Auditory Research.* Springer, 2005.

BIBLIOGRAPHY

[16] T. H. Bullock, R. H. Hamstra, and H. Scheich. The jamming avoidance response of high frequency electric fish. *J Comp Physiol A*, 77(1):1–22, Mar. 1972.

[17] T. H. Bullock and C. D. Hopkins. *Explaining Electroreception*. Springer, 2005.

[18] A. Caputi and R. Budelli. Peripheral electrosensory imaging by weakly electric fish. *J Comp Physiol A*, 192(6):587–600, 2006.

[19] B. A. Carlson. Phantoms in the brain: ambiguous representations of stimulus amplitude and timing in weakly electric fish. *J Physiol Paris*, 102(4-6):209–22, 2008.

[20] B. A. Carlson and C. D. Hopkins. Stereotyped temporal patterns in electrical communication. *Anim Behav*, 68(4):867–878, 2004.

[21] B. A. Carlson and M. Kawasaki. Behavioral responses to jamming and 'phantom' jamming stimuli in the weakly electric fish *Eigenmannia*. *J Comp Physiol A*, 193(9):927–41, Sept. 2007.

[22] J. Chowning. The synthesis of complex audio spectra by means of frequency modulation. *J Audio Eng Soc*, 21(7):526–534, 1973.

[23] W. Crampton and J. Albert. Evolution of electric signal diversity in gymnotiform fishes. *Communication in fishes*, 2:647–731, 2006.

[24] M. A. Elgar. Predator vigilance and group size in mammals and birds: a critical review of the empirical evidence. *Biol Rev*, 64(1):13–33, 1989.

[25] D. J. Field. Relations between the statistics of natural images and the response properties of cortical cells. *J. Opt. Soc. Am. A*, 4(12):2379–2394, Dec. 1987.

[26] T. E. Finger, C. C. Bell, and C. E. Carr. Comparisons among electroreceptive teleosts: why are electrosensory systems so similar. *Electroreception. Wiley, New York*, pages 465–481, 1986.

[27] E. Fortune. The decoding of electrosensory systems. *Curr Opin Neurobiol*, 16(4):474–480, 2006.

[28] E. S. Fortune and G. J. Rose. Voltage-gated Na+ channels enhance the temporal filtering properties of electrosensory neurons in the torus. *J Neurophysiol*, 90(2):924–929, 2003.

[29] M. Hagedorn. Ecology and behavior of a pulse-type electric fish, *Hypopomus occidentalis* (gymnotiformes, hypopomidae), in a fresh-water stream in panama. *Copeia*, 1988(2):324–335, 1988.

[30] W. Heiligenberg. Electrolocation of objects in the electric fish *Eigenmannia* (Rhamphichthyidae, Gymnotoidei). *J Comp Physiol*, 87(2):137–164, 1973.

[31] W. Heiligenberg. Theoretical and experimental approaches to spatial aspects of electrolocation. *J Comp Physiol*, 103(3):247–272, 1975.

[32] W. Heiligenberg. The jamming avoidance response of the electric fish *Eigenman-*

nia: computational rules and their neuronal implementation. *Semin Neurosci*, 3:3–18, 1991.

[33] W. Heiligenberg. *Neural nets in electric fish*. The MIT Press, 1991.

[34] W. Heiligenberg, C. Baker, and J. Matsubara. The jamming avoidance response in *Eigenmannia* revisited: The structure of a neuronal democracy. *J Comp Physiol A*, 127(3):267–286, Sept. 1978.

[35] W. Heiligenberg and J. Bastian. The control of *Eigenmannia*'s pacemaker by distributed evaluation of electroreceptive afferences. *J Comp Physiol A*, 136(2):113–133, 1980.

[36] É. Hitschfeld, S. Stamper, K. Vonderschen, E. Fortune, and M. Chacron. Effects of restraint and immobilization on electrosensory behaviors of weakly electric fish. *ILAR J*, 50:361–372, 2009.

[37] E. M. Hitschfeld, S. A. Stamper, K. Vonderschen, E. S. Fortune, and M. J. Chacron. Effects of restraint and immobilization on electrosensory behaviors of weakly electric fish. *ILAR J*, 50(4):361–72, Jan. 2009.

[38] C. D. Hopkins. Electric communication: Functions in the social behavior of *Eigenmannia virescens*. *Behaviour*, 50(3/4):270–305, 1974.

[39] G. J. Hupé and J. E. Lewis. Electrocommunication signals in free swimming

brown ghost knifefish, *Apteronotus leptorhynchus*. *J Exp Biol*, 211(10):1657–1667, May 2008.

[40] J. Justice. Analytic signal processing in music computation. *IEEE Trans Audio Speech Lang Process*, 27(6):670 – 684, Dec. 1979.

[41] W. Kaplan. *Advanced calculus, 4th ed.*, volume 4, pages 286–291. Addison-Wesley, Reading, MA, 1991.

[42] M. Kawasaki. Independently evolved jamming avoidance responses employ identical computational algorithms: a behavioral study of the african electric fish, *Gymnarchus niloticus*. *J Comp Physiol A*, pages 9–22, 1993.

[43] Keeley. Large, slow changes of electric organ discharge frequency in the weakly electric fish, *Eigenmannia virescens*, 2004.

[44] M. Kelly, D. Babineau, A. Longtin, and J. E. Lewis. Electric field interactions in pairs of electric fish: modeling and mimicking naturalistic inputs. *Biological cybernetics*, 98(6):479–90, June 2008.

[45] E. I. Knudsen. Spatial aspects of the electric fields generated by weakly electric fish. *J Comp Physiol*, 99(2):103–118, 1975.

[46] B. Kramer. The sexually dimorphic jamming avoidance response in the electric fish *Eigenmannia* (teleostei, gymnotiformes). *J Exp Biol*, 130(1):39–62, 1987.

[47] J. L. Larimer and J. A. MacDonald. Sensory feedback from electroreceptors to electromotor pacemaker centers in gymnotids. *Am J Physiol*, 214:1253–1261, June 1968.

[48] G. Lauder and K. Liem. Patterns of diversity and evolution in ray-finned fishes. *Fish neurobiology*, 1:1–24, 1983.

[49] R. Lerner. A matched filter detection system for complicated doppler shifted signals. *IRE Trans Inf Theory*, 6(3):373–385, 1960.

[50] H. Lissmann. On the function and evolution of electric organs in fish. *J Exp Biol*, 35(1):156–191, 1958.

[51] H. Lissmann and K. Machin. The mechanism of object location in *Gymnarchus Niloticus* and similar fish. *J Exp Biol*, 35(2):451–486, 1958.

[52] A. Longtin, J. W. Middleton, J. Cieniak, and L. Maler. Neural dynamics of envelope coding. *Math Biosci*, 214(1-2):87–99, 2008.

[53] M. S. Madhav, S. A. Stamper, E. S. Fortune, and N. J. Cowan. Closed-loop stabilization of the jamming avoidance response reveals its locally unstable and globally nonlinear dynamics. *J Exp Biol*, 216(22):4272–4284, 2013.

[54] J. Matsubara and W. Heiligenberg. How well do electric fish electrolocate under jamming? *J Comp Physiol A*, 125(4):285–290, Dec. 1978.

[55] P. McGillivray, K. Vonderschen, E. S. Fortune, and M. J. Chacron. Parallel coding of first- and second-order stimulus attributes by midbrain electrosensory neurons. *J Neurosci*, 32(16):5510–24, Apr. 2012.

[56] M. G. Metzen and M. J. Chacron. Weakly electric fish give behavioral responses to envelopes naturally occurring during movement: implications for neural processing. *J Exp Biol*, Dec. 2013.

[57] W. Metzner. The jamming avoidance response in *Eigenmannia* is controlled by two separate motor pathways. *J Neurosci*, 13(5):1862–78, May 1993.

[58] W. Metzner. Neural circuitry for communication and jamming avoidance in gymnotiform electric fish. *J Exp Biol*, 202(10):1365, 1999.

[59] J. Middleton, E. Harvey-Girard, L. Maler, and a. Longtin. Envelope gating and noise shaping in populations of noisy neurons. *Phys Rev E*, 75(2):021918, Feb. 2007.

[60] J. W. Middleton, A. Longtin, J. Benda, and L. Maler. The cellular basis for parallel neural transmission of a high-frequency stimulus and its low-frequency envelope. *Proc Nat Acad Sci*, 103(39):14596–14601, Sept. 2006.

[61] P. Moller. *Electric fishes: history and behavior*, volume 17. Chapman & Hall London, 1995.

[62] K. Moortgat, C. Keller, T. Bullock, and T. Sejnowski. Submicrosecond pacemaker precision is behaviorally modulated: the gymnotiform electromotor pathway. *Proc Nat Acad Sci*, 95(8):4684–4689, 1998.

[63] B. L. Partridge and W. Heiligenberg. Three's a crowd? Predicting *Eigenmannia*'s responses to multiple jamming. *J Comp Physiol A*, 136(2):153–164, 1980.

[64] J. U. Ramcharitar, E. W. Tan, and E. S. Fortune. Effects of global electrosensory signals on motion processing in the midbrain of *Eigenmannia*. *J Comp Physiol A*, 191(9):865–72, Sept. 2005.

[65] B. Rasnow. The effects of simple objects on the electric field of *Apteronotus*. *J Comp Physiol A*, 178(3):397–411, 1996.

[66] A. Rihaczek and E. Bedrosian. Hilbert transforms and the complex representation of real signals. *Proc IEEE*, 54(3):434–435, 1966.

[67] J. Roddey, B. Girish, and J. Miller. Assessing the performance of neural encoding models in the presence of noise. *J Comp Neurol*, 8(2):95–112, 2000.

[68] S. Rosen. Temporal information in speech: acoustic, auditory and linguistic aspects. *Philosophical Transactions of the Royal Society of London. Series B: Biological Sciences*, 336(1278):367–373, 1992.

[69] E. Roth, M. B. Reiser, M. H. Dickinson, and N. J. Cowan. A task-level model for optomotor yaw regulation in *Drosophila Melanogaster*: A frequency-domain

system identification approach. In *Proc IEEE Int Conf on Decision Control*, pages 3721–3726. IEEE, 2012.

[70] M. Savard, R. Krahe, and M. J. Chacron. Neural heterogeneities influence envelope and temporal coding at the sensory periphery. *Neuroscience*, 172:270–284, Jan. 2011.

[71] H. Scheich and T. Bullock. The detection of electric fields from electric organs. In A. Fessard, editor, *Electroreceptors and Other Specialized Receptors in Lower Vertrebrates*, volume 3 / 3 of *Handbook of Sensory Physiology*, pages 201–256. Springer Berlin Heidelberg, 1974.

[72] H. Scheich, T. H. Bullock, and R. H. Hamstra. Coding properties of two classes of afferent nerve fibers: high-frequency electroreceptors in the electric fish, *Eigenmannia*. *J Neurophysiol*, 36(1):39–60, 1973.

[73] J. Schnapf, T. Kraft, and D. Baylor. Spectral sensitivity of human cone photoreceptors. *Nature*, 325(6103):439, 1987.

[74] S. A. Stamper, E. Carrera-G, E. W. Tan, V. Fugère, R. Krahe, and E. S. Fortune. Species differences in group size and electrosensory interference in weakly electric fishes: implications for electrosensory processing. *Behav Brain Res*, 207(2):368–376, 2010.

[75] S. A. Stamper, E. S. Fortune, and M. J. Chacron. Perception and coding of envelopes in weakly electric fishes. *J Exp Biol*, 216(13):2393–2402, 2013.

[76] S. A. Stamper, M. S. Madhav, N. J. Cowan, and E. S. Fortune. Beyond the jamming avoidance response: Weakly electric fish respond to the envelope of social electrosensory signals. *J Exp Biol*, 215(23):4196–4207, 2012.

[77] M. Stone. An asymptotic equivalence of choice of model by cross-validation and Akaike's criterion. *J R Stat Soc B*, 39(1):pp. 44–47, 1977.

[78] E. W. Tan, J. M. Nizar, E. Carrera-G, and E. S. Fortune. Electrosensory interference in naturally occurring aggregates of a species of weakly electric fish, *Eigenmannia virescens*. *Behav Brain Res*, 164(1):83–92, 2005.

[79] F. A. Triefenbach and H. H. Zakon. Changes in signalling during agonistic interactions between male weakly electric knifefish, *Apteronotus leptorhynchus*. *Anim Behav*, 75(4):1263–1272, Apr. 2008.

[80] G. Von der Emde. Non-visual environmental imaging and object detection through active electrolocation in weakly electric fish. *J Comp Physiol A*, 192(6):601–612, 2006.

[81] G. von der Emde. Electroreception. In C. G. Galizia and P.-M. Lledo, editors, *Neurosciences - From Molecule to Behavior: a University textbook*, pages 409–425. Springer Berlin Heidelberg, Berlin, Heidelberg, 2013.

[82] G. von der Emde, K. Behr, B. Bouton, J. Engelmann, S. Fetz, and C. Folde. 3-dimensional scene perception during active electrolocation in a weakly electric pulse fish. *Frontiers in behavioral neuroscience*, 4(May):26, Jan. 2010.

[83] A. Watanabe and K. Takeda. The change of discharge frequency by a.c. stimulus in a weak electric fish. *J Exp Biol*, 40:57–66, 1963.

[84] N. Yu, G. Hupé, C. Garfinkle, J. E. Lewis, and A. Longtin. Coding conspecific identity and motion in the electric sense. *PLoS Comp Biol*, 8(7):e1002564, 2012.

[85] H. Zakon and K. Dunlap. Sex steroids and communication signals in electric fish: a tale of two species. *Brain Behav and Evol*, 54(1):61–69, 1999.

[86] H. H. Zakon, J. Oestreich, S. Tallarovic, and F. A. Triefenbach. EOD modulations of brown ghost electric fish: JARs, chirps, rises, and dips. *J Physiol Paris*, 96(5):451–458, 2002.

[87] M. M. Zupanc, G. Engler, A. Midson, H. Oxberry, L. A. Hurst, M. R. Symon, and G. K. Zupanc. Light-dark-controlled changes in modulations of the electric organ discharge in the teleost *Apteronotus leptorhynchus*. *Anim Behav*, 62(6):1119–1128, Dec. 2001.

Vita

Manu S. Madhav received his B.Tech. Degree in Mechanical Engineering from National Institute of Technology Calicut, India in 2008, and enrolled in the Master of Science in Engineering (M.S.E.) program in the Mechanical Engineering Department at Johns Hopkins University in the Fall of 2008. While enrolled in the Masters program, he worked with Dr. Allison Okamura on a project investigating the efficacy of providing haptic feedback to the feet. Manu joined Dr. Noah Cowan's Locomotion in Mechanical and Biological Systems (LIMBS) lab to pursue his Ph.D. in the Spring of 2009. His research has since focused on developing and executing novel experimental paradigms to investigate and characterize behavior in animals at task as well as neural circuit levels.

Manu did his primary research on understanding the emergence and relevance of nonlinear features in the electrosensory system of weakly electric fish. A low-latency

closed-loop experimental rig allowed him to fully characterize the Jamming Avoidance Response (JAR) and discover the Social Envelope Response (SER) in these fish. His paper on the SER in Electric Fish was ranked as one of the top three publications in 2012 in the Journal of Experimental Biology. Under his mentorship, Eva Siehmann's work on envelope coding in electric fish won her the best undergraduate thesis award at Westflischen Hochschule. Manu has also worked on understanding the impact of assuming symmetry while modeling human locomotion, in collaboration with Dr. Amy Bastian's lab at the JHU School of Medicine. In addition, he is actively involved in a collaboration with Dr. Charles Duffy at the University of Rochester investigating the role of MSTd in integrating cues and driving navigation in primates.

For his post-doctoral work, Manu will investigate the coding and processing of spatial navigation in the rodent brain using a unique virtual reality experimental system, in collaboration with Dr. Jim Knierim from JHU and Dr. Hugh T. Blair from UCLA. Manu has worked either directly with, or on data from, several animal models, including electric fish, cockroaches, rats, primates, and humans. In the future he hopes to expand this repertoire and continue understanding the algorithms that drive complex behavior in animals. Doing so will help bridge the gap between "biological" and "artificial" machines and drive the next generation of bio-inspired robotics research, while simultaneously helping biologists and neuroscientists use careful mathematical analyses to better understand the systems they investigate.